Analytic Modelling and Resource Dimensioning of Optical Burst Switched Networks

Daniele Tafani

MEng in Telecommunications Engineering

A Dissertation submitted in fulfilment of the

requirements for the award of

Doctor of Philosophy (Ph.D.)

to

School of Electronic Engineering

Faculty of Engineering and Computing

Dublin City University

Supervisors: Prof. Liam P. Barry, Dr. Conor J. McArdle

24 February 2012

Declaration

I hereby certify that this material, which I now submit for assessment on the programme of study leading to the award of Doctor of Philosophy is entirely my own work, that I have exercised reasonable care to ensure that the work is original, and does not to the best of my knowledge breach any law of copyright, and has not been taken from the work of others save and to the extent that such work has been cited and acknowledged within the text of my work.

Signed:

Student ID: 58119931

Date: 24 February 2012

To my brother Stefano

"A mind is like a parachute. It doesn't work if it is not open." (Frank Zappa)

Acknowledgments

This is certainly the section of the thesis that I enjoyed writing the most. First and foremost I would like to thank my supervisor Prof. Liam Barry for giving me the privilege of being one of his PhD students and for his constant advise and support through this very enduring period of my life. Thank you for believing in me and basically for changing my life in accepting me for this research adventure. My eternal gratitude goes to Dr. Conor McArdle for sharing with me all the challenges, for the millions of hours spent on the whiteboard of his office developing new ideas and trying to improve the old ones. Without your never-ending support, advises and kindness this thesis would not exist. Thank you for everything!

I am most grateful to Dublin City University for giving me the opportunity to research in the Radio and Optical Communications Lab while earning my PhD (probably one of the best optics lab on the planet), and the Science Foundation of Ireland for the scholarship grants awarded during this period.

I would like to thank all the past and present members of the Lab for all their infinite support, friendship and for the FUN (!) particularly Antonio, Colm, Eamonn, Elif, Frank, Hayman, Josue, Kai, Karl, Kevin, Krzysztof, Prince, Ramon, Regan, Rob, Rui, Sly and Tam.

These three years in Ireland gave me the opportunity to meet unforgettable marvelous people that are impossible to list and this thesis is dedicated to all of them. A special dedication goes to my best mates (in alphabetical order and ladies first) Elena Halfstuff, Cormacchio Bolgero, Davide Legnolago, Fabiana, Paolesello, Paula Houston and Zambo. Thank you for your precious friendship and the infinite indelible great memories.

Last but not least, I would like to thank the most important people in my life without whom it would not have been possible to write this doctoral thesis. My eternal gratitude goes to my parents Angela and Ubaldo, to my brother Stefano and to my girlfriend Wany for their infinite patience, support and love. This is for you.

Abstract

The realisation of optical network architectures may hold the key to delivering the enormous bandwidth demands of next generation Internet applications and services. Optical Burst Switching (OBS) is a potentially cost-effective switching technique that can satisfy these demands by offering a high bit rate transport service that is bandwidth-efficient under dynamic Internet traffic loads. Although various aspects of OBS performance have been extensively investigated, there remains a need to systematically assess the cost/performance trade-offs involved in dimensioning OBS switch resources in a network. This goal is essential in enabling the future deployment of OBS but poses a significant challenge due to the complexity of obtaining tractable mathematical models applicable to OBS network optimisation. The overall aim of this thesis lies within this challenge.

This thesis firstly develops a novel analytic performance model of an OBS node where burst contention is resolved by combined use of Tuneable Wavelength Converters (TWCs) and Fibre Delay Lines (FDLs) connected in an efficient share-per-node configuration. The model uses a two-moment traffic representation that gives a good trade-off between accuracy and complexity, and is suitable for extension to use in network modelling.

The OBS node model is then used to derive an approximate analytic model of an OBS network of switches equipped with TWCs and FDLs, again maintaining a two-moment traffic model for each end-to-end traffic path in the network. This allows evaluation of link/route loss rates under different offered traffic characteristics, whereas most OBS network models assume only a single-moment traffic representation.

In the last part of this thesis, resource dimensioning of OBS networks is performed by solving single and multi-objective optimisation problems based on the analytic network model. The optimisation objectives relate to equipment cost minimisation and throughput maximisation under end-to-end loss rate constraints. Due to non-convexity of the network performance constraint equations, a search heuristic approach has been taken using a constraint-handling genetic algorithm.

Contents

List of Tables

List of Figures

List of Acronyms

BHP	Burst Header Packet
BPP	Bernoulli Poisson Pascal method
DR	Deflection Routing
E-BPP	Extended Bernoulli Poisson Pascal method
EDFA	Erbium Doped Fibre Amplifier
EFPA	Erlang Fixed Point Approximation
EFPA-S	Erlang Fixed Point Approximation with Streamline
EON	European Optical Network
ERT	Equivalent Random Theory
FDL	Fibre Delay Line
FMM	Factorial Moment Matching
GA	Genetic Algorithm
IPP	Interrupted Poisson Process
JET	Just Enough Time
JIT	Just In Time
LAUC	Latest Available Unscheduled Channel
LAUC-VF	Latest Available Unscheduled Channel with Void Filling
LAUT	Latest Available Unscheduled Time
NSFNET	National Science Foundation NETwork
OBS	Optical Burst Switching
OCS	Optical Circuit Switching
OPS	Optical Packet Switching
OXC	Optical Cross Connect
RLA	Reduced Load Approximation
RWA	Routing and Wavelength Assignment
RWGA	Random Weighted Genetic Algorithm
SBNM	Shared Buffer Network Model
SCU	Switch Control Unit
SOA	Semiconductor Optical Amplifier
TAG	Tell And Go
TAS	Tune and Select
TAS-dFDL	Tune and Select with Dedicated Fibre Delay Line
TAS-shFDL	Tune and Select with Shared Fibre Delay Line
TAW	Tell And Wait
TWC	Tunable Wavelength Converter
WDM	Wavelength Division Multiplexing

Chapter 1

Introduction

The ever increasing bandwidth demands required by next-generation applications and services of Internet Protocol (IP) networks motivates the search for alternative solutions to traditional electronic transmission and switching networks. Wavelength Division Multiplexing (WDM) is one such technology capable of delivering future bandwidth demands [82]. WDM enables multiple optical wavelength channels to be established on the same optical fibre, increasing the available bandwidth and providing good utilisation of the potential network capacity. Optical networks based on WDM use multiple independent optical communication channels each at typical data rate of 10 Gbps, resulting in a possible available bandwidth of over 50 Tbps [82, 96]. Additionally, compared to traditional networks where data is sent in the electronic domain, WDM networks can benefit from lower signal attenuation (0.2 dB/Km), lower bit error rates and lower signal distortion [82, 96]. In recent years, research attention has been focused on developing switching techniques that can exploit the enormous potential offered by WDM technology. Emerging optical systems are expected to provide static all-optical connections that can be established between a source node and a destination node of the network for the entire duration of a communication session. These connections, known as *lightpaths*, have the advantage of avoiding bottlenecks due to opto-electronic conversions at intermediate nodes of the network. Normally, a lightpath uses the same wavelength on each link of its end-to-end path (*wavelength continuity constraint*) [82]. Alternatively, through wavelength conversion via Tunable Wavelength Converters (TWCs), a lightpath can be setup using any available wavelength on each link of

the path. This switching paradigm is known as Optical Circuit Switching (OCS). Although commercially viable, this scheme does not provide an optimal utilisation of network bandwidth, particularly in the case of bursty Internet traffic. To avoid non-optimal resource usage, it is desirable that optical networks have the capability to dynamically switch IP packets.

Optical Packet Switching (OPS) [131] is a promising switching technique that has gained considerable attention for the deployment of next generation WDM networks as it allows finer-grained all-optical switching at packet level. Networks based on this switching paradigm can achieve a better bandwidth utilisation than OCS networks and have the efficiency of packet switching and routing being performed without opto-electronic conversion. Since network resources are not reserved in advance, a major drawback of OPS is that different optical packets may contend for the same wavelength channel over a common fibre link, resulting in packet loss. In OPS, packet loss can be addressed with buffering strategies in the time domain, realised by holding data packets in Fibre Delay Lines (FDLs) for a fixed amount of time determined by the fibre length [82]. Although attractive, OPS can not be employed yet since, at the time of writing, the technology is not mature enough to deliver fast packet-level optical switching [96]. Additionally, a recent study conducted in [117] illustrates that future OPS networks may not be as efficient as current electronic networks in terms of energy savings.

Optical Burst Switching (OBS) [8, 93, 117] is a network switching paradigm for WDM networks that can be placed conceptually between OCS and OPS. In an OBS network, IP packets are assembled into *bursts* and sent over the network all-optically. Before the burst transmission, an associated header packet is sent in a dedicated out-of-band wavelength channel in order to configure the switches along the burst's path prior to its arrival. The configuration of an OBS node performed by the header mainly consists of reservation of a wavelength channel on one of the switch's output ports. The header is processed electronically in the switches along the path and it is separated in time from its associated burst by a specifically dimensioned interval of time called the *offset interval*. After the offset interval expires, the burst is sent without waiting for an acknowledgment of a successful path setup.

The increasing attention of the research community to OBS is justified by the following

advantages that this switching scheme provides compared to OCS and OPS:

- OBS allows multiple node pairs to share the bandwidth over the same link thanks to statistical multiplexing whereas OCS can not switch traffic at granularity lower than a wavelength. Consequently, the bandwidth utilisation is greater than for OCS.

- OBS uses a one-way signaling scheme as opposed to OCS where dedicated send and release messages must be exchanged between a node pair for the management of a lightpath; thus, OBS has a lower setup latency and overhead than OCS.

- Differently from OPS, OBS is a more easily realised technology as it does not require fast-switching times in the optical domain. Furthermore, the complexity of header processing is lower than in OPS, where the control information has to be extracted from each packet within a very short time period. In OBS, each header is associated with a set of assembled packets, relaxing the processing times at each intermediate node of the network.

- OCS can not efficiently accommodate bursty IP traffic because of its high setup latency and wavelength granularity. On the contrary OBS can efficiently cope with bursty traffic thanks to its statistical multiplexing.

The feasibility of OBS networks has been demonstrated in the past decade through several test-bed implementations [1,5,63,69], however, experimental investigations alone may not be sufficient to extend the design of OBS networks to more generic scenarios, and a deeper understanding of their behaviour is needed. In this regard, analytic modelling of OBS is indispensable to achieve this objective and, along with experimental test-beds, contributes to the derivation of tools capable of quantifying the performance of OBS networks. The aim of the work presented in this thesis is to determine and validate new analytic models and optimisation methods in order to enable optimal design and resource dimensioning of future OBS networks.

1.1 Thesis Contributions

Similarly to OPS, burst loss, arising from contention between bursts at switch output ports, is the major performance issue for OBS. Thus, it is essential to derive analytic tools that provide performance evaluation of OBS networks in terms of burst loss probability. The present thesis addresses this issue by developing a novel approximate model of an OBS network with the objective of defining and resolving optimisation problems mainly in relation to dimensioning of OBS network infrastructure. The contributions presented in this thesis can be categorised as three main achievements as follows.

- We first focus our attention on a cost-effective OBS switch architecture where burst contentions are resolved with the joint action of TWCs and a share-per-node FDL in a feedback configuration. We develop an analytic model by adopting a two-moment matching technique in order to gain a good approximation of the characteristics of burst traffic. Particularly, we take into account the contribution of the load and of the peakedness of the burst offered traffic.

- A novel OBS network model is then built from the realised OBS switch model, where all network nodes are configured with TWCs and shared FDLs. A "path-centric" approach is used, that is the blocking probability values are calulcated separately for each path, gaining a better accuracy as opposed to "link-centric" approaches that tend to overestimate burst blocking at downstream links. Once again, the traffic streams in the network model are characterised by their average load and peakedness.

- The network model is finally used for the definition and the resolution of multi-objective optimisation problems with a major focus on network resource dimensioning of the wavelength channels in the network links and in FDLs. We address this topic by means of single/multi-objective genetic algorithms, drawing conclusions on the optimal configuration of resources in the network that allow minimisation of the total network hardware cost, simultaneously achieving a desired performance goal in terms of reducing burst blocking probability.

1.2 Thesis Overview

The thesis is organised as follows:

In Chapter 2 we present an overview of the main features of Optical Burst Switching. We describe the burst assembly process, signaling schemes, channel reservation protocols and the main contention resolution techniques. We further present a brief summary on the major research contributions in the current literature on different aspects of OBS with a specific focus on contention resolution schemes, proposals on cost-efficient buffered OBS architectures and especially on analytic modelling and performance evaluation of OBS architectures.

In Chapter 3 we analyse a particular OBS node architecture where burst contentions are resolved with a share-per-node FDL in a feedback configuration. We derive an approximate analytic model of this OBS node that allows performance evaluation in terms of burst blocking probability at the output ports. We validate our model by comparison with results obtained with a discrete-event simulation of the switch.

In Chapter 4 a buffered OBS network model is developed on the basis of the realised OBS node model of the previous chapter. We adapt well-known circuit switching techniques such as the Reduced Load Approximation to an analysis of the OBS network based on a path-centric approach. We further discuss the influence on the burst blocking probability of the streamline effect and we quantify its impact on the overall performance of the network. Once again, analytic results are validated by comparison to simulations.

In Chapter 5, optimisation problems related to pertinent dimensioning of OBS networks are defined and resolved on the basis of the realised OBS network model. Particularly, we focus our attention on the optimal dimensioning and allocation of link and FDL wavelength channels. Genetic algorithms are defined and used to resolve the optimisation problems.

In Chapter 6, the conclusions of the thesis are presented providing final comments on the obtained results and proposing ideas for future improvements related to the subjects under investigation.

Chapter 2

Optical Burst Switching

In this chapter we introduce the Optical Burst Switching (OBS) paradigm and provide a description of its main features. In Section 2.1 we introduce the ideas behind OBS and the general architecture of an OBS network. In Section 2.2 we illustrate the principal burst assembly procedures and their impact on network traffic. In Section 2.3 we introduce the main signaling schemes and in Section 2.4 a brief overview of the major channel scheduling policies is presented. Strategies to prevent burst contentions are discussed in Section 2.5. Finally, in Section 2.6 we provide a brief survey of the major contributions found in research literature, mainly in relation to analytic modelling, performance evaluation and resource optimisation of OBS networks. We further identify the topics that we believe have received less attention in the research community and that the methods proposed in this thesis are attempting to address.

2.1 Optical Burst Switching: General Overview and Architecture

In Optical Burst Switching, IP packets are assembled together into larger data packets called *bursts*. Each burst has associated with it a control packet called a *Burst Header Packet* (BHP). The BHP carries the control information necessary to deliver its associated burst to the destination node. Before the burst transmission, the BHP is sent in a dedicated out-of-band control wavelength channel in order to configure the switches along the burst's path

prior to its arrival at each switch. The configuration of the switches mainly consists of the reservation of a wavelength channel at the switches' output ports, thus establishing an all-optical transparent path for the incoming burst. The information contained in the BHP is processed electronically at the intermediate network nodes and it is separated in time from its burst by an interval of time known as the *offset interval* or *offset time* [52, 93]. The transmission of a burst and the BHP over a WDM link is depicted in Figure 2.1. At the offset interval expiration, the burst is sent on the optical transparent path determined by the BHP without waiting for an acknowledgment of successful path setup. There may be contention issues at the output ports of intermediate nodes between incoming bursts directed to the same wavelength channel, thus potentially causing burst loss.

The typical architecture of an OBS network is depicted in Figure 2.2. As shown in the figure, OBS is implemented as a technology for all-optical core networks, though there are numerous proposals in the research literature about its potential application in metro and access networks [49, 56, 109]. The nodes of an OBS network are categorised into *core nodes* and *edge nodes*. Edge nodes can be further classified into *ingress* nodes and *egress* nodes. The ingress nodes are responsible for the assembly of bursts coming from the access network, for signaling, for routing and for wavelength assignment. Additionally, they are also responsible for the generation of the BHP and its related offset time. The core nodes implement the switching functionality of the OBS network by scheduling a wavelength channel according to the information contained in the BHP. They are further respon-

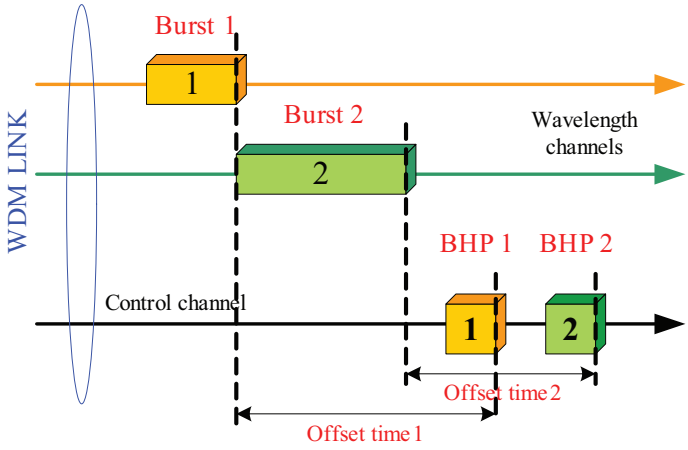

Figure 2.1: Transmission of bursts and associated BHPs over a WDM link.

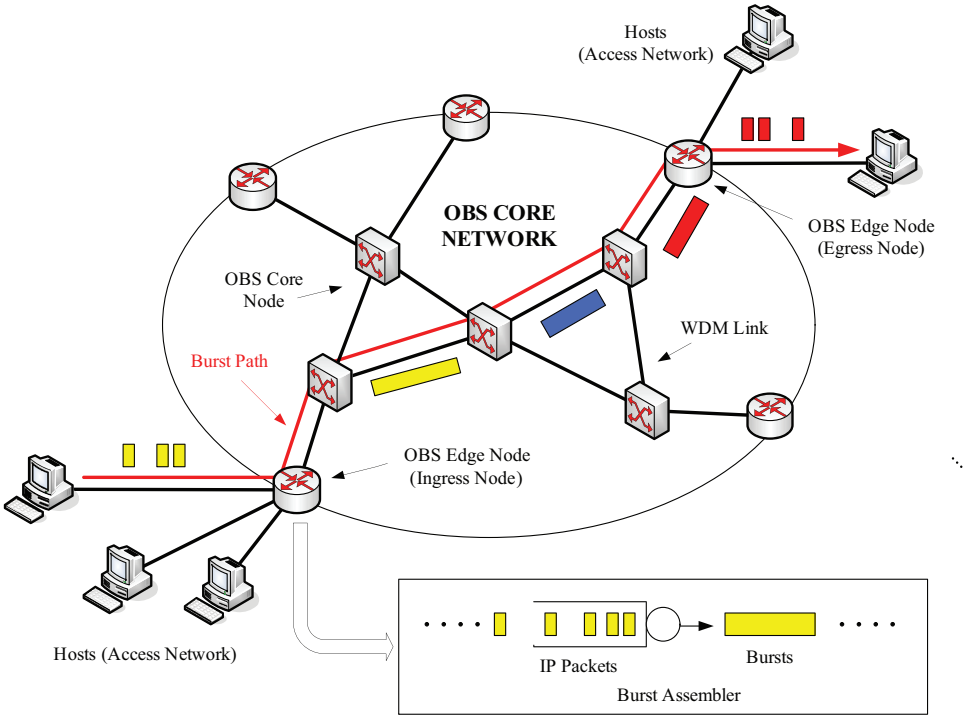

Figure 2.2: OBS core network architecture

sible for resolving contentions between bursts. The egress nodes disassemble the incoming bursts and forward them to the access network. From an architectural point of view, an OBS core node consists of a *Switch Control Unit* (SCU), an *Optical Cross Connect* (OXC) and input/output ports connected to network WDM links comprising multiple wavelength channels. The SCU receives the BHP, extracts the contained control information and processes it, allocating a wavelength channel of an output port for the incoming burst. On the other hand, the ingress node consists of the *burst assembler* (or burst aggregator) and a channel scheduler. The burst assembler, as the name suggests, is the unit of the ingress node that is responsible for aggregating data packets for the formation of a burst. It is typically organised into packet queues associated with different destination (egress) nodes and, potentially, with different classes of service [52]. Once a burst is formed its BHP is generated along with a properly determined offset time and an outgoing wavelength channel is scheduled for transmission. Figure 2.3 illustrates the general architecture of an OBS core node. Basic architectures and design issues of OBS core and edge nodes have been extensively studied in research. Notable examples can be found in [1, 17, 20, 32, 40, 69].

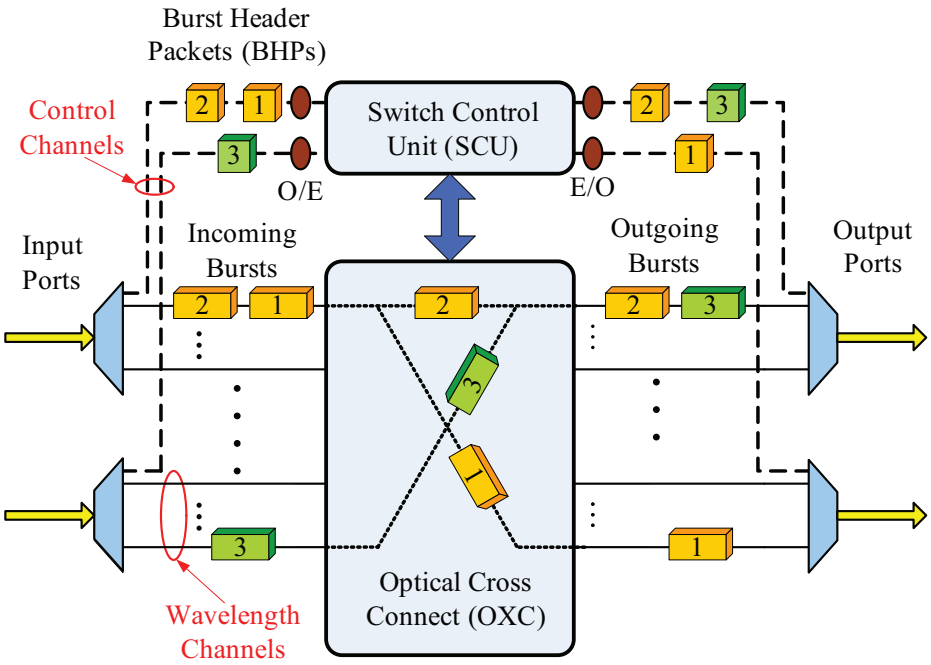

Figure 2.3: OBS core node architecture

2.2 Burst Assembly Strategies

Burst assembly (or burst aggregation) is the procedure of assembling data packets into bursts to be transmitted from an ingress node of the OBS network. There are two main mechanisms of assembling data into bursts: *size-based* and *timer-based*. Their main functionality is depicted in Figure 2.4.

In the size-based strategy, the incoming packets are collected until a burst of a defined fixed size is formed; in this way, the generation of bursts is aperiodic in time and all the bursts have the same length. In the timer-based strategy, the burst is assembled within a constant interval of time, resulting in a periodic transmission of bursts of different lengths. Both strategies may have considerable issues under low and heavy loads. In fact, the value of the threshold has a major impact on both the assembly processes. Particularly, under low loads, if the size threshold is too high the average burst latency becomes too large. Conversely, under heavy loads the time-based strategy yields large burst sizes, thus the average waiting time becomes greater than in the case of the size-based assembly. The advantages and the disadvantages of using one scheme as opposed to the other depend on the requirements of the OBS network. For example, if there are service requirements

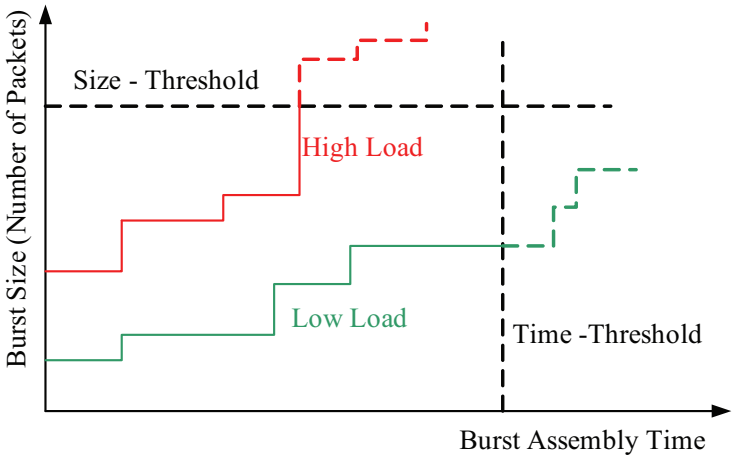

Figure 2.4: Burst assembly strategies: in the size-based strategy (red line), the threshold is defined by a maximum number of packets whereas in the time-based strategy (green line) packets are assembled until a defined timer expires.

in terms of ensuring a maximum transmission delay, then a timer-based scheme will be preferred to a size-based one. Generally, the size-based scheme is preferred under heavy loads, whereas the timer-based scheme is more effective at low loads. In most applications, the best solution is often to choose a *hybrid* strategy using a combination of size-based and timer-based schemes, where the burst assembly strategy can be dynamically chosen on the basis of the traffic intensity conditions. Notable works on this topic have been presented in [21] and [22]. It has been generally demonstrated that hybrid schemes can perform better than the fixed ones, at the price of a higher complexity [23, 87, 108, 119, 123, 138].

The burst assembly process has a considerable impact on the shaping of OBS traffic and may significantly influence the performance of an OBS network. There are several studies on the effects introduced by the aggregation procedure and numerous analytic models have been proposed in research literature on this subject. A frequently made assumption is that burst inter-arrival times are exponentially distributed, that is burst traffic can be modelled as a *Poisson* process [42, 57]. In research literature it is common to find analytic models of OBS networks with these assumptions [34, 66, 103, 134]; however, it has been demonstrated that IP traffic generally tends to manifest *self-similarity*, that is it is bursty at all time scales [4, 24]. This means that modelling network traffic as a Poisson process may lead to inaccuracies and it is more likely that IP core networks dimensioned on the

basis of the Poisson assumption may exhibit unexpected performance behaviour. Simulation studies conclude that the burst assembly procedure can reduce the level of traffic self-similarity [41, 135]; however, the nature of the traffic at the output of a burst aggregator depends on multiple factors such as the type of input traffic coming from the access networks, its intensity and the adopted burst aggregation scheme. Assumptions on the nature of the traffic offered to the burst assembler lead to different OBS traffic models. Recently, Mountrouidou and Perros have studied burst aggregation algorithms at ingress nodes and proposed that the Poisson assumption may not be accurate enough to accommodate OBS traffic characteristics [79]. In fact, it has been shown that the burst inter-arrival times distribution strongly depends on the burst aggregation method and the packet arrival process at the aggregator. For example, in [135], it has been shown that for Poisson input traffic, OBS traffic converges to a Gaussian distribution for both time-based and size-based strategies. Similar results can be found in [136]. Thus, in general it is not possible to draw conclusions on the burst traffic characteristics at the output of a burst aggregator. As for burst length distribution, Gauger [40] has found from simulation that performance is relatively insensitive to burst length distribution. Rostami and Wolisz [106], through analysis, also show that burst length distribution has little impact on performance, concluding that assuming exponentially distributed burst lengths is appropriate in analysis. As we will see in Chapters 3 and 4, to form tractable network models we will assume a simple generic approximation of offered burst traffic by using two-moment matching techniques [42], yielding accuracy better than one-moment Poisson based methods.

2.3 Signaling Schemes

The resource reservation performed by the BHP could be defined through different signaling schemes. The most popular strategies proposed by the research community fall into the categories of the *Tell And Wait* (TAW) and the *Tell And Go* (TAG) protocols [52]. In the former, after the BHP reaches its destination and all the resources necessary for burst transmission are reserved, an acknowledgment (ACK) message is sent back to the source over the same path and, after its reception, the burst is transmitted. An additional ACK message

follows the burst in order to perform explicit release of the allocated resources. The adoption of TAW leads to very low values of burst loss compared to other signaling schemes but has high transmission delay since it has to wait for the acknowledgment control packet to reach the source [52]. In the TAG protocol, there is no acknowledgment. Following the BHP transmission and at the expiration of the offset time the burst is sent and does not wait for any acknowledgment on the channel resource reservation over its path. In this way, burst loss is higher but average delay and complexity are lower than in the TAW protocol. TAG is further divided in *Just In Time* and in *Just Enough Time* variants [133]. In JIT, wavelength channels are immediately reserved after the BHP is processed and are subsequently and explicitly released by a dedicated ACK message. In JET, as depicted in Figure 2.5, wavelength channels are reserved only for the burst duration. The expected burst arrival time and its expected length are extracted from the BHP at intermediate nodes and determine the instants of reservation and release of the wavelength channels. The primary benefit of using JIT and JET strategies is in reducing end-to-end transmission delays, offering efficient bandwidth utilisation and lowering signaling complexity compared to TAW schemes, however these advantages come at the cost of a higher burst loss. Relevant contributions on performance analysis of JIT and JET strategies are proposed in [5, 6, 31, 121].

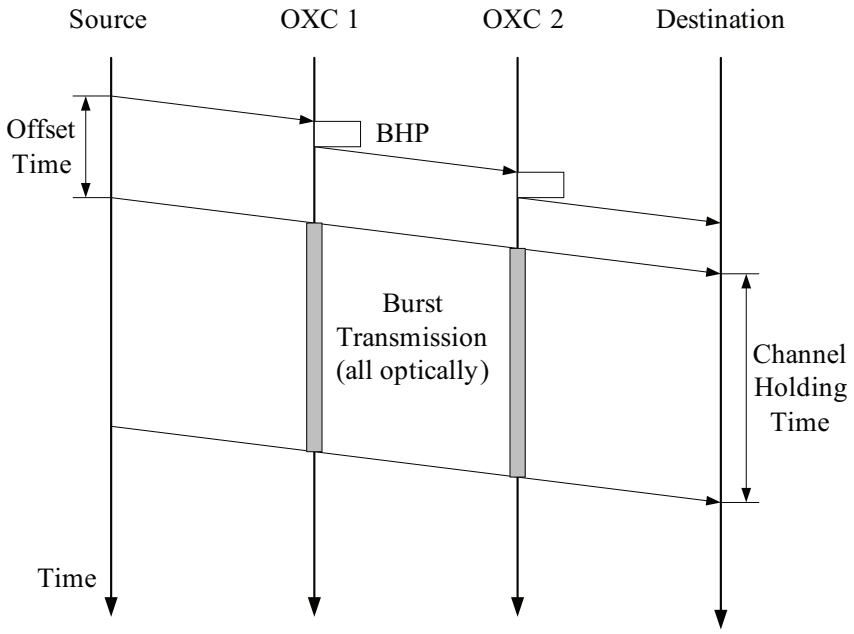

Figure 2.5: Just Enough Time signaling scheme.

2.4 Channel Scheduling Algorithms

In this section we provide a brief overview of the most popular channel scheduling algorithms proposed for OBS networks. The input information required for the scheduling process is stored in the BHP of an unscheduled burst and it is processed by the SCU at core nodes to properly configure the switches for the incoming burst. The key parameters for OBS channel scheduling are:

- $s_s^{i,j}$ and $e_s^{i,j}$: the scheduled burst arrival and departure times for burst *j* on channel *i* respectively.
- s_u and e_u : the unscheduled burst arrival and departure times respectively.
- l_u : the unscheduled burst length ($l_u = e_u - s_u$).
- $LAUT_i$: the *Latest Available Unscheduled Time* (LAUT) or the *Horizon Time* of channel i. The LAUT is the earliest time at which a data channel is available to schedule an unscheduled burst.

Figure 2.6 shows all the above mentioned parameters in a burst scheduling scenario example. Channel scheduling strategies can be divided into algorithms *without void filling* and *with void filling*. The void is traditionally defined as the interval of time between the scheduled burst departure time and the next scheduled burst arrival time, namely $s_s^{i+1,j} - e_s^{i,j}$. The main channel scheduling algorithm without void filling is the *Latest Available Unscheduled Channel* (LAUC) also known as the *Horizon algorithm*; on the other hand, the most popular algorithm with void filling is the *Latest Available Unscheduled Channel with Void Filling* (LAUC-VF) [128]. As shown in Figure 2.6 the LAUC checks all the LAUTs on each channel of the node. It then chooses the channel which has the lowest time distance from the burst unscheduled arrival time to the selected LAUT. To do so, this algorithm needs to know all the LAUTs for each channel as well as the unscheduled burst arrival and departure time instants. Differently from LAUC, LAUC-VF is able to check the channel with the lowest available gap between two already scheduled bursts and, if possible, it fills this void with the unscheduled burst. To do so, it requires to know the arrival and departure times of all

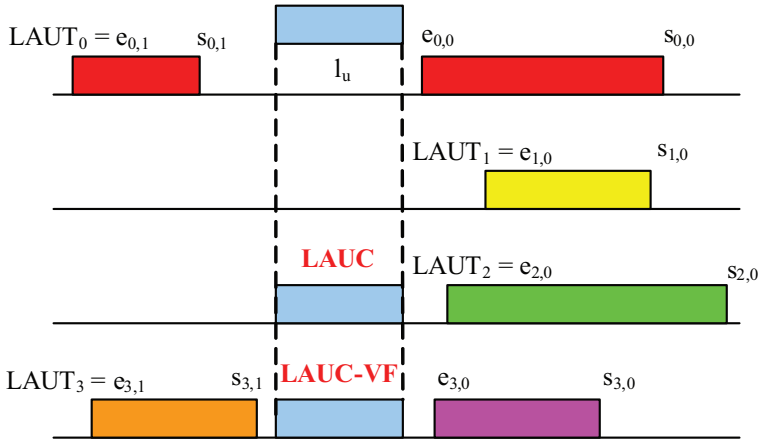

Figure 2.6: Channel Scheduling: LAUC vs LAUC-VF.

the bursts in each channel as well as the departure and arrival times of the unscheduled burst. The LAUC-VF algorithm is more complex to realise than LAUC but it gives significantly better performance in terms of lower burst loss probability and better utilisation of the available bandwidth [8, 128, 129].

2.5 Contention Resolution Techniques

In an OBS network, contention occurs when multiple incoming bursts are simultaneously directed to the same outgoing wavelength channel of a common switch output port. When this happens a burst could be dropped or a contention resolution strategy could be adopted in order to prevent burst loss. In OBS networks, burst contentions can be resolved with the employment of *Fibre Delay Lines* (FDLs), *Tunable Wavelength Converters* (TWCs) and *Deflection Routing* (DR) strategies. The storage of optical data in buffers for WDM networks is not possible due to lack of an optical equivalent of traditional buffers in the electronic domain. In the past decade, FDLs have been introduced as an alternative buffering solution for WDM networks [50, 134]. An FDL, as the name suggests, is a fibre segment which acts as a buffer in the time domain by delaying an optical burst contending for an outgoing wavelength channel. Particularly, in case of contention between two or more bursts, an attempt is made to schedule a free wavelength channel of the FDL and a free wavelength channel of the output port where the contention occurred. If this is possible, the burst will be delayed

by the FDL and sent to the free wavelength channel of the output port. This delay depends on the size of the FDL which, in turn, strictly depends on the physical constraints of the switch (e.g., it requires over 200 Km of fibre in order to delay a burst of 1ms) [52]. An example of a burst contention resolved with an FDL is illustrated in Figure 2.7. A key issue in design of FDLs is the choice of the fixed delay time. If FDL time delays are significantly shorter than burst transmission times then the likelihood of successfully removing overlap between contending bursts is low; however, if FDLs are very long, signal degradation issues may arise and average delay in the switch increases [38].

FDL buffers can be constructed in *single-stage* and *multi-stage* structures [38, 50, 82]. In single-stage structures the delay is determined by a single block of fixed-length FDLs while, in multi-stage structures, the delay is determined by a cascade of FDLs in parallel. FDLs can be further categorised in *feed-forward* and *feedback* architectures. In the first case, the data is delayed from the output port of a switching element to the input port of another switching element at the next stage. In the feedback architecture the data is delayed from the output port of a switching element to the input port of the same stage. It is common to find these architectures in a *share-per-port* configuration (where the FDLs are shared amongst the wavelength channels of a switch output port) or in a *share-per-node* configuration (where the pool of FDLs is shared amongst the output ports of the switch). An example of these structures is illustrated in Figure 2.8.

The performance evaluation of different FDL architectures has been widely analysed

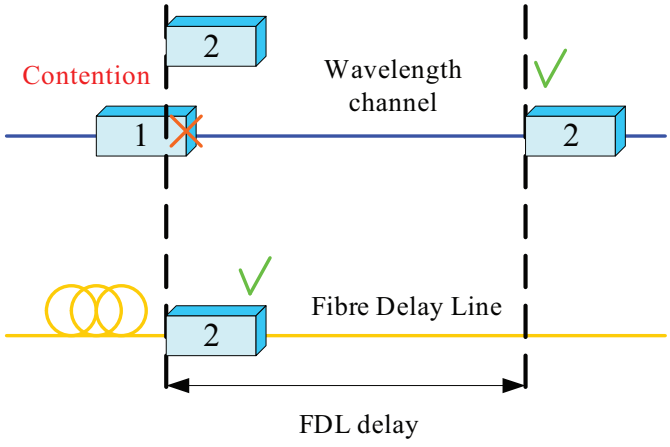

Figure 2.7: Burst contention resolved with an FDL.

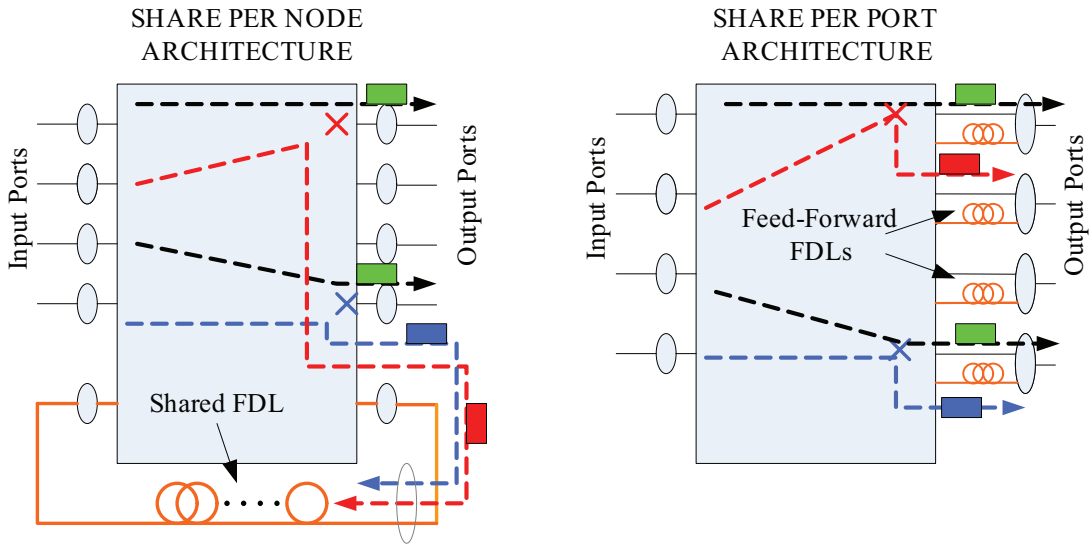

Figure 2.8: OBS node (a) with a share-per-node FDL in a feedback configuration and (b) with share-per-link FDLs in a feed-forward configuration.

in literature [38–40, 50, 72]. As we will see in the next chapter, it has been demonstrated that share-per-node feedback architectures generally offer a more cost-efficient solution compared to share-per-port feed-forward architectures.

Another important scheme of contention resolution is provided by the use of Tunable Wavelength Converters (TWCs) [82]. A TWC is a device that can convert burst data from an input wavelength to one of the available output wavelengths of the system. The number of all the available convertible wavelengths is called *range of conversion*. Similarly to FDLs, wavelength converters can significantly improve the efficiency of OBS networks by switching a contending burst from its current wavelength to an alternative free wavelength within the range of conversion as depicted in Figure 2.9. For this reason, wavelength converter pools are employed in OBS nodes and, frequently, in tandem with FDLs [101, 102, 120]. There are several configuration schemes for the placement of wavelength converters. Inside an OBS switch, one could have a wavelength converter per channel (*dedicated wavelength convertible switch*) or a shared pool of converters (*partial wavelength convertible switch*) [52]. The first scheme is expensive but provides wavelength conversion capability to all wavelength channels whereas the second strategy is less expensive but achieves lower performance in terms of burst blocking. The pool of converters can be further shared *per link* or *per node* [52, 82]. TWCs can be also categorised on the basis of their conversion

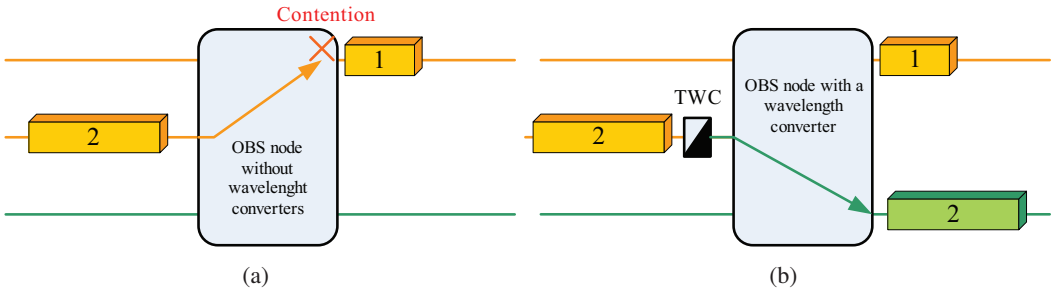

Figure 2.9: Burst contention resolved with using of a Tunable Wavelength Converter.

range. If the converter allows switching of data among all wavelengths it is said to have *full wavelength conversion* capability; on the other hand, when a selected range of wavelengths is available for conversion, then the converter is said to have *limited range conversion* capability [52]. Finally, in relation to the allocation of TWCs over the network, we can define the following configurations:

- *Full-complete*: all nodes have full wavelength conversion capability.
- *Partial*: all nodes have limited range conversion capability.
- *Sparse*: selected nodes have full complete conversion capability.
- *Sparse-partial*: selected nodes have limited range conversion capability.

The first allocation offers the best performance but it is the most expensive. Though numerous analytic and simulation studies of OBS architectures have considered full-complete conversion capability [66, 105, 134] and realisable designs of this configuration have been proposed [71], it is more likely that this assumption may not find realistic applications in the foreseeable future. TWCs are expensive devices [68] and studies on sparse and sparse-partial configurations demonstrated that it is still possible to achieve levels of performance comparable to a full-complete scheme but at lower cost [126, 127]. Qin and Yang [92], evaluated a very detailed analytic model of an OBS node under limited-range wavelength conversion capability. Based on link-independence and wavelength-independence assumptions, they calculate the expressions of the blocking probabilities for limited conversion degrees. An analytic approximate model of OBS nodes with shared wavelength converters has been presented in [98] while in [105] a framework has been developed for calculating

path blocking probabilities in an OBS network for nodes with limited wavelength conversion.

The last contention resolution strategy is Deflection Routing (DR). In DR, the contention problem is solved by sending the burst on an alternative path from another output port rather than the one originally planned. This technique is generally not favoured for electronic switching networks [82] and its implementation for OBS networks still requires further investigation. In [125], a performance analysis of an OBS network has been conducted where contention is resolved by employing TWCs in combination with DR. In [48, 139] it has been shown that DR may cause network instability mainly in relation to unexpected drops in the network throughput under specific load conditions. In the present work we do not consider the employment of DR for resolving burst contention.

It is worth mentioning that the employment of contention resolution techniques such as FDLs or deflection routing may have a major impact on the performance of the network when considering *TCP over OBS*. More generally, the TCP congestion control scheme is severely affected by both the burst assembly process and out-of-order TCP packet delivery [110, 111, 137]. In the first case, a burst loss may cause multiple TCP packets to be dropped, consequently provoking a drastic reduction of the TCP congestion avoidance window at the source node (thus, lowering the overall network throughput). In the second case, FDLs or deflection routing may introduce delays on the TCP flow transmission, causing out-of-order packet delivery. The TCP protocol detects this occurrence as a packet loss and sends duplicate ACK messages to inform the sender of the failed packet reception (provoking a False Fast Retransmit). This introduces synchronisation problems at the receiver causing a wastage of bandwidth (Figure 2.10). For these reasons it is essential to investigate and predict the behaviour of TCP over OBS. Several schemes have been proposed in order to address these issues. One way is to delay the transmission of the burst at the sender in order to realise a synchronised transmission of the TCP flow (OBS source-ordering) [59]; performance evaluation of TCP implementations over OBS have been proposed in [110] and [137]. This topic is out of the scope of the work presented in this thesis, hence it has not been taken into consideration for the development of the proposed OBS network model. The interested reader may find a survey on the performance improvements of different TCP

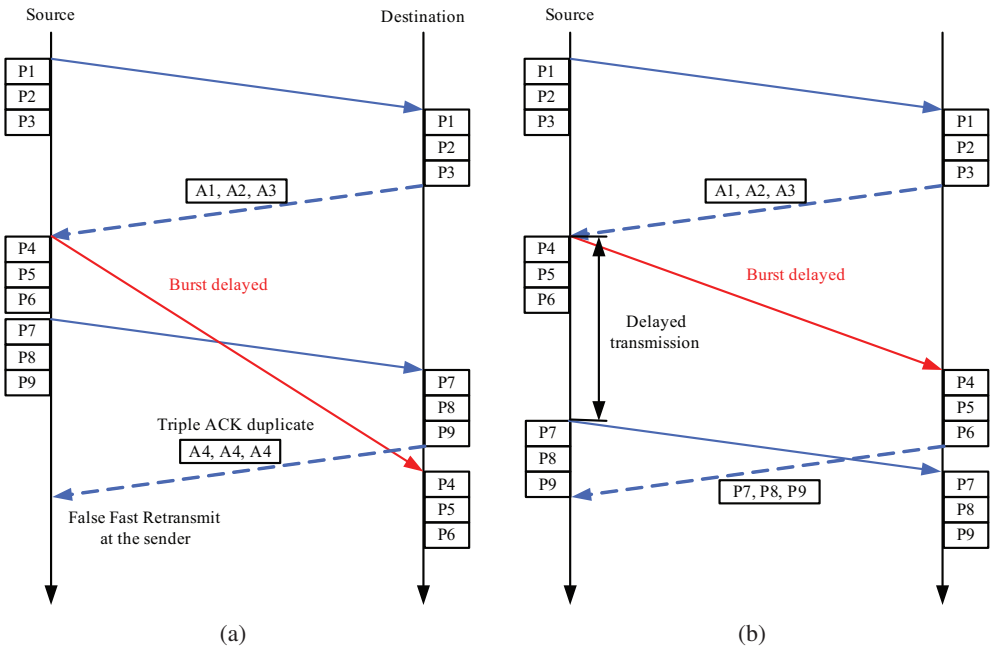

Figure 2.10: TCP over OBS. The introduction of FDLs or deflection routing provokes out-of-order delivery of TCP packets at the receiver, causing False Fast Retransmit at the sender (a); the out-of-order delivery can be solved with source-ordering at the OBS layer by delaying the transmission of the burst.

over OBS variants in [111].

2.6 State-of-the-Art in OBS Analytic Modelling and Motivation of the Present Work

Research literature is rich with works devoted to analytic modelling and performance evaluation of the OBS paradigm applied to WDM networks. Particularly, during the past decade, significant contributions have been made in the analysis of FDL-bufferd OBS nodes and networks where burst contentions are resolved with the joint employment of FDLs and TWCs. As we said Section 2.2, an assumption frequently made in the majority of the works in the literature is that the burst traffic from a burst assembler can be described by a Poisson process. This means that the burst inter-arrival times at intermediate nodes of the network are negative-exponentially distributed. This assumption can be found in several works focusing on isolated FDL architectures and FDL-buffered OBS nodes and networks, frequently in combination with TWCs. In [18] Callegati models an FDL as an $M/M/1$ queue with

balking with asynchronous packets of variable length (where M denotes the exponential distribution). This model was one of the first to capture the *balking* property of the FDL, that is, if the delay introduced by the FDL is not sufficient to avoid burst contention the contending burst has to be dropped. Analyses of the impacts introduced by different inter-arrival distributions on modelling a single FDL have been conducted in [2]. The authors consider the cases of deterministic, uniform, exponential and Weibull distributions. Performance evaluations of a single wavelength FDL with general burst length distribution have been made in [64] and [65]. In [99], Rogiest et al. provide an exact Markov chain analysis while an investigation for correlated arrivals has been conducted in [100]. In [134], Yoo et al. proposed a model of an OBS node with feed-forward FDLs for different traffic classes, specifically they model the node with FDLs as an $M/M/k/k$ system (for classless traffic) and as an $M/M/k/D$ queue (for prioritised traffic). This analysis has been generalised in [34], where the FDL buffer is modelled as an $M/M/k/D$ queue, providing union bounds for burst loss probability and for both classes of traffic. In [66], Lu and Mark characterise an OBS node with share-per-port FDLs as a multidimensional continuous-time Markov chain. They developed an asymptotic approximation model of FDLs considering separately the cases of short FDLs and long FDLs. An OBS node architecture with shared-per-port FDLs has been analysed in [95] where, once again, the burst inter-arrival distribution is assumed to be exponential. An approximate analytic model of an OBS/OPS node architecture with feed-forward and feedback shared FDL buffers and general burst lengths has been presented in [140, 141]. Recently, Hayat et al. [45] have proposed a model of an OBS node with a shared pool of converters and a dedicated FDL buffer per link, focusing their analysis on the trade-off between the utilisation of FDLs and TWCs. OBS node architectures with limited number of wavelength converters have been analysed in [76, 98, 102]. In [98] burst traffic flows are characterised with their first two moments by employing the *Equivalent Random Theory* (ERT) [42, 124], a moment-matching technique that allows approximation of non-Poissonian traffic flows. In [3], Akar et al. model an OBS node with share-per-link wavelength converters deriving a Markovian analysis where the burst arrival process is described with an Engset model. A 3-state Markovian process is used in [130] to model short and long burst arrivals for a OBS edge node architecture. The authors further assume

the burst lengths to be Coxian distributed. Limited-range conversion capabilities have been studied in [75, 91, 105, 116].

A major achievement on bufferless OBS network modelling has been presented in [103, 104, 122] where the performance of the OBS network is evaluated in terms of link blocking probabilities. The analysis is based on a modified version of the well-known Erlang Fixed Point Approximation (EFPA) [54], leading to a link-centric evaluation of the OBS network. Simultaneous possession of multiple links by a single burst is also accounted for in the analysis in [9, 11]. Castro et al. proposed in [19] a method to optimise the number of FDLs in an OBS network where each node is modelled according to the analysis derived in [66]. The performance analysis of an OBS tandem network where burst traffic arrivals are modelled with the *Interrupted Poisson Process* (IPP) has been presented in [10]. The IPP process has been successfully used in network analysis for modelling bursty traffic [42]. Mountrouidou et al. [80] derive a model of a hub-based OBS network architecture where burst arrivals are characterised by a bulk slotted process. In [107] a two-moment analysis of a bufferless OBS network is presented where contentions are resolved with deflection routing. The authors provide a more accurate path-oriented analytic approach to resolve the OBS network, that is the blocking probability of each end-to-end path is separately calculated. Additionally, accuracy is improved by modelling burst arrival traffic with the *Bernoulli-Poisson-Pascal* (BPP) method proposed in [27, 28] as opposed to one-moment Poisson based analyses.

All of the above mentioned works significantly contribute to the derivation of analytic models that allow design and optimal dimensioning of OBS networks; however, we note a less concentration on in the following research topics that, in our opinion, still require to be fully investigated and understood:

- An assumption frequently made in the majority of the works found in research literature is that burst traffic can be modelled with a Poisson process, that is burst inter-arrival times are exponentially distributed. An equivalent assumption is often made for the burst length distribution as well. As it has been shown in notable works [4,24], IP traffic tends to manifest self-similarity, particularly it is bursty at all time scales.

Thus, the Poisson assumption, although generally leading to easier modelling and dimensioning, might not be suitable to accurately accommodate the bursty nature of IP traffic. More importantly, as we said in Section 2.2, it is not possible to draw general conclusions as to the nature of the burst traffic emanating from a burst aggregator. Thus, a Poisson-based analytic model of an OBS architecture may not consider unexpected behaviours arising from the non-Poissonian nature of the burst traffic, ultimately leading to undesirable inaccuracies for the design and the dimensioning of OBS networks.

- Research effort in FDL-based OBS node modelling is minimal compared to simulation studies on the same subject. Furthermore, although efficiently capturing the impact on performance of several features related to OBS (balking effect, offset time effect, etc.), most of the proposed analytic models devoted their attention to modelling OBS nodes with feed-forward/shared-per-link FDLs, frequently assuming exponentially distributed inter-arrival times. We believe that more effort should be put on modelling of practical FDL-buffered OBS architectures, particularly on analytic models of OBS with share-per-node FDLs where non-Poissonian traffic assumptions should be considered.

- Similarly to OBS node modelling, less emphasis has been put on OBS network modelling where contentions are resolved with FDLs. Furthermore, a link-centric approach based on EFPA is adopted in the vast majority of the works proposed in research literature, where burst traffic is characterised with standard one-moment Poisson analysis. A performance evaluation based on EFPA often overestimates link blocking probabilities [107]. We believe that a path (stream)-centric approach is desirable in order to gain a better accuracy for the estimation of burst blocking probabilities compared to a link-centric approach.

- Research literature is rich with proposals on optimal OBS resource dimensioning, predominantly on Routing and Wavelength Assignment (RWA) [29, 113] and on optimal allocation of TWCs in OBS/OPS networks [37, 126]. As we will see in Chapter 5, little research effort has focused on optimal dimensioning and allocation of FDLs,

with some few exceptions [19]. It is largely accepted that FDLs will play a predominant role for resolving contentions in deployable OBS networks [38,82,134]. The author believes that pertinent investigations of FDL dimensioning should be conducted in order to derive more efficient methods for optimising OBS networks in order to assess their cost/benefit in comparison to other candidate optical architectures and to enable their future deployment.

This thesis attempts to address all the above mentioned issues with the realisation of the following:

- **Optical Burst Switch Node Modelling** : A novel approximate analytic OBS node model with a share-per-node FDL is developed. The node model can handle general burst inter-arrival times. In order to do so we rely on *moment-matching* techniques, that is a set of analytic tools used to approximate non-Poisson arrival processes by way of the first two moments of the channel occupancy distribution of the system. We first model the switch output port by approximating its channel occupancy distribution with a Bernoulli-Poisson-Pascal (BPP) distribution and by using the Equivalent Random Theory (ERT). We characterise the traffic flows with the mean and the variance of the output port channel occupancy distribution. Finally, we model a cost-effective buffered OBS node architecture by allowing the switch to be equipped with multiple input/output ports, each one connected to an optical fibre carrying multiple wavelength channels. The switch is further equipped with one FDL shared among the output ports in a feed-back configuration and employs full wavelength conversion.

- **Optical Burst Switch Network Modelling** : A novel FDL-buffered OBS network model is proposed, where nodes are modelled according to the analytic model above mentioned. The aim is to provide a mathematical framework that allows performance evaluation of OBS network by describing burst traffic flows in terms of moment-matching, resulting in a better accuracy compared to standard one-moment Poisson-based analysis. The network model further allows evaluation of the burst blocking probabilities at stream (path) level, resulting in an increased accuracy compared to a link-centric approach. Finally, the analysis is refined by neglecting network links

whose blocking probability is zero due to the streamline effect.

- **Resource Dimensioning and Optimisation of OBS Network**: A method for dimensioning link wavelength channels and for determining an optimal allocation of FDL buffers for OBS networks is presented. We focus on minimising the total hardware cost of the network under requirements defined in terms of a guaranteed level of end-to-end burst blocking probability and physical constraints determined by maximum and minimum allowable number of link/FDL wavelength channels. We further define and study multi-objective optimisation problems where we wish to simultaneously minimise the total network hardware cost and the maximum tolerable end-to-end burst loss. The optimisation problems are resolved by means of genetic algorithms.

Table 2.1 illustrates the differences between the modelling contributions available in the research literature for OBS networks and the features of the model proposed in this work. In the next chapter we start our analysis with the description of the approximate model of the buffered OBS node.

Table 2.1: Overview of research contributions on modelling of OBS networks. FF/FB: feed-forward/feedback, FWC/PWC/LWC: full/partial/limited wavelength conversion, LC/PC: link/path centric, SH: shared.

OBS node model	Burst arrivals model	FDL config.	TWC config.	Network modelling approach
Akar et al. [3]	Engset model	-	SH-LWC	-
Battestilli et al. [9]	Poisson	-	FWC	PC
Battestilli et al. [10]	IPP	-	FWC	LC
Castro et al. [19]	Poisson	FF/FB	FWC	LC
Hayat et a. [45]	Poisson	SH-FF	SH-FWC	-
Lu et al. [66]	Poisson	FF/FB	FWC	-
Mountrouidou et al. [80]	Bulk Slotted	-	FWC	-
Rajabi et al. [95]	Poisson	SH-FF	FWC	LC
Reviriego et al. [98]	ERT model	-	SH-FWC	-
Rosberg et al. [105]	Poisson	-	FWC	LC
Sahasrabudhe et al. [107]	BPP model	-	FWC	PC
Wong et al. [125]	Poisson	-	FWC	LC
Xu et al. [130]	3-State Markovian	-	FWC	-
Zhang et al. [141]	Poisson	SH-FF/FB	FWC	-
Proposed method	BPP/ERT model	SH-FB	FWC	PC

Chapter 3

Modelling of the Optical Burst Switched Node

In this chapter we derive an approximate analytic model of an optical burst switch where contentions are resolved with the employment of a Fibre Delay Line (FDL). The chapter is organised as follows. In Section 3.1 we select and describe a potentially cost-effective buffered OBS node architecture with a share-per-node FDL employed in a feedback configuration. The description of the node model is presented in Section 3.2. We first focus our attention on modelling a single output port of the selected switch architecture. We conduct an approximate two-moment matching flow analysis by assuming that each traffic stream may be represented with a non-Poisson process. Burst loss performance at the output port is evaluated by deriving expressions for the burst blocking probability perceived by all traffic flows offered to the node. In Section 3.3 we validate the analytic model by comparison with results obtained from a discrete-event simulation of the node realised in Opnet Modeler^{TM} [85]. Finally conclusions are given in Section 3.4.

3.1 The Architecture of the Optical Burst Switch

As mentioned in Chapter 1, a contention between bursts directed to the same wavelength channel on a common output link may be resolved with the employment of Tunable Wavelength Converters (TWCs) or Fibre Delay Lines (FDLs). In the research literature it is

common to find performance analyses of OBS architectures where TWCs and FDLs are used in tandem to resolve burst contentions [38,39,66,95,102,140]. An extensive overview of OBS architecture designs is provided in [38, 40] and [17] where the basic *Tune-And-Select* (TAS) OBS node architecture [15] is studied in relation to the addition of FDLs for resolving burst contention. The analysis presented in this chapter starts with the description of this particular OBS node architecture and its extended versions employing FDLs for contention resolution. The general TAS node architecture is shown in Figure 3.1. The switch is equipped with P input/output ports (connected to input/output fibre links) each comprising W_p wavelength channels, with $p = 1, \ldots, P$. Burst switching is performed with the combined action of TWCs and *Semiconductor Optical Amplifiers* (SOAs) [82]. Each wavelength channel of an input port comprises a number of SOAs that is equivalent to the number of output ports of the switch, for a total of $P \sum_{p=1}^{P} W_p$ SOAs [17, 40]. Furthermore, all wavelength channels on each port are equipped with a TWC for a total of $\sum_{p=1}^{P} W_p$ TWCs, allowing full wavelength conversion. This configuration permits both burst wavelength conversion and switching to a desired wavelength channel. Particularly, after being demultiplexed at the input ports, the burst signal is converted into an outgoing wavelength channel by the TWC then is split and directed to all output ports. The desired output port is finally selected by "turning on" its associated SOA and "turning off" all the SOAs associated with the rest of the output ports. An *Erbium-Doped Fibre Amplifier*

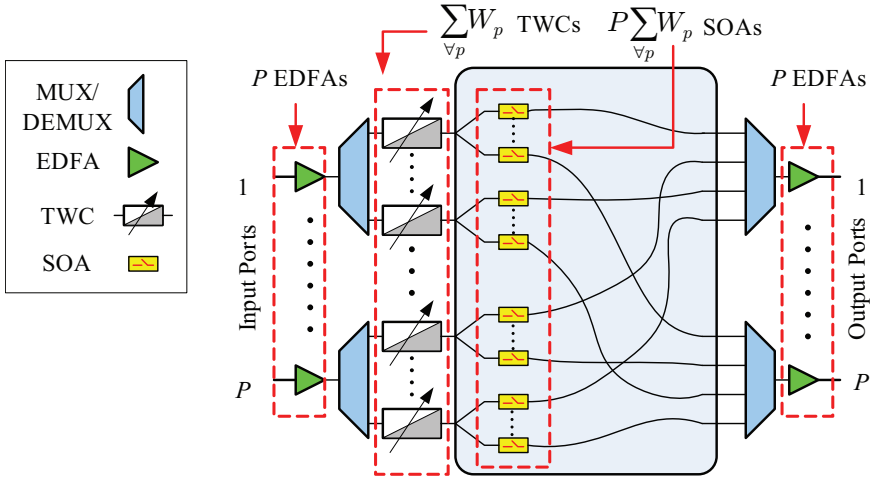

Figure 3.1: Tune and Select (TAS) OBS node architecture.

(EDFA) [82] is required at each input/output port for amplifying the optical signal and compensating the loss due to signal splitting [15, 16]. It has been extensively proven in [15, 17] that, as opposed to other switch architectures such as the basic *Broadcast and Select* (BAS) OBS architecture [36] (where wavelength conversion is performed at the output stage with tunable filters and wavelength converters), the TAS node architecture may potentially yield more cost-effective switch designs thanks to its low signal degradations [15].

Figures 3.2(a) and 3.2(b) illustrate two of the most common buffered OBS TAS node architectures employing FDLs for contention resolution. We generally denote with K the number of wavelength channels comprised in an FDL and, following [66], we refer to them as *FDL virtual buffers*. Figure 3.2(a) depicts a TAS node architecture where a single FDL is dedicated to each output port (*TAS-dFDL*) in a feed-forward configuration. In this case, the optical cross-connect redirects an incoming burst to one of the available channels in an FDL, in order to avoid a contention. With wavelength converters present at input ports, any available FDL channel may be selected. After being delayed in the FDL, the burst is transmitted on the same wavelength at the output port. Note that the reservation of a wavelength channel at the output port and a virtual buffer in the FDL is simultaneous and is prior to the burst entering the FDL buffer (*PreRes strategy*) [38]. If it is not possible to

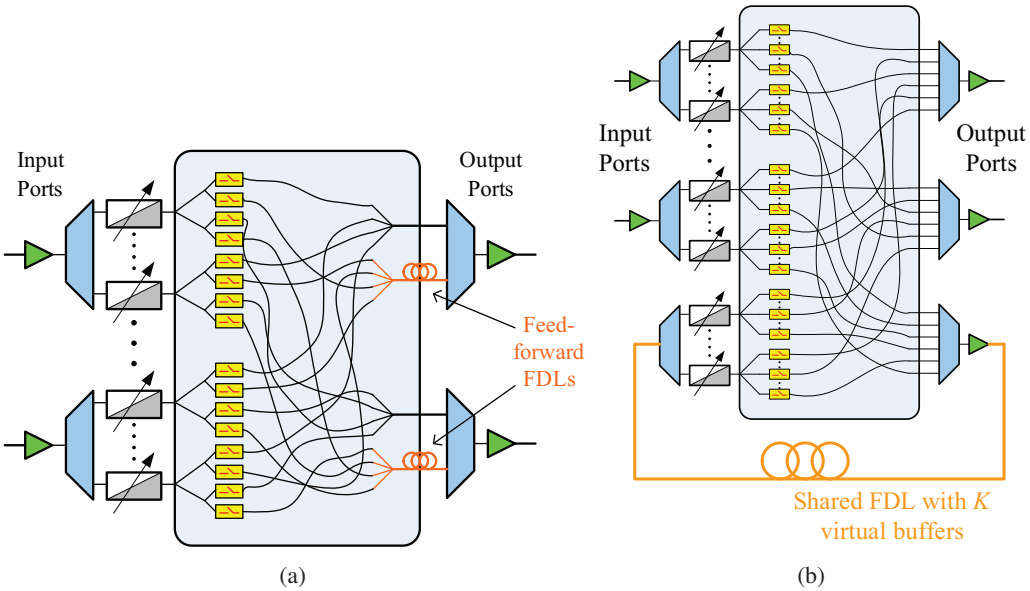

Figure 3.2: OBS TAS-dFDL (a) and TAS-shFDL (b) node architectures.

select a wavelength that is available both in the FDL and the output port, then the burst is dropped. Although a further decrease in burst loss could be gained by introducing additional wavelength converters between the FDL and the output port, this arrangement would result in a considerable increase of hardware costs. Figure 3.2(b) depicts a TAS node architecture where extra input/output ports are dedicated to FDLs shared amongst the output ports in a feedback configuration (TAS-shFDL). The node depicted in Figure 3.2(b) illustrates an example with one shared FDL. In this configuration, a contending burst may be directed to any free channel of the FDL thanks to the action of TWCs at input ports. The number of channels in the FDL may be less than the number of channels at the input port, allowing the FDL ports (and associated switch matrix) to be scaled according to cost/performance trade-offs. This flexibility is afforded by the additional K wavelength converters at each FDL return port, which allow re-conversion of packets to any of P output port channels. It is theoretically possible that a burst may recirculate multiple times through the switch and FDL bank, although signal degradation issues may limit the number of recirculations in practice and there are diminishing performance gains as FDL resource usage per packet increases with each recirculation [40].

Note that both configurations adopt the so called *prefer conversion* strategy, that is an attempt to resolve burst contention is first performed by using the TWCs and, only in case of failure, a final attempt is made with the employment of the FDL [38]. An extensive evaluation of performance and technology for these architectures has been presented in [17, 38, 40]. It is shown that the TAS-shFDL architecture yields a more cost-efficient solution than the one offered with the TAS-dFDL architecture. This is mainly due to the fact that, in a TAS-shFDL configuration, the presence of TWCs at the FDL return port allows another burst conversion in additon to the one already performed by the TWCs equipped at the switch input ports. Additionally, nodes with a TAS-dFDL configuration have been shown to achieve lower wavelength utilisation and lower effective throughput under dynamic traffic conditions compared to TAS-shFDL nodes [40]. Finally, it has been demonstrated that the number of FDLs employed in the TAS-shFDL architecture has a minor impact on burst loss performance compared to a TAS-shFDL switch employing a single FDL with an *equivalent* total number of virtual buffers. The differences in performance between the two cases

become more evident for higher numbers of wavelength channels in the FDL [40] (e.g., for 32 and 64 virtual buffers). Nevertheless, in this case, issues regarding the technical feasibility of these buffered architectures may affect their applicability on realistic OBS network deployments [40]. Simulation results that illustrate the above mentioned characteristics of the TAS-shFDL architecture are presented in Figure 3.3. We consider a hypothetical TAS OBS switch with a single input/output port comprising $W = 10$ wavelength channels with full wavelength conversion capability. Burst traffic is offered to the input port according to a Poisson process and burst lengths are assumed exponentially distributed. We compare the burst blocking probability at the output port with different values of virtual buffers K for the TAS-dFDL and the TAS-shFDL architectures.

The buffer configuration is coded as $X - Y$ where X is the number of FDLs and Y is the number of virtual buffers in each FDL. We first note that the addition of FDLs is highly effective in lowering the burst loss rate as opposed to a bufferless TAS node, obtaining in some cases a performance gain of several orders of magnitude. The TAS-dFDL configuration is generally outperformed by the TAS-shFDL in both scenarios of one FDL with

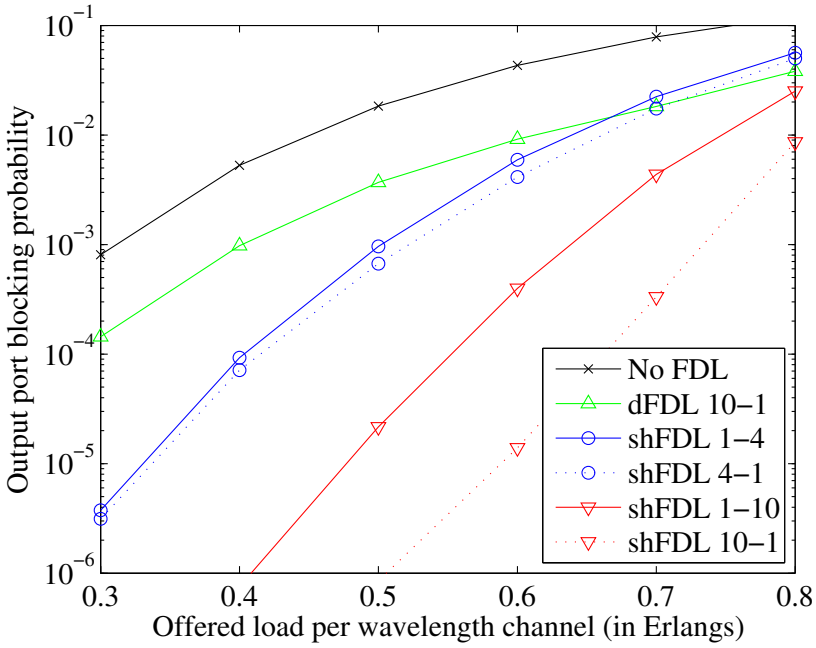

Figure 3.3: Burst loss probability of different buffered architectures from discrete-event simulations.

10 virtual buffers (shFDL 1-10) and 10 FDLs with one virtual buffer each (shFDL 10-1). We further note that there are no major differences in loss performance between the cases of shFDL 1-4 and shFDL 4-1, however the situation is substantially different for the comparison between shFDL 1-10 and shFDL 10-1, where the latter configuration considerably outperforms the former. Nevertheless, the shFDL 10-1 arrangement leads to an unrealistic solution for buffered OBS node design, mainly in relation to switch complexity constraints and increasing hardware cost [17, 40]. In this regard, Tables 3.1-3.3 illustrate a cost comparison for different TAS-shFDL architectures with the same total number of virtual buffers K. We see that adding FDLs while keeping K constant always yields to an increase of the cost in terms of unit components. An extensive set of similar results drawing equivalent conclusions can be found in [40], where the cases of $K = 16, 32$ and 64 virtual buffers are examined. Additionally, it is further shown that the channel utilisation and the effective throughput offered by an shFDL $1 - X$ architecture are equal or greater than the ones offered by an sh-FDL $Y - Z$ configuration, with $X = YZ$. From this we conclude that the OBS TAS-shFDL node architecture with one FDL may achieve performances close to TAS-shFDL architectures with multiple FDLs and equivalent number of virtual buffers but at lower hardware cost. For these reasons, in this thesis we focus our attention on the analysis of the TAS-shFDL architecture with a single FDL in a feedback configuration which,

Table 3.1: Unit cost comparisons between TAS-shFDL architectures for a switch with 4 ports each comprising $W = 8$ wavelength channels.

	shFDL 1-4	shFDL 2-2	shFDL 4-1
TWCs	36	36	36
SOAs	60	60	72
EDFAs	9	10	12
TOT.	105	106	120

Table 3.2: Unit cost comparisons between TAS-shFDL architectures for a switch with 4 ports each comprising $W = 16$ wavelength channels.

	shFDL 1-8	shFDL 2-4	shFDL 4-2	shFDL 8-1
TWCs	72	72	72	72
SOAs	120	120	144	204
EDFAs	9	10	12	16
TOT.	201	202	228	292

Table 3.3: Unit cost comparisons between TAS-shFDL architectures for a switch with 4 ports each comprising $W = 32$ wavelength channels.

	shFDL 1-16	shFDL 2-8	shFDL 4-4	shFDL 8-2	shFDL 16-1
TWCs	144	144	144	144	144
SOAs	240	240	288	408	660
EDFAs	9	10	12	16	18
TOT.	393	394	444	568	828

we believe, may be an attractive candidate architecture for buffered OBS nodes with TWCs and FDLs.

Before starting with the description of the analytic node model we provide some insights on the impact on loss performance introduced by the FDL delay and by the burst length distribution. In Figure 3.4(a) we show an example of the FDL delay impact on burst loss for an output port comprising 10 wavelength channels and 5 FDL channels being offered with Poisson burst traffic. We see that increasing values of FDL delay yield a reduction in burst loss probability until a lower bound is reached. After a delay equal to 3 times the burst transmission time no substantial improvements in burst loss can be observed. For these reasons we assume a value of FDL delay equal to at least twice the burst transmission time for our analysis. Similar conclusions have been drawn in [38,40] where more evidence of this effect is shown for different scenarios. As discussed in the previous chapter, it has also been shown that burst loss ratio are generally insensitive to the burst length distribution. Figure 3.4(b) depicts the burst blocking probability of a 4-ports bufferless TAS-shFDL node architecture when burst lengths are constant or exponentially distributed for $W = 8, 16, 32$ wavelength channels. It can be seen that both cases exhibit approximately the same level of burst loss ratio. Additional simulation results illustrating this aspect for the case of exponential, gamma and Gaussian distributed burst lengths are provided in [40] whereas further evidence from an analytic perspective is provided in [106]. Thus, we conclude that assuming exponentially distributed lengths may be appropriate for the TAS-shFDL node analysis.

The OBS node architecture under study is the same as Figure 3.2(b). The switch is assumed to have P input/output ports each one connected to an optical fibre link comprising

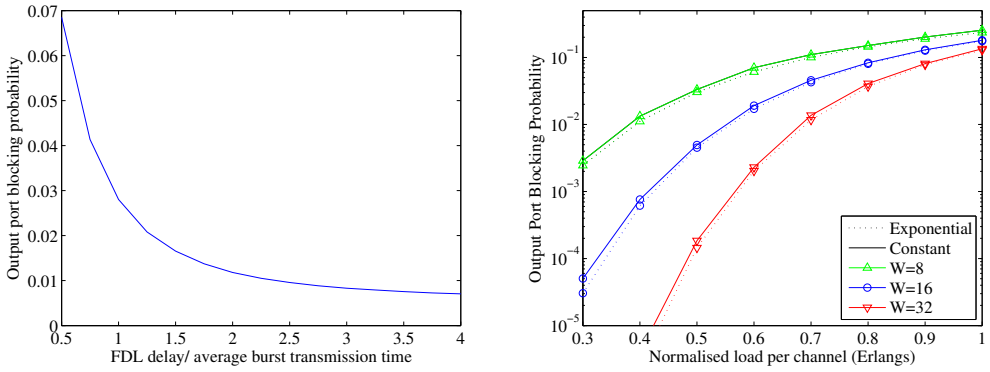

(a) (b)

Figure 3.4: Impact of FDL delay (a) and of the burst length distribution (b) on burst loss probability.

W wavelength channels. An extra input/output port is dedicated to a single FDL comprising K wavelength channels (virtual buffers). The adopted contention resolution scheme uses both TWCs and the FDL in a prefer conversion strategy. Furthermore, the reservation of the wavelength channels in the output ports and in the FDL follows the PreRes strategy as described in [38]. We do not assume burst recirculations in the shared FDL. Finally, we assume the switch employs the JET signaling scheme and schedules all wavelength channels according to the LAUC-VF strategy. As discussed in Sections 2.3 and 2.4, these signalling and channel scheduling methods are amongst the most promising for OBS network deployment due to their good trade-off between achievable performance and complexity. The aim for developing the node model is to quantify the intensity of the burst traffic streams that overflows from the switch and that are considered lost from the system in order to determine their blocking probabilities.

3.2 The Analytic Model of the Switch

In this section an approximate analytic model of the OBS TAS-shFDL switch with a shared FDL in a feedback configuration is presented. The analysis is firstly conducted for a single port in isolation to facilitate the description of the complete multi-port switch model. Note that from an analytic perspective, the proposed output port model is equivalent to the model of a network *link* connected to that port. Subsection 3.2.1 presents a brief theoret-

ical background on the available methods used to derive a flow model of the OBS node architecture under study. The model of a single output port of the switch in isolation is proposed in Subsection 3.2.2 whereas Subsection 3.2.3 deals with the model of a single output port equipped with a feedback FDL. The overall flow model of the OBS TAS-shFDL node architecture is derived in Subsection 3.2.4. Finally, an additional procedure to refine the blocking probability values by increasing their accuracy is presented in Section 3.2.5.

3.2.1 Background

We model the output port of the TAS-shFDL as a group of wavelength channels (or *servers*) being contended by incoming burst packets. Incoming bursts are analytically characterised by the concept of a *traffic flow* (or *stream*). In our model, a traffic flow conceptually corresponds to the aggregation of multiple burst packets emanating from different input ports of the switch and directed to a common output port. The average intensity of a traffic flow *offered* to the port in question is quantified with the *mean* of the busy channel distribution of a system equivalent to the output port but with an infinite number of channels [42].

Figure 3.5 illustrates the model of a hypothetical OBS node with a single output port being offered with burst traffic following a Poisson process, that is, burst inter-arrival times are exponentially distributed with average arrival rate equal to λ bursts/s. We assume burst lengths are also exponentially distributed with average burst service time equal to s bursts/s. As depicted in the figure, the output port can be modelled as an $M/M/W/W$ queuing system where W is the number of wavelength channels in the port (link) [57]. The burst traffic flow F offered to the port is quantified by its mean m, that is the mean of the busy channel distribution of an $M/M/\infty$ queuing system. Thus m represents the average burst load offered to the port by flow F and is given by the ratio λ/s (in *Erlangs*) [57]. We refer to the portion of burst traffic that (on average) will be served by the output port as *burst carried traffic*, characterised by flow $\bar{F}$; conversely, the portion of traffic that cannot be served determines the *burst overflow traffic* represented by $\hat{F}$. The mean and variance of these flows have been calculated by Kosten [42] for a group of channels being offered with a Poisson traffic flow of mean m. Particularly, the mean $\hat{m}$ and the variance $\hat{v}$ of the overflow traffic are given by

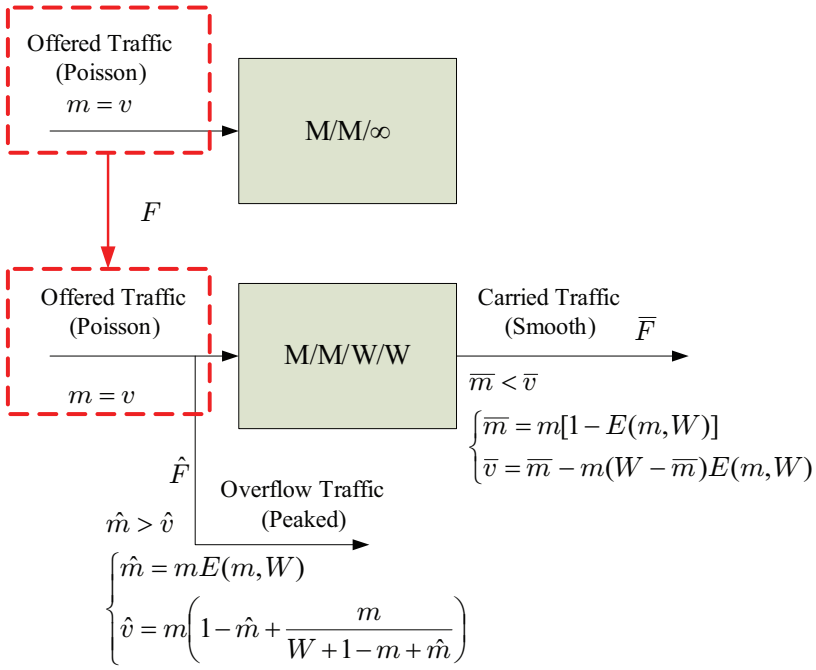

Figure 3.5: Model of the output port as an $M/M/W/W$ queue.

$$\hat{m} = m \cdot E(m, W), \tag{3.1}$$

$$\hat{v} = \hat{m}\left(1 - \hat{m} + \frac{m}{W + 1 + \hat{m} - m}\right), \tag{3.2}$$

where $E(m, W)$ is the well-known *Erlang B* formula [57] defined as

$$E(m, W) = \frac{m^W / W!}{\sum_{i=0}^{W} m^i / i!}. \tag{3.3}$$

Additionally, the mean $\bar{m}$ and variance $\bar{v}$ of the carried traffic flow are calculated as

$$\bar{m} = m\left[1 - E(m, W)\right], \tag{3.4}$$

$$\bar{v} = \bar{m} - m\left(W - \bar{m}\right) E(m, W). \tag{3.5}$$

All the above defined traffic streams are shown in Figure 3.5, along with their moments. It can be demonstrated that, if the offered traffic is Poisson, the variance of the overflow traffic is always greater than its mean. Conversely, the variance of the carried traffic is always lower [42]. Thus the overflow and carried traffic streams cannot be characterised

by a Poisson process, which has variance equal to the mean. We quantify the deviation of a traffic flow from being Poisson with its *peakedness* Z defined as the ratio of its variance and its mean, that is $Z = v/m$. If $Z > 1$ the traffic is said to be *peaked* whereas if $Z < 1$ the traffic is characterised as *smooth*. Finally, for Poisson traffic, $Z = 1$. In a network analysis scenario, traffic streams carried or overflowing from an output port of a node may generally be offered to another network element (e.g., an alternative output port of another network node). Thus, modelling these traffic flows with the Poisson process may lead to inaccuracies due to their non-Poissonian nature. Furthermore, in an OBS network, as we discussed in Chapter 2, burst traffic emanating from an assembler is not Poisson and, in general, it may not be possible to define a unique distribution for the burst inter-arrival times. Therefore, a model alternative to a traditional Poisson analysis should be taken into consideration for characterising these traffic flows. Generally, when a group of channels is offered non-Poisson traffic, its analysis becomes more challenging and it is often preferred to rely on approximate methods for the derivation of tractable analytic models. For the OBS node analysis, we propose the employment of alternative approximate techniques that take into consideration the contribution of higher moments for representing burst traffic flows. These techniques are known as *moment-matching* methods [42].

In a moment-matching method, the arrival process defining the offered traffic flow is substituted with an "equivalent" process. This process is selected in such a way that the analysis of the system becomes more tractable, allowing parameters of interest to be computed, such as the moments of the carried and overflow traffic streams or performance metrics such as the blocking probability. The process substitution is performed by matching the moments of the original arrival process with the moments of the equivalent one. Though the accuracy of the model increases with the number of matched moments, the analysis becomes too complex, often resulting in the derivation of intractable models. Typically, a good compromise is achieved with a two-moment description, that is the mean and the variance of the arrival process.

Research literature is rich with proposals of two-moment methods. One of the most celebrated techniques is the so called *Equivalent Random Theory* (ERT) [124] which allows modelling of a group of channels being offered a peaked traffic stream. This technique is

computationally simple and accurate and its main features will be described in more detail during the analysis of the port model. A peaked traffic stream can also be modeled by moment-matching with an *Interrupted Poisson Process* (IPP) as proposed by Kuczura in [61]. In this case, in addition to the mean and the variance, an extra parameter is required for using the method. Both ERT and IPP are very efficient and accurate for peaked traffic flows but can not handle smooth traffic. In this regard, various attempts have been made to extend the ERT method for handling smooth and peaked traffic, most notably in [14, 53, 84, 89], however issues regarding accuracy, model limitations and numerical instability may affect their practical implementations. A unified model capable of handling smooth, peaked and Poisson traffic is provided by the *Bernoulli-Poisson-Pascal* (BPP) method as proposed by Delbrouck in [27] and [28]. The model approximates the arrival process by matching its mean and variance with those of a Pascal process (for peaked traffic) or a Bernoulli process (for smooth traffic). The BPP method is an attractive solution often used in network analysis despite some drawbacks that limit its applicability under particular scenario, as documented in [27] and [28]. Nevertheless, we found this technique suitable for the analysis of the TAS-shFDL switch as described in the following section. Another significant benchmark has been established by Brandt et al. in [13] where non-Poisson traffic streams are represented by their *factorial moments* [42]. Although the complexity of the proposed method grows quadratically with the number of channels in the system, its very good accuracy may justify its application for computing the moments of the carried and overflow traffic streams.

3.2.2 Analysis of the Bufferless Port

The model of the output port is depicted in Figure 3.6. The port comprises W wavelength channels each one equipped with a TWC and is offered with I independent heterogeneous traffic flows. We assume general burst inter-arrival times and exponentially distributed burst lengths. Under these premises, the port can be modelled as a $G/M/W/W$ queuing system being offered with multiple independent traffic streams. Burst packets coming from the switch input ports are represented by traffic flows F_i and quantified by mean and variance (m_i, v_i), for $i = 1, \ldots, I$. The i-th burst traffic flow carried by the output port is indicated as $\bar{F}_i$ with mean and variance $(\bar{m}_i, \bar{v}_i)$ whereas the i-th burst traffic overflowing from the

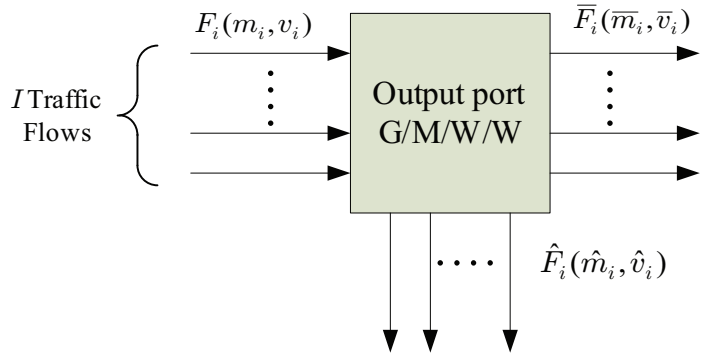

Figure 3.6: Analytic flow model of the OBS TAS output port.

output port is denoted by $\hat{F}_i$ and characterised by mean and variance $(\hat{m}_i, \hat{v}_i)$. The average burst inter-arrival rate of flow F_i is equal to λ_i bursts/s while the average burst service time is given by s bursts/s, thus $m_i = \lambda_i/s$ Erlangs. Our aim is to calculate the quantities $(\bar{m}_i, \bar{v}_i)$ and $(\hat{m}_i, \hat{v}_i)$ given the number of channels W and the offered moments (m_i, v_i) for $i = 1, \ldots, I$. We solve the model by assuming that each burst traffic flow is represented by a *Bernoulli-Poisson-Pascal* (BPP) process applying Delbrouck's *BPP method* as proposed in [27] and [28]. Particularly, each flow follows the BPP distribution given by

$$p_i(x) = p_i(x = X_i) = \binom{-C}{x} \beta_i^x (1 - \beta_i)^C, \tag{3.6}$$

where X_i is the channel occupancy of the i-th offered traffic flow and $C = \alpha_i/\beta_i$ with α_i and β_i defined as

$$\alpha_i = m_i/Z_i, \tag{3.7}$$

$$\beta_i = 1 - 1/Z_i. \tag{3.8}$$

Figure 3.7 depicts the state transition diagram related to the output port when offered with BPP traffic flow i. The system can be modelled as a group of channels with a limited number of sources C_i which alternate between an idle state and a busy state. The intervals of time when a source is idle or busy are both exponentially distributed with average intensity respectively given by β_i and γ_i. We note that when $Z_i < 1$, Equation (3.6) becomes a Bernoulli distribution whereas when $Z_i > 1$ we obtain a Pascal distribution. The prob-

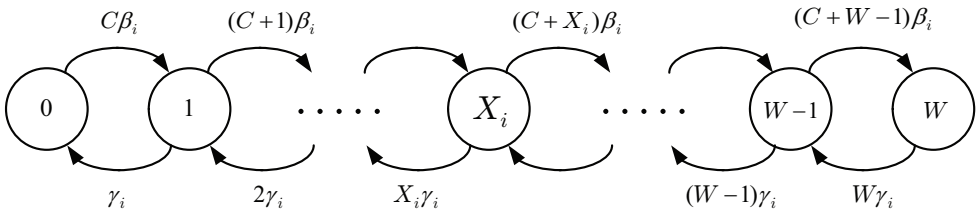

Figure 3.7: State transition diagram representation of the output port being offered with BPP traffic flow i.

lem of deriving the expressions of the carried mean and variance of a group of channels being offered multiple independent BPP arrival processes has been solved by Delbrouck in [28]. Particularly, the marginal distribution $\theta_i(x)$ associated with flow i can be obtained by convolving the joint busy channel distribution over all but the i-th flow. Thus, from the marginal distribution $\theta_i(x)$, it is possible to calculate all the moments of the carried traffic of flow i. Delbrouck achieved the same objective with a more efficient recursive procedure as described in [28] and summarised by Algorithm 1. At each iteration, an estimate of the *time congestion* T of the system is calculated. We remind the reader that the time congestion of a group of channels is defined as the portion of time that the group of channels is busy [42]. From the time congestion, it is possible to estimate the carried mean $\bar{m}_i$, the carried second moment $\bar{c}_i$ and, consequently, the carried variance $\bar{v}_i$ of each traffic flow i. Providing a demonstration of this procedure is out of the scope of this thesis. The interested reader can find a detailed mathematical proof of the method in [28].

Once $\bar{m}_i$ and $\bar{v}_i$ are calculated, the next step is to derive expressions for the overflow

Algorithm 1 Evaluation of $\bar{\mathbf{m}}_j$ and $\hat{\mathbf{m}}_j$ for output port j

1: Input : m_i, v_i, W for $i = 1, ..., I$
2: Initialisation : $\bar{m}_i^{(0)} \leftarrow 0$, $\hat{m}_i^{(0)} \leftarrow 0$, $c_i^{(0)} \leftarrow 0$
3: **for** $k \leftarrow 1, W$ **do**
4: $\quad T^{(k)} \leftarrow \sum_{i=1}^{I} \tilde{Z}_i \hat{m}_i^{(k-1)} / \left(k + \sum_{i=1}^{I} \tilde{Z}_i^{(k)} \hat{m}_i^{(k-1)}\right)$
5: $\quad \bar{m}_i^{(k)} \leftarrow (1 - T^{(k)})[\alpha_i + \beta_i \cdot \bar{m}_i^{(k-1)}]$
6: $\quad \bar{c}_i^{(k)} \leftarrow (1 - T^{(k)})[(\alpha_i + \beta_i) \cdot \bar{m}_i^{(k-1)} + \alpha_i + \beta_i \cdot \bar{c}_i^{(k-1)}]$
7: $\quad \bar{v}_i = \bar{c}_i - \bar{m}_i^2$
8: **end for**
9: **return** $\bar{m}_i, \bar{v}_i$

mean $\hat{m}_i$ and variance $\hat{v}_i$. The value of $\hat{m}_i$ for flow i can be calculated straightforwardly as

$$\hat{m}_i = m_i - \bar{m}_i. \tag{3.9}$$

Similarly to the overflow mean, the overflow variance $\hat{v}_i$ can be calculated by neglecting the existing correlations between the offered and carried traffic flows as $\hat{v}_i = v_i - \bar{v}_i$ [42], however this may lead to significant inaccuracies. This issue is overcome with the employment of ERT.

As previously mentioned, ERT is a two-moment matching technique that can efficiently compute the mean and the variance of a stream overflowing from a group of channels being offered with peaked traffic, as depicted in Figure 3.8. A peaked traffic flow can be represented as a stream overflowing from a group of channels being offered with Poisson traffic. Thus, we assume the existence of such a fictitious system by denoting its number of channels as W^* and the mean intensity of its Poisson offered traffic as A^*. These values can be computed by solving numerically Equation (3.1), that is

$$m = A^* \cdot E(A^*, W^*). \tag{3.10}$$

A good starting point for solving (3.10) is given by the following approximate values of A^*

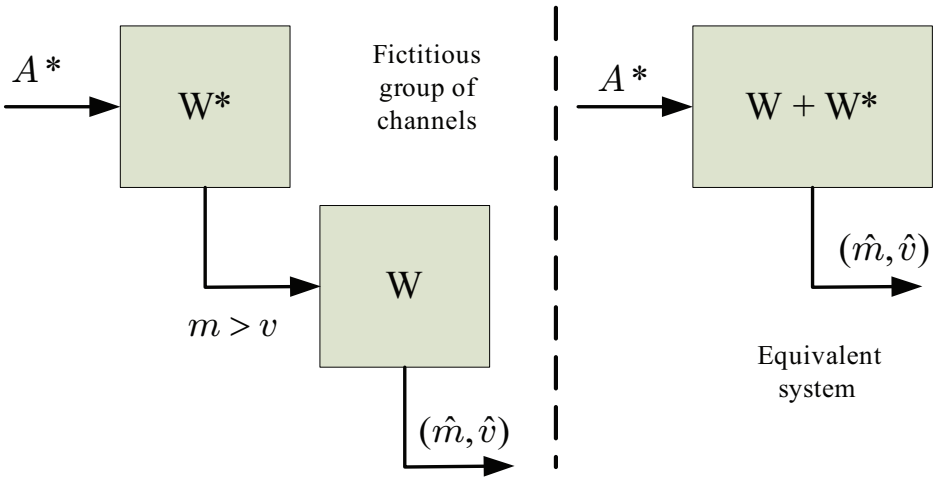

Figure 3.8: Application example of the Equivalent Random Theory.

and W^*, derived by Rapp in [97]

$$A^* \approx v + 3Z\,(1 - Z)\,, \tag{3.11}$$

$$W^* = \frac{A^*(m + Z)}{m + Z - 1} - m - 1. \tag{3.12}$$

Once the parameters of the fictitious group of channels have been computed, the mean and variance of the traffic overflowing from the original group of channels can be obtained as

$$\hat{m} = m \cdot E(A^*, W + W^*), \tag{3.13}$$

$$\hat{v} = \hat{m}\left(1 - \hat{m} + \frac{A^*}{W + W^* + 1 + \hat{m} - A^*}\right). \tag{3.14}$$

The employment of ERT allows a considerable increase in the accuracy when evaluating the overflow variance $\hat{v}_i$ of the i-th traffic flow compared to a simpler difference $\hat{v}_i = v_i - \bar{v}_i$. Following Deschamps in [30], we first define the mean of the total traffic offered to the output port from all the streams as

$$\hat{M} = \sum_{i=1}^{I} \hat{m}_i. \tag{3.15}$$

Then, we apply ERT, deriving the value of A^* by numerically solving

$$\hat{M} = A^* \cdot E(A^*, W). \tag{3.16}$$

Equation (3.16) can be solved with a standard numerical procedure such as the Newton-Raphson method [42]. Consequently, using Equation (3.14), we obtain

$$\hat{V} = \hat{M}\left(1 - \hat{M} + \frac{A^*}{W + 1 + \hat{M} - A^*}\right). \tag{3.17}$$

The values of the overflow variances are finally approximated by assuming that each overflowing stream is independent and that all variances are proportional to the mean of the offered traffic, that is

$$\hat{v}_i = \left(\frac{m_i}{M}\right)\hat{V}, \tag{3.18}$$

where $M = \sum_{i=1}^{I} m_i$. Algorithm 1 and Equations (3.9), (3.15)-(3.18) define the procedure to calculate the mean and the variance of all the carried and overflow streams of the output port. For simplicity, we refer to the entire procedure described so far as the *Extended BPP* (*E-BPP*) *method*.

A major limitation of this technique is in its inaccuracy in modelling an arbitrarily smooth traffic stream. In fact, when offered with a traffic flow of mean intensity m and peakedness $Z < 1$, the values of the time congestion T may become negative unless $W \leq m/(1-Z)$, a condition generally met in practical situations. Nevertheless, for unrealistically low values of peakedness this condition might not be satisfied. In this case, since the blocking probability experienced from the traffic stream is nearly zero, we overcome this issue by assuming that no overflow occurs from the group of channels.

3.2.3 Analysis of the Buffered Port

We complete the analysis of the TAS output port by considering the employment of a shared FDL, comprising K virtual buffers. Once again, our goal is to determine the mean and variance of the traffic carried by the output port and of the traffic that is considered lost from the system. As we mentioned in Section 3.1, a burst contention will be resolved only if it is possible to simultaneously reserve a free virtual buffer and a free wavelength channel of the output port. The delay introduced by the FDL is sufficient to de-correlate returned traffic from offered traffic so that the output port is seen as free to returned FDL burst traffic. Hence, burst traffic re-directed by the FDL to the output port will not experience burst contention. This situation is depicted in Figure 3.9(a) for the scenario of a single Poisson stream of mean intensity m Erlangs. We note that if $K \leq W$, bursts in the feedback flow quantified by $\bar{m}$ do not contend with each other for channels in the output port as they have been "streamlined" when passing through the FDL channels. Furthermore, "future" offered traffic of average intensity m will perceive a system with fewer available numbers of channels than W, say W^{-}, as previously delayed FDL traffic is partially occupying the W channels. From a queuing analysis perspective, the traffic characterised by $\bar{m}$ can be interpreted as a stream with priority higher than the one of the flow represented by m. Under these assumptions, the output port of Figure 3.9(a) can be seen as a queuing

system with *preemptive priorities* [46], whose exact analysis in our context would appear to be intractable. Instead, we propose a modelling approximation for which we provide the following mathematical interpretation.

For a group of channels being offered with J independent Poisson streams of mean m_j (where j traffic denotes the traffic priority) [46], the overflow mean of stream j can be computed exactly as

$$\hat{m}_j = Of(\sum_{\forall j} m_j) - \sum_{\forall i, i \neq j} Of(m_j), \tag{3.19}$$

where the operator $Of(x)$ denotes the overflow mean originating from a stream with mean intensity x and where $Of(m_j) = \hat{m}_j$. Applying Equation (3.19) to the scenario depicted in Figure 3.9(a) yields

$$\hat{m} = Of(m + \bar{m}) - Of(\bar{m}) = Of(m + \bar{m}), \tag{3.20}$$

where we implicitly resolve $Of(\bar{m}) = 0$ because the traffic flow carried back by the FDL is not affected by contention (streamlined). From this we conclude that, for Poisson offered traffic streams, the overflow associated with the incoming stream of intensity m can be obtained from the overflow of an equivalent stream of mean intensity given by $m + \bar{m}$. Hence, from a modelling perspective the system of Figure 3.9(a) can be substituted with the system of Figure 3.9(b).

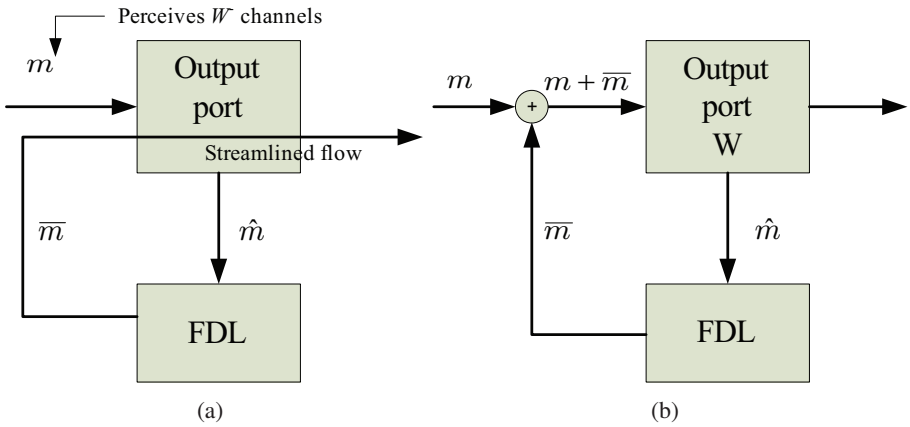

Figure 3.9: Flow model of a buffered output port: exact analysis (a) and approximate analysis (b).

An alternative intuitive but less rigorous interpretation of this phenomenon is as follows. The traffic flow offered to the output port and quantified by m perceives a system with less capacity because some of the channels are occupied by the FDL carried traffic; thus, in this situation the average portion of offered traffic that is blocked is greater than the case without the presence of the carried traffic. We approximate the level of blocking perceived by the offered traffic by keeping the number of channels constant and virtually increasing the intensity of the offered traffic. Therefore, "it is like" the amount of carried traffic from the FDL drives the virtual intensity of the offered traffic, achieving the same approximate level of blocking obtainable by keeping the same intensity m but varying the number of channels perceived by the offered traffic flow. Although (3.20) is only exact for Poisson streams, we assume its validity also for smooth and peaked traffic flows. In the last section of this chapter we show that this approximation yields a good compromise between complexity and accuracy of the model and we validate it by comparison with simulation results over different scenarios.

Before continuing with the description of the analysis, it is worth mentioning that the assumption of independence between the traffic flows (that is, the traffic flows offered to both the output port and the FDL) approximates the queuing behaviour of a system where wavelength channels are scheduled in a random fashion. Basically, the proposed method models the behaviour of a channel scheduling algorithm where voids between successive bursts are *randomly* filled. This seems to be in contrast with the initial assumption made in Section 3.1 where instead a LAUC-VF scheduling strategy has been considered for the switch architecture under study. Nevertheless, as shown in [128], there is a small difference in terms of burst blocking probability between the LAUC-VF and other random VF-based scheduling schemes (although the complexity related to different algorithms is different). Hence, we approximate the LAUC-VF channel scheduling mechanism with that of a scheduler that randomly selects the void to fill with an incoming burst. This approximation is validated by comparison with simulation results in the last section of this chapter.

Under these premises, we model the output port and the FDL with the approximate analytic model depicted in Figure 3.10. In addition to the already mentioned flows associated with the output port, we also define $\bar{F}_{K,i}$ as the i-th traffic flow carried by the FDL with

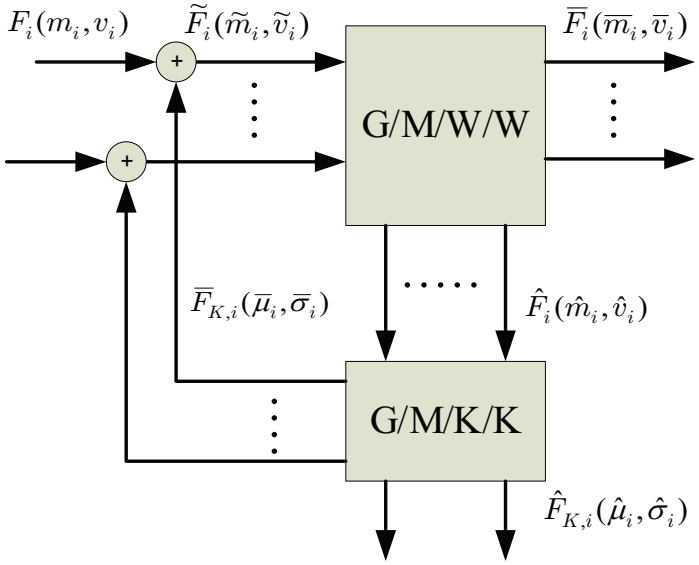

Figure 3.10: Analytic model of the buffered output port.

mean and variance given by $(\bar{\mu}_i, \bar{\sigma}_i)$ and $\hat{F}_{K,i}$ as the i-th traffic overflowing from the FDL with mean and variance equal to $(\hat{\mu}_i, \hat{\sigma}_i)$. The latter represents the portion of traffic that is lost from the system and cannot be recovered. Furthermore, we also denote with flow $\tilde{F}_i$ the i-th traffic flow effectively offered to the port, that is the virtual traffic obtained from the sum of the i-th original offered stream and the i-th stream carried back from the FDL. Its mean and variance are denoted as $(\tilde{m}_i, \tilde{v}_i)$. Our aim is to evaluate the quantities $(\bar{\mu}_i, \bar{\sigma}_i)$ and $(\hat{\mu}_i, \hat{\sigma}_i)$ for $i = 1, \ldots, I$.

The traffic overflowing from the port is notionally offered to the FDL and is non-Poisson in nature. Thus, the FDL is modelled as a $G/M/K/K$ queuing system and, similarly to the output port analysis, we again use the Extended BPP method to derive the FDL carried and overflow moments. By applying Algorithm 1 and Equations (3.9), (3.15)-(3.18) we obtain $(\bar{\mu}_i, \bar{\sigma}_i)$ and $(\hat{\mu}_i, \hat{\sigma}_i)$, where, this time, the input moments are given by $(\hat{m}_i, \hat{v}_i)$ for all traffic flows. Hence, according to the previously discussed modelling approximation, the mean and variance of the i-th effective traffic flow are obtained with the following set of equations

$$\tilde{m}_i = m_i + \bar{\mu}_i, \tag{3.21}$$

$$\tilde{v}_i = v_i + \bar{\sigma}_i. \tag{3.22}$$

Note that we are neglecting the correlations between the input and the FDL carried flows in evaluating (3.21) and (3.22).

We resolve the entire port model with a recursive procedure defined as follows. At iteration $k = 0$, we set $\tilde{m}_i^{(0)} = m_i$ and $\tilde{v}_i^{(0)} = v_i$. Thus, we evaluate $(\bar{m}_i^{(0)}, \bar{v}_i^{(0)})$ and $(\hat{m}_i^{(0)}, \hat{v}_i^{(0)})$ by applying the E-BPP method to the output port. In a similar way, we use again the E-BPP method to compute $(\bar{\mu}_i^{(0)}, \bar{\sigma}_i^{(0)})$ and $(\hat{\mu}_i^{(0)}, \hat{\sigma}_i^{(0)})$ for the FDL. Thus, we estimate the mean and variance of the effective offered traffic at iteration $k = 1$ as

$$\tilde{m}_i^{(1)} = m_i + \bar{\mu}_i^{(0)}, \tag{3.23}$$

$$\tilde{v}_i^{(1)} = v_i + \bar{\sigma}_i^{(0)}, \tag{3.24}$$

The procedure is then repeated where, this time, the input traffic is quantified by $(\tilde{m}_i^{(1)}, \tilde{v}_i^{(1)})$ rather than (m_i, v_i). We stop the recursion once a desired level of accuracy ϵ on all I overflow means is reached, that is

$$\Delta = \left| \hat{\mu}_i^{(k+1)} - \hat{\mu}_i^{(k)} \right| / \hat{\mu}_i^{(k)} < \epsilon \quad i = 1, ..., I. \tag{3.25}$$

Providing a mathematical proof of convexity of the problem or uniqueness of the solution is challenging and is out of the scope of the present work. Nevertheless, convergence of the algorithm has always been observed for all the scenarios under study, as we will show in Section 3.3.

3.2.4 Analytic Model of the Multi-port Buffered Switch

The extension of the model to a multi-port switch architecture is straightforward. We consider an OBS TAS-shFDL switch architecture with P input/output ports each one comprising W_j wavelength channels for $j = 1, \ldots, P$. The switch has a shared FDL with K virtual buffers. The node architecture is interpreted as a combination of multiple buffered output port models, as depicted in Figure 3.11. Note that, in this case, each moment is qualified with two subscripts: i denotes the stream and j denotes the associated output port. For example, $v_{i,j}$ is the variance of the i-th traffic flow offered to the j-th out-

put port. Also, in order to simplify the presentation of the analysis, all moments associated with a specific output port are grouped together as a vector. For example, the traffic flows carried by output port j are represented by vectors $\bar{\mathbf{m}}_j = [\bar{m}_{1,j}, \bar{m}_{2,j}, \ldots, \bar{m}_{p_j,j}]$ and $\bar{\mathbf{v}}_j = [\bar{v}_{1,j}, \bar{v}_{2,j}, \ldots, \bar{v}_{p_j,j}]$ where p_j denotes the number of traffic streams offered to port j. Table 3.4 summarises all the moments considered in the analysis of the switch.

The procedure to solve the switch is analytically equivalent to the one described for the hypotethical buffered node with a single output port. The carried and overflow moments of each output port are calculated with the E-BPP method. The vectors $(\hat{\mathbf{m}}_j, \hat{\mathbf{v}}_j)$ comprising the means and variances of the streams overflowing from all output ports are concatenated together as $\hat{\mathbf{M}} = [\hat{\mathbf{m}}_1, \ldots, \hat{\mathbf{m}}_P]$ and $\hat{\mathbf{V}} = [\hat{\mathbf{v}}_1, \ldots, \hat{\mathbf{v}}_P]$, representing the collection of streams offered to the FDL. Hence, using once again the E-BPP method for the FDL, we obtain the vectors $\hat{\mathbf{M}}_K = [\hat{\boldsymbol{\mu}}_1, \ldots, \hat{\boldsymbol{\mu}}_P]$, $\hat{\mathbf{V}}_K = [\hat{\boldsymbol{\sigma}}_1, \ldots, \hat{\boldsymbol{\sigma}}_P]$ and $\bar{\mathbf{M}}_K = [\bar{\boldsymbol{\mu}}_1, \ldots, \bar{\boldsymbol{\mu}}_P]$, $\bar{\mathbf{V}}_K = [\bar{\boldsymbol{\sigma}}_1, \ldots, \bar{\boldsymbol{\sigma}}_P]$. Similarly to the case of a single output port, the mean and variance of the

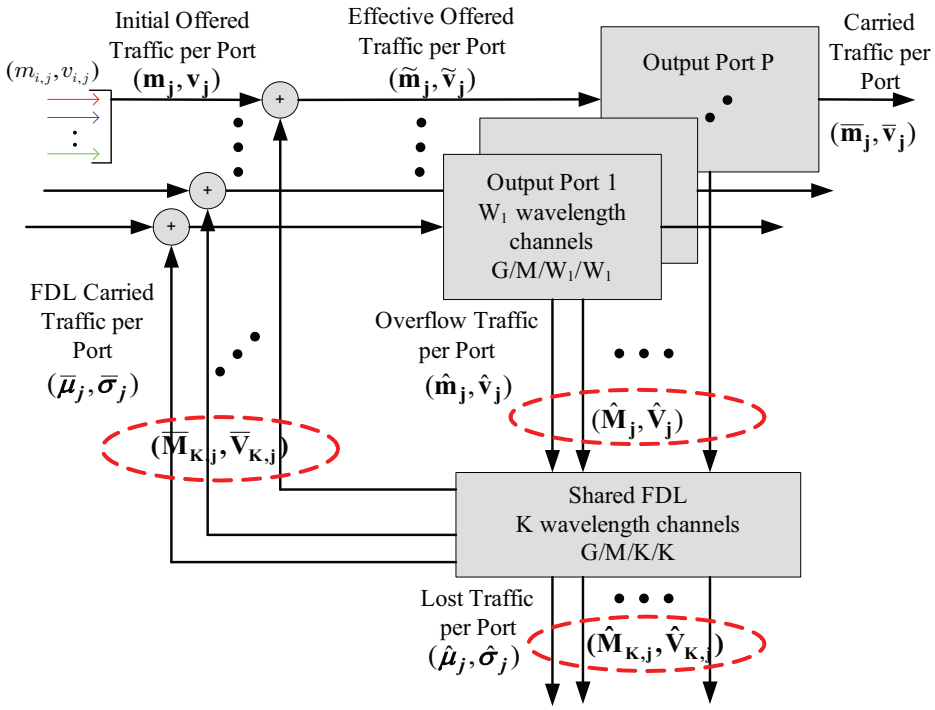

Figure 3.11: The analytic flow model of the OBS TAS-shFDL switch architecture.

Table 3.4: Moments describing the traffic flows within the OBS flow model.

Moments	Description of the Traffic Flow
$(\mathbf{m}_j, \mathbf{v}_j)$	Traffic initially offered to output port j
$(\tilde{\mathbf{m}}_j, \tilde{\mathbf{v}}_j)$	Traffic effectively offered to output port j
$(\bar{\mathbf{m}}_j, \bar{\mathbf{v}}_j)$	Traffic carried by output port j
$(\hat{\mathbf{m}}_j, \hat{\mathbf{v}}_j)$	Traffic overflowing from output port j
$(\hat{\mathbf{M}}, \hat{\mathbf{V}})$	Aggregate traffic offered to the FDL
$(\bar{\mathbf{M}}_K, \bar{\mathbf{V}}_K)$	Aggregate traffic carried by the FDL
$(\hat{\mathbf{M}}_K, \hat{\mathbf{V}}_K)$	Aggregate traffic lost from the switch
$(\bar{\boldsymbol{\mu}}_j, \bar{\boldsymbol{\sigma}}_j)$	Traffic carried by the FDL for output port j
$(\hat{\boldsymbol{\mu}}_j, \hat{\boldsymbol{\sigma}}_j)$	Traffic lost from the FDL for output port j

traffic flows effectively offered to each output port are obtained as

$$\tilde{\mathbf{m}}_j = \mathbf{m}_j + \bar{\boldsymbol{\mu}}_j, \tag{3.26}$$

$$\tilde{\mathbf{v}}_j = \mathbf{v}_j + \bar{\boldsymbol{\sigma}}_j, \tag{3.27}$$

for $j = 1, \ldots, P$. Once again, we solve (3.26) and (3.27) with an analogous recursive algorithm as proposed for the single output port, that is

$$\tilde{\mathbf{m}}_j^{(k+1)} = \mathbf{m}_j + \bar{\boldsymbol{\mu}}_j^{(k)}, \tag{3.28}$$

$$\tilde{\mathbf{v}}_j^{(k+1)} = \mathbf{v}_j + \bar{\boldsymbol{\sigma}}_j^{(k)}, \tag{3.29}$$

with starting point given by $\tilde{\mathbf{m}}_j^{(0)} = \mathbf{m}_j$ and $\tilde{\mathbf{v}}_j^{(0)} = \mathbf{v}_j$. The complete procedure to calculate the mean and variance of the carried and overflow streams of the switch is illustrated in Figure 3.12.

3.2.5 Burst Blocking Probability

Once the means of all traffic streams overflowing from the FDL are computed, it is possible to evaluate the burst blocking probability experienced by each flow. Specifically, the average blocking probability perceived by a burst belonging to traffic flow i offered to output

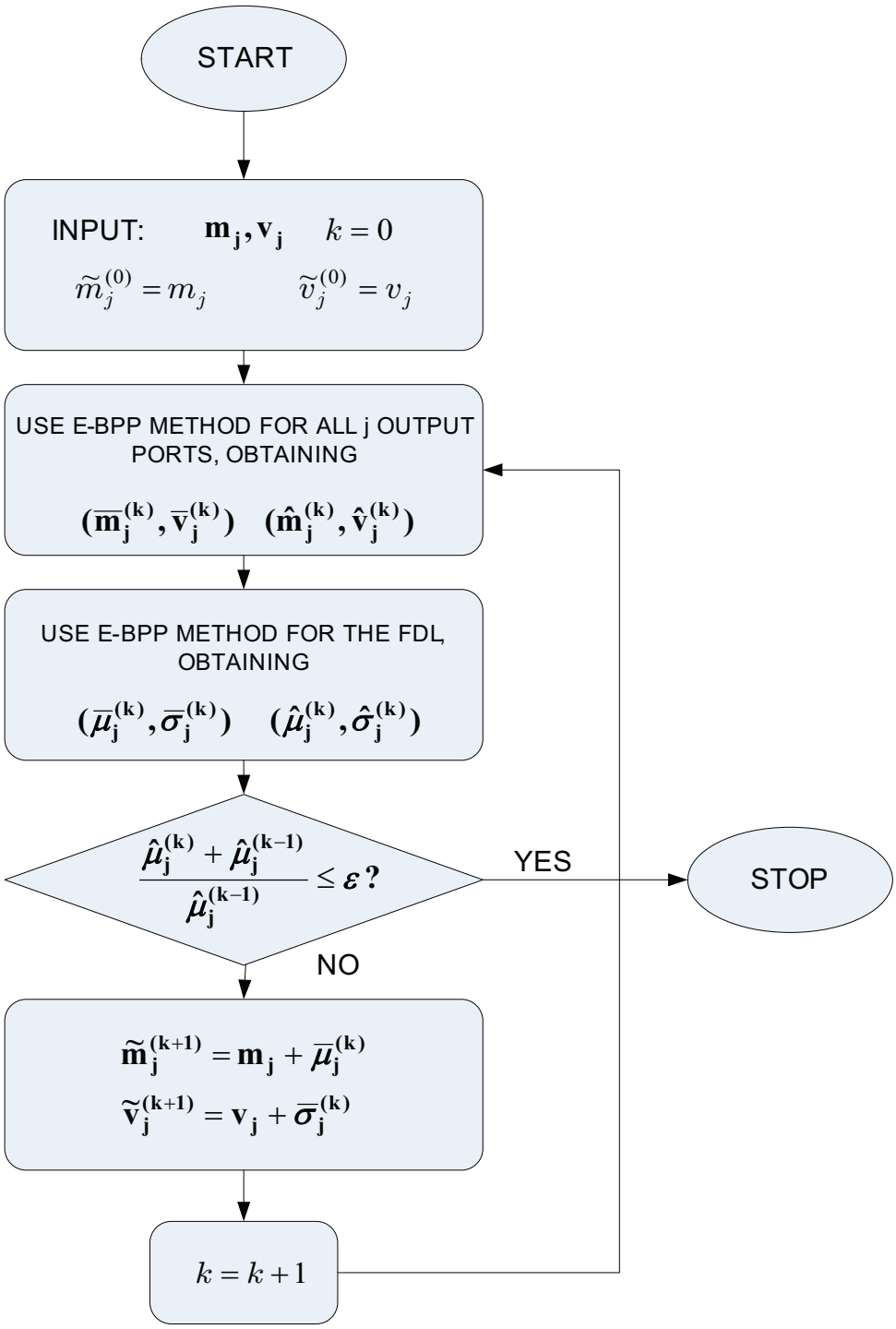

Figure 3.12: Procedure to evaluate the mean and variance of the carried and overflow traffic streams of the OBS TAS-shFDL switch.

port j may be calculated as

$$B_{i,j} = \hat{\mu}_{i,j}/m_{i,j}, \tag{3.30}$$

while the total blocking probability at output port j is evaluated as

$$B_j = \sum_{i=1}^{p_j} \hat{\mu}_{i,j} / \sum_{i=1}^{p_j} m_{i,j}. \tag{3.31}$$

Equations (3.30) and (3.31) lead to good estimates of the blocking, however we observed a substantial increase in the inaccuracy of the method when the values of blocking probabilities reach the order of $\approx 10^{-4}$ or below. This is due to that fact that the BPP method may be inaccurate for calculating the moments of overflow traffic at low loads as opposed to the estimation of the moments of the traffic flows carried by a group of channels (for which it is very efficient and accurate). Additionally, there is a general intrinsic limit on the accuracy obtainable by approximating the characteristics of a traffic flow with two moments, which manifests its weakness with more evidence at low loads as shown in [51]. Thus, for blocking probability values equal or lower than $\approx 10^{-4}$ the E-BPP mehtod alone might not be accurate enough in estimating $B_{i,j}$ and B_j. We attempt to address this issue by considering the contribution of higher moments of the overflow traffic. Particularly, we propose an additional procedure to evaluate the means $\hat{\mu}_{i,j}$ for all offered traffic flows and all output ports, basing our analysis on the work proposed by Brandt et al. in [13] and applied to OBS node modelling for the first time in [73]. We refer to this procedure as the *Factorial Moment Matching* (FMM) method. We want to remark that this procedure is performed only one time after the final estimates of vectors $\tilde{\mathbf{m}}_j$ and $\tilde{\mathbf{v}}_j$ for $j = 1, \ldots P$, have been evaluated. We conduct our analysis by characterising the traffic flows of interest in terms of their *factorial moments* as illustrated in Figure 3.13. Let us consider traffic flow $\mathcal{A}_j$ which comes from the aggregation of all the traffic flows effectively offered to output port j. We define the mean of $\mathcal{A}_j$ as $\tilde{M}_j = \sum_{i=1}^{p_j} \tilde{m}_{i,j}$ and its variance as $\tilde{V}_j = \sum_{i=1}^{p_j} \tilde{v}_{i,j}$. We want to calculate $\tilde{M}_{j,(g)}$, that is the g-th factorial moment of this traffic flow. The distribution of $\mathcal{A}_j$ is assumed to be BPP, thus, following [51], the factorial moments of (3.6) are given by

$$\tilde{M}_{j,(g)} = (a_j + g - 1)_g \left(\frac{b_j}{1 - b_j} \right)^g, \; g = 1, 2, 3, \ldots. \tag{3.32}$$

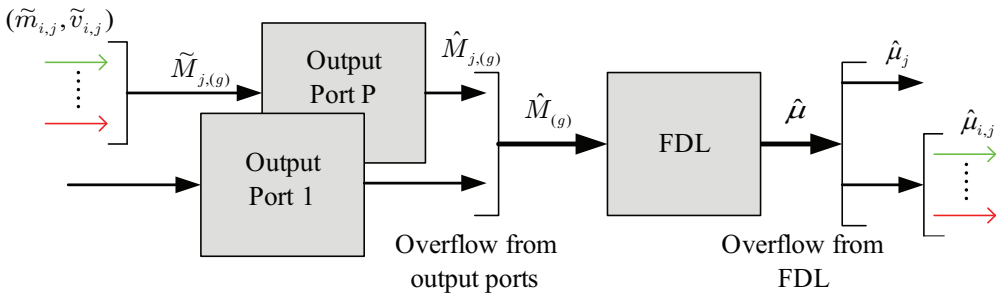

Figure 3.13: The Factorial Moment Matching procedure.

for $j = 1, \ldots, P$, where $(\cdot)_g$ denotes the g-th falling factorial defined as $(x)_g = x(x-1)\ldots(x-g+1)$ and where

$$a_j = \tilde{M}_j \left(\frac{1 - b_j}{b_j} \right), \tag{3.33}$$

$$b_j = 1 - 1/\tilde{Z}_j. \tag{3.34}$$

We denote with $\tilde{Z}_j$ the peakedness of flow $\mathcal{A}_j$ given by $\tilde{Z}_j = \tilde{V}_j / \tilde{M}_j$. We then calculate the factorial moments of the total traffic that overflows from the output ports following the method proposed by Potter in [90] and expressed by the following equation,

$$\hat{M}_{j,(g)} = \left[\sum_{k=0}^{N} \binom{N}{k} \frac{(g+k-1)!}{(g-1)!\, \tilde{M}_{j,(g+k)}} \right]^{-1}, \; g = 1, 2, 3, \ldots. \tag{3.35}$$

for $j = 1, \ldots, P$. At this point, we determine the total traffic offered to the FDL as the aggregation of all the traffic flows that are rejected from the output ports as depicted in Figure 3.13. This operation can be performed by deriving the cumulants [42] of the traffic flows, summing them and computing the associated factorial moments, that is

$$[\, \hat{M}_{(1)} \cdots \hat{M}_{(g)} \cdots] = \mathcal{F}\Big(\sum_{\forall j} \mathcal{C} \left([\, \hat{M}_{j,(1)} \cdots \hat{M}_{j,(g)} \cdots] \right) \Big) \tag{3.36}$$

where the vector-valued function $\mathcal{C}(\cdot)$ transforms factorial moments to cumulants and $\mathcal{F}(\cdot)$ the reverse. Functions $\mathcal{C}(\cdot)$ and $\mathcal{F}(\cdot)$ are defined as follows.

Let m_r, $m_{(r)}$, and κ_r be respectively the r^{th} raw moment, factorial moment and cumulant of a random variable. The cumulants can be derived in terms of raw moments with the

following recursive expression

$$\kappa_r = m_r - \sum_{i=1}^{r-1} \binom{r-1}{i} \kappa_{r-i} m_i, \quad r = 1, 2, 3, \ldots \tag{3.37}$$

whereas raw moments can be represented in terms of the factorial moments as

$$m_r = \sum_{i=1}^{r} S(r, i) m_{(i)}, \quad r = 1, 2, 3, \ldots, \tag{3.38}$$

where $S(r, i), i = 1, 2, \ldots, r$ are the Stirling numbers of the second kind. Combining these expressions yields the following recursion expressing cumulants in terms of factorial moments

$$\kappa_r = \sum_{i=1}^{r} S(r, i) m_{(i)} - \sum_{i=1}^{r-1} \kappa_{r-i} \binom{r-1}{i} \sum_{j=1}^{i} S(i, j) m_{(j)}. \tag{3.39}$$

Similarly, for factorial moments in terms of cumulants,

$$m_{(r)} = \kappa_r - \sum_{i=1}^{r-1} S(r, i) m_{(i)} + \sum_{i=1}^{r-1} \kappa_{r-i} \binom{r-1}{i} \sum_{j=1}^{i} S(i, j) m_{(j)}. \tag{3.40}$$

These formulae define respectively $\mathcal{C}(\cdot)$ and $\mathcal{F}(\cdot)$.

Once all $\hat{M}_{(g)}$ are obtained, we can again use (3.35) to evaluate the mean of the total traffic lost from the FDL,

$$\hat{\mu} = \hat{\mu}_{(1)} = \left[\sum_{k=0}^{K} \binom{K}{k} \frac{k!}{\hat{M}_{(g+1)}} \right]^{-1}, \; g = 1, 2, 3, \ldots. \tag{3.41}$$

At this point, similarly to the evaluation of the variances in (3.18), the mean $\hat{\mu}_j$ of the aggregate traffic overflowing from the FDL and associated with each output port j is calculated by assuming that each overflow is independent and proportional to the mean $\hat{M}_{j,(1)}$ of the aggregate traffic offered to the FDL from output port j. Therefore we have

$$\hat{\mu}_j = \left(\hat{M}_{j,(1)} / \sum_{j=1}^{P} \hat{M}_{j,(1)} \right) \hat{\mu}. \tag{3.42}$$

for $j = 1, \ldots, P$. We then derive $\hat{\mu}_{i,j}$ as

$$\hat{\mu}_{i,j} = \left(\hat{m}_{i,j} / \hat{M}_{j,(1)} \right) \hat{\mu}_j. \tag{3.43}$$

Having computed $\hat{\mu}_{i,j}$ for all traffic flows and for $j = 1, \ldots, P$ we can finally calculate the values of the burst blocking probabilities with (3.30) and (3.31).

As demonstrated in [72] the FMM method alone is sufficient to resolve the OBS node model for the case of single stream per-port scenarios. In fact, by providing the factorial moments of the offered traffic streams, it is possible to estimate the burst blocking probability at each port; however, the method may lead to an intractable analysis when used for network modelling due to its high complexity. Nevertheless, resolving the node model with the E-BPP method and computing the blocking values with only a single pass of the FMM analysis yields approximately the same results as obtained by conducting the entire analysis exclusively with the FMM method. Thus, we first compute the mean and variance of the carried and overflow streams with the less complex E-BPP method and then we "refine" the values of the blocking by applying the FMM analysis as a final iteration.

3.3 Results

We validate our analytic method by comparison with blocking probability results obtained with a discrete-event simulation of the OBS TAS-shFDL node architecture realised with Opnet Modeler™ [85]. This simulation tool offers to accurately model different protocols, devices and behaviors with an extensive set of special-purpose modelling functions. Its user-friendly Graphical User Interface along with the considerable amount of documentation and study cases are amongst its most attractive features. An analysis of its performance and accuracy when simulating and quantifying parameters of interests for packet switched networks has been presented in [67] where the authors further propose a comparison with the C++ based freeware simulation tool *Ns-2*. From the results of this investigation we conclude that the Opnet Modeler™well suits our needs and therefore we use it for simulating the OBS node architecture under study. The simulator implements the following features:

- up to eight input/output ports per switch (eight bi-directional WDM links),
- configurable number of data wavelength channels per link,
- burst offsets configurable for each traffic path,
- an incoming burst header queue and processor(s),
- the Just Enough Time (JET) reservation scheme,
- the LAUC-VF scheduling algorithm,
- configurable share-per-node feed-back fibre delay lines.

Aggregation queues and the detail of the burst aggregation process are not implemented, thus burst priority schemes are not considered. We simulate the transmission of burst packets with exponentially distributed burst lengths of average duration equal to 1ms. The switch dedicates one extra input/output port to a shared FDL employed in a feedback configuration comprising K virtual buffers. The FDL introduces a delay of 10 times the average burst transmission time, in order to minimise the FDL delay impact on burst blocking. We analyse the cases of a switch with an isolated output port and with 4 output ports all comprising the same number of wavelength channels W. Burst arrivals are modeled according to a BPP process as indicated in [43]. The simulated BPP traffic flow i is generated by considering burst packets transmitted from C_i sources with the same arrival intensity of β_i bursts/s, as depicted in Figure 3.7. The total burst arrival rate varies according to the number of channels of the output port occupied by flow i, that is $\lambda = (C_i + X_i)\beta_i$ bursts/s with $X_i = 1, 2, \ldots, W$. In this way, the simulated offered traffic can have its traffic moments matched to those of the BPP distribution. We note that this is not an exact match as, although offered traffic moments may be matched exactly, the inter-arrival process cannot be matched as the BPP model essentially assumes a fictitious renewal inter-arrival process that yields BPP offered traffic moments and no such renewal process exists [42].

In [72], we have investigated this subject in a single-stream modelling scenario by applying the FMM method to resolve a buffered OBS node model assuming gamma distributed burst inter-arrival times. The gamma distribution allows modelling arbitrary peaked-

ness in a unified model. Similar conclusions have been drawn in [12] where the authors derive a traffic model with gamma-distributed inter-arrival times parameterised for high variances approximating systems subjected to self-similar traffic. Therefore, to allow an exact comparison between analysis and simulation, the accuracy of the method is evaluated also for gamma burst arrivals. In this regard, denoting with τ the burst interarrival times, the factorial moments of the offered traffic may be expressed in terms of the gamma interarrival distribution as

$$M_{(g)} = \frac{1}{\mu E[\tau]} \cdot \prod_{i=1}^{g-1} \frac{i\, F^*(i\mu)}{1 - F^*(i\mu)}, \quad g \in \mathbb{N}, \tag{3.44}$$

where $F^*(\cdot)$ is the Laplace-Stieltjes transform (LST) of the interarrival cumulative distribution function, μ is the parameter of the exponentially distributed holding times in and $E[\tau]$ is the mean interarrival time. For the gamma case, $F^*(\cdot)$ is given by

$$f_\tau(t) = \frac{\theta^{-k}\, t^{k-1}\, e^{-t/\theta}}{\Gamma(k)} \quad t \geq 0 \tag{3.45}$$

where $k > 0$ is the shape parameter, $\theta > 0$ is the scale parameter and $\Gamma(k)$ is the gamma function. The LST $F^*(s)$ of the corresponding cumulative distribution function $F_\tau(t)$ is given as

$$F^*(s) = \int_0^\infty e^{-st} f_\tau(t)\, dt = (1 + \theta s)^{-k} \tag{3.46}$$

from which the first moment of the interarrival time τ is

$$E[\tau] = -\Big[\frac{dF^*(s)}{ds}\Big]_{s=0} = \theta k. \tag{3.47}$$

We now wish to find values of the parameters θ and k such that burst traffic with interarrival time τ has a given mean intensity m and peakedness Z. From (3.44) and (3.46) we may calculate the first two factorial moments of the traffic as

$$M_{(1)} = \frac{1}{\mu E[\tau]} = m \tag{3.48}$$

$$M_{(2)} = \frac{1}{\mu E[\tau]} \cdot \frac{(1 + \theta\mu)^{-k}}{1 - (1 + \theta\mu)^{-k}} = \frac{m}{(1 + \frac{1}{Mk})^k - 1}. \tag{3.49}$$

The mean and peakedness expressed in terms of the factorial moments of the offered traffic are

$$m = M_{(1)} \quad \text{and} \quad Z = 1 - M_{(1)} + M_{(2)}/M_{(1)}, \tag{3.50}$$

and so we may relate the mean and peakedness of the traffic to the gamma distribution parameters by the equations:

$$\theta = \frac{1}{m\mu k} \tag{3.51}$$

$$Z = 1 - m + \frac{1}{(1 + \frac{1}{mk})^k - 1}. \tag{3.52}$$

Given desired values of mean m and peakedness Z of the offered traffic, we may solve (3.52) numerically to yield corresponding values of k and θ.

3.3.1 Single Port Case

Figures 3.14 and 3.15 illustrate the burst blocking probability of a hypothetical TAS-shFDL switch with a single output port comprising $W = 8$ wavelength channels and a shared FDL with $K = 4$ virtual buffers. Burst loss is computed by applying the E-BPP + FMM analysis according to the procedure described in Section 3.2 for BPP and gamma distributed burst arrivals. The performance evaluation is conducted for offered load m varying from 0.3 to 1 Erlangs per channel and for peakedness values $Z = 0.8, 1, 1.2$. We further compare our model to one proposed in [66]. In this case, an output port is assumed to be equipped with a dedicated FDL shared amongst its wavelength channels and is modeled as an $M/M/W/W + K$ queue. Thus, the burst blocking probability of port p is calculated with the following formula,

$$B_p = \frac{m^{W+K}/(W^K \cdot W!)}{\sum_{j=0}^{W-1} m^j/j! + \sum_{j=W}^{W+K} m^j/(W^{j-K} \cdot W!)}, \tag{3.53}$$

where m is the load of the traffic flow offered to the output port. Also shown in Figure 3.14, for comparison, is the simple modelling of the port as an $M/M/W/W$ queue where the blocking is calculated with the Erlang B formula $E(m, W)$. Finally, a simple modelling of the output port as an $M/M/W + K/W + K$ queue is also considered, where the burst

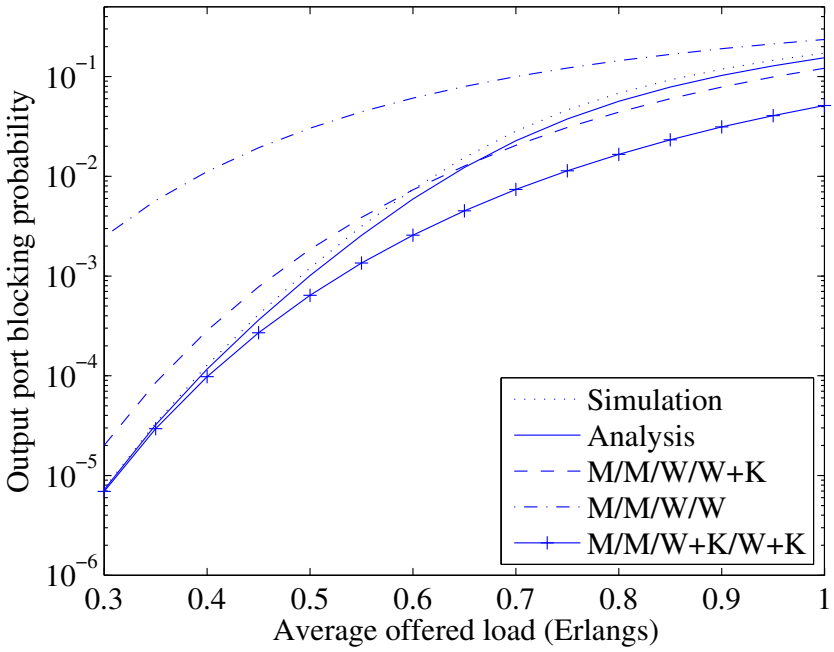

Figure 3.14: Blocking probability of the output port for Poisson offered traffic with $W = 8$ and $K = 4$. Burst arrivals are gamma distributed.

blocking probability is computed as $E(m, W + K)$.

First of all, note that modelling the output port as an $M/M/W/W$ does not give a good estimate of blocking when the FDL is employed to reduce contention. The estimate improves somewhat for high loss rates due to the fact that as load increases the FDL virtual buffers become increasingly less effective at resolving contentions. Results from the graph further indicates that a simple calculation of $E(m, W + K)$ will do better than $E(m, W)$. In fact, at low loads it provides a good approximation. This prompts the conclusion that, in so far as blocking performance is concerned for low intensity Poisson offered traffic, an output port with W wavelength channels and K FDL virtual buffers would behave similarly to a port with $W + K$ output channels and no FDL. At higher loads, however, the accuracy of the simple estimate $E(m, W + K)$ diminishes due to the fact that it does not reflect contention between input traffic and delayed traffic from the FDL. We further note that the $M/M/W/W + K$ queuing model proposed in [66] performs better than the previously examined Poisson models; however, in this case the blocking curve crosses the simulation curve at medium loads and its accuracy decreases for high and low loads. The best estima-

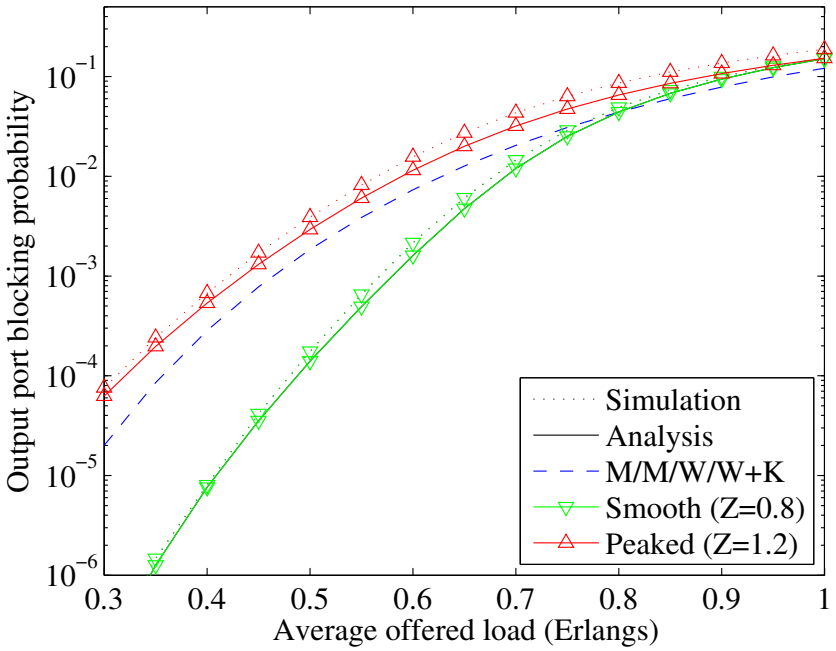

Figure 3.15: Blocking probability of the output port for smooth and peaked offered traffic with $W = 8$ and $K = 4$. Burst arrivals are gamma distributed.

tion of blocking is provided by the derived E-BPP + FMM analysis. Particularly, it can be observed that the analytic curve follows the shape of the simulation curve at all values of offered load, with a maximum relative error of ≈ 10.5 %.

The advantages offered by the proposed analytic model become even more evident when considering non-Poisson input traffic. Figure 3.15 illustrates this aspect by showing the average blocking probability of the same output port when offered traffic with peakedness $Z = 0.8$ and $Z = 1.2$. We note that our analytic model compares quite favourably with the blocking curves obtained by simulation. In this case also, it can be observed a maximum relative error of ≈ 15.7 %. The importance of considering the contribution of the traffic variance in the analysis is justified by the observable impact that different peakedness values have on loss performance. In fact, there is a very high sensitivity of the burst blocking level to the peakedness of the offered traffic and we note that the analytic method is successful in tracking it. The figure further demonstrates the decrease in accuracy when neglecting the traffic peakedness by assuming exponentially distributed inter-arrival times with the analytic model proposed in [66]. In this case, the introduced error is of almost an

order of magnitude for the peaked case and more than an order of magnitude for the smooth case.

3.3.2 Multi-port Case

In this case we consider a more realistic OBS TAS-shFDL switch equipped with P=4 output ports, that is the general average node degree that can be found in a core network. Each port has the same number of channels W and is offered burst traffic of equal average intensity and peakedness. The analysis is focused mainly on $W = 8, 16, 32$ wavelength channels, values of capacity that may be considered appropriate in relation to a future practical deployment of OBS architectures. Performance evaluations of OBS architectures conducted in recent test-bed experiments confirm this hypothesis as demonstrated in [1] and [63]. Due to lack of existing analytic network models with FDLs that can be used for an exact comparison with the proposed multi-port node analysis (where each node's architecture is assumed to be TAS-shFDL), burst blocking probability values are further computed with the $M/M/W/W + K$ model proposed in [66]. The model is not capable of reflecting the TAS-shFDL architecture, in fact it approximates the performance behaviour of a TAS-dFDL switch where each port has a dedicated FDL shared amongst its wavelength channels. Hence, "it is like" the proposed $M/M/W/W + K$ analysis models a TAS-shFDL architecture where different traffic streams overflowing from the output ports do not contend amongst each other for virtual buffers in the share-per-node FDL; however, we expect the model to be quite accurate at low loads, as opposed to high load scenarios, where the impact on blocking probability of the correlations between different traffic streams contending for FDL virtual buffers is higher.

Figure 3.16 depicts an illustrative example of the different performances of the proposed node model and the above mentioned Poisson queuing model, for $W = 8$ channels, $K = 4$ virtual buffers and Poisson offered traffic. Observe the very high accuracy of the E-BPP + FMM method when compared to simulation data, resulting in a maximum relative error of ≈ 7.5 %. Similarly to the previous case, the $M/M/W/W + K$ queuing model yields low accuracy and is not capable of following the shape of the blocking curve given by simulation data. The situation is even worse than the one port case. As expected, this is

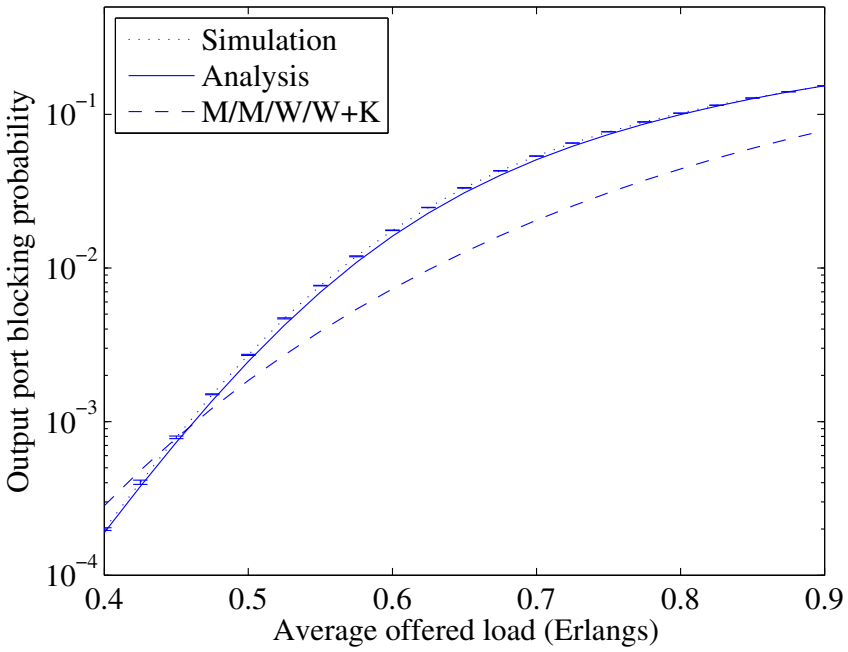

Figure 3.16: Blocking probability at the output port of a 4-port OBS node for Poisson traffic where $W = 8$ wavelength channels and $K = 4$ FDL virtual buffers.

particularly evident at high loads where the correlations between traffic streams offered to the FDL have a large influence on the final value of burst blocking probability.

The same conclusions on the accuracy of the proposed E-BPP + FMM model can be drawn in the scenarios depicted in Figures 3.17-3.21. Once again we observe a very good accuracy of the analysis when compared to simulation data. We note that the analytic model performs better in the multi-port case than in the single port case mainly because of lower amount of traffic carried back by the FDL. The accuracy is even better in the case of gamma distributed arrivals because of an exact comparison between the arrival processes in the simulation and analysis. The accuracy of the model is acceptable but generally decreases for higher number of virtual buffers. This is mainly due to the fact that a high value of K produces an increase in the amount of traffic carried back by the FDL. This may challenge the assumption of independence between the carried and offered streams made for Equation (3.22), however we still note how the analytic model can successfully track the very high sensitivity of the blocking to the load and the peakedness of the offered traffic.

Figures 3.22 and 3.23 illustrate the blocking probability of a 4-ports TAS-shFDL switch

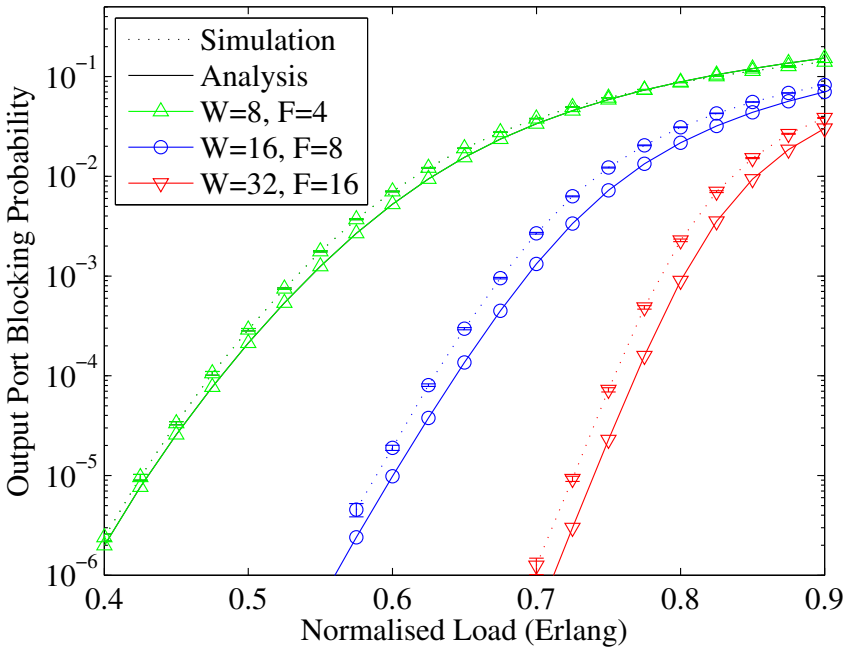

Figure 3.17: Blocking probability at the output port of a 4-port OBS node for smooth traffic ($Z = 0.8$). Burst arrivals are BPP distributed.

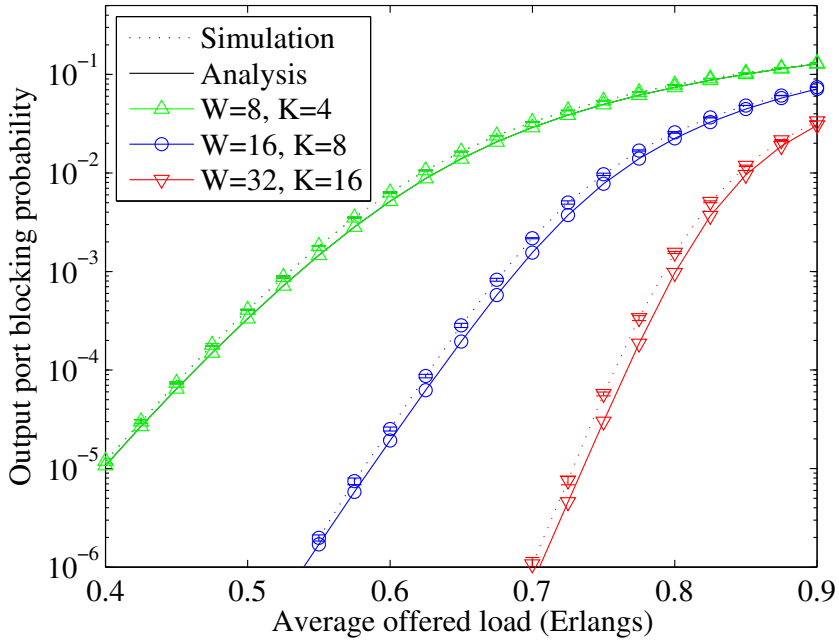

Figure 3.18: Blocking probability at the output port of a 4-port OBS node for smooth traffic ($Z = 0.8$). Burst arrivals are gamma distributed.

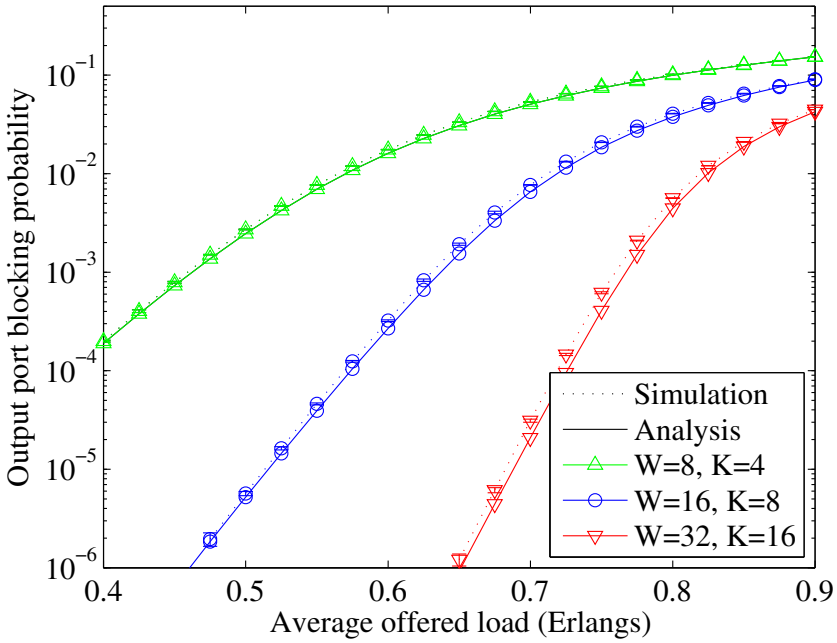

Figure 3.19: Blocking probability at the output port of a 4-port OBS node for Poisson traffic ($Z = 1$).

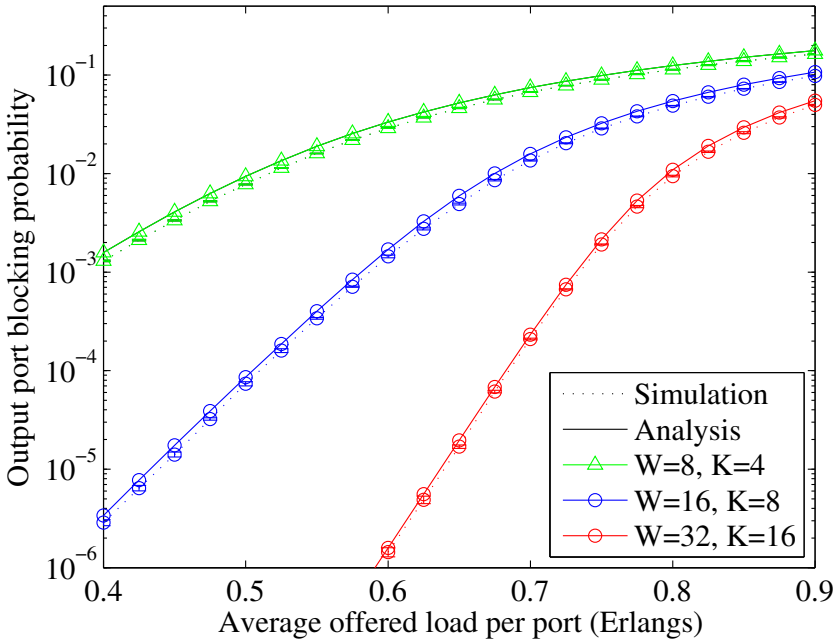

Figure 3.20: Blocking probability at the output port of a 4-port OBS node for peaked traffic ($Z = 1.2$). Burst arrivals are BPP distributed.

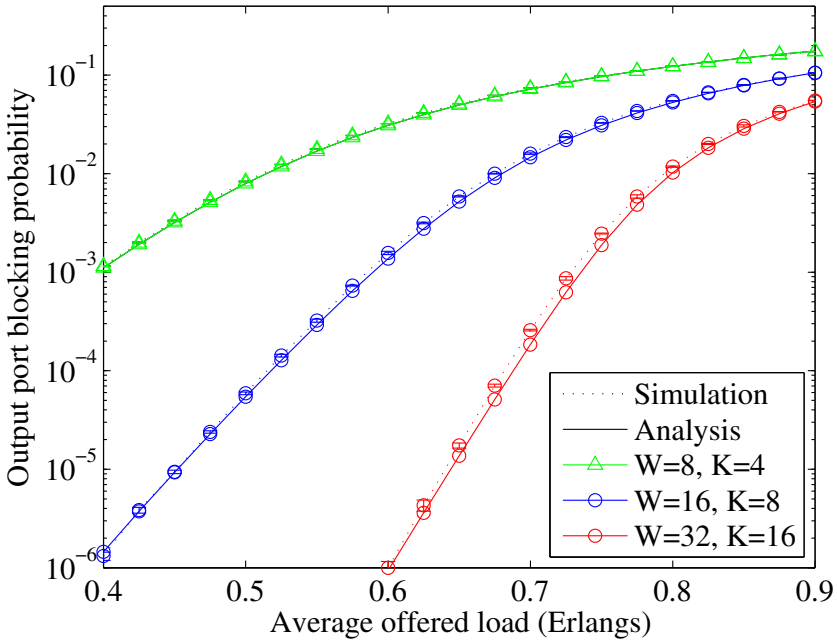

Figure 3.21: Blocking probability at the output port of a 4-port OBS node for peaked traffic ($Z = 1.2$). Burst arrivals are gamma distributed.

where each port is offered with traffic flows of different mean intensity and peakedness. Note that the values of m are scaled by a factor L for each output port. The number of channels per port is $W = 64$ and the FDL comprises $K = 32$ virtual buffers. The validity of the analytic method is challenged by choosing values of peakedness where the BPP method manifests its inaccuracies. In this case, the analytic results exhibit a lower accuracy than the scenarios of Figures 3.17-3.21 but are still successful in following the shape of the blocking curves and tracking their sensitivity to loads and peakednesses, especially for gamma arrivals. An example of the scalability of the method is illustrated in Figure 3.24 where burst loss is evaluated for a 4-ports switch with $W = 128$ channels and $K = 64$ virtual buffers for Poisson and peaked traffic and gamma burst arrivals. The analytic results are still quite close to simulation in both cases. We note that, in this case, a small change in the offered load provokes a substantial change in the experienced loss rate due to the high number of channels.

The impact of the offered traffic peakedness on loss rate is shown in Figure 3.25, for different W and K and for gamma offered traffic of mean intensity equal to 0.6 Erlangs

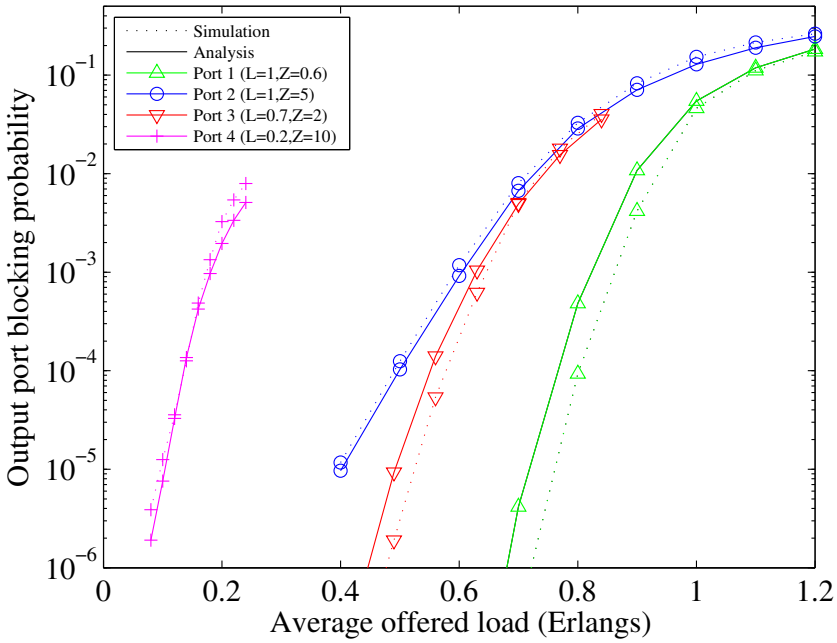

Figure 3.22: Blocking probability of a 4-port switch for non-uniform offered traffic conditions and gamma burst arrivals.

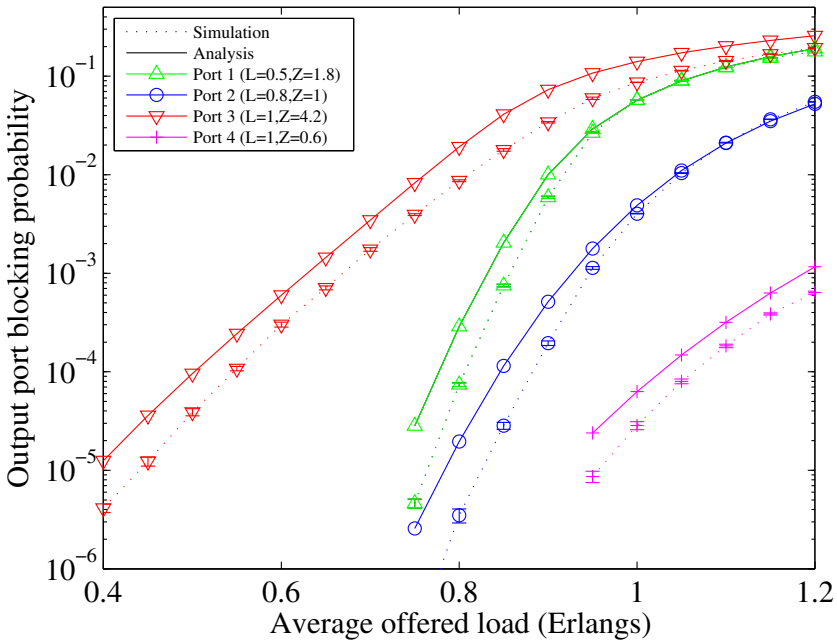

Figure 3.23: Blocking probability of a 4-port switch for non-uniform offered traffic conditions and BPP burst arrivals.

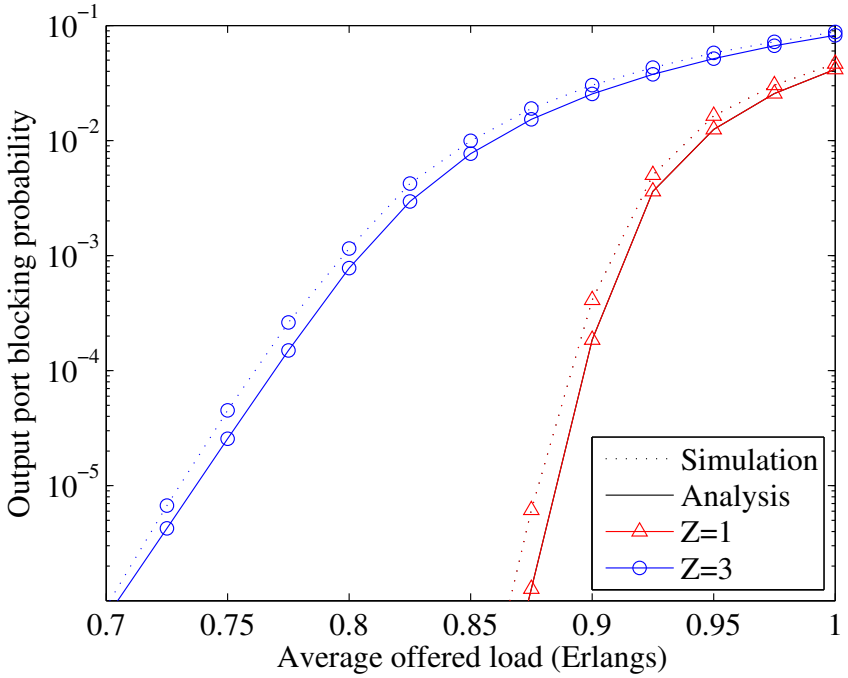

Figure 3.24: Blocking probability of a 4-port switch for $W = 128$, $K = 64$ and gamma burst arrivals.

per channel. Also in this case, the method compares favourably with simulation results especially for traffic near to Poisson. The inaccuracies tend to increase for traffic flows with very high peakedness.

Table 3.5 illustrates the percentage of the maximum allowable offered load for increasing numbers of virtual buffers at a loss rate level of 10^{-4} and for Poisson offered traffic. We observe that the analysis exhibits acceptable accuracy until the number of virtual buffers doubles the number of wavelength channels at the output ports. Nevertheless, in this region the increment in utilisation is very low as we register approximately less than 10% gain from a ratio $K/W = 2$ to a ratio $K/W = 4$. The situation is different when K is less than or equal to W, reaching considerable gains at maximum allowable load for a relatively small number of virtual buffers. From this we conclude that adopting a number of virtual buffers greater than the number of channels at the output port may result in only marginal improvements of the performance of the OBS switch and that $K \leq W$ may be an appropriate choice for buffered OBS switch dimensioning.

The analytic model of the switch has been implemented in Matlab^{TM} [70]. Convergence

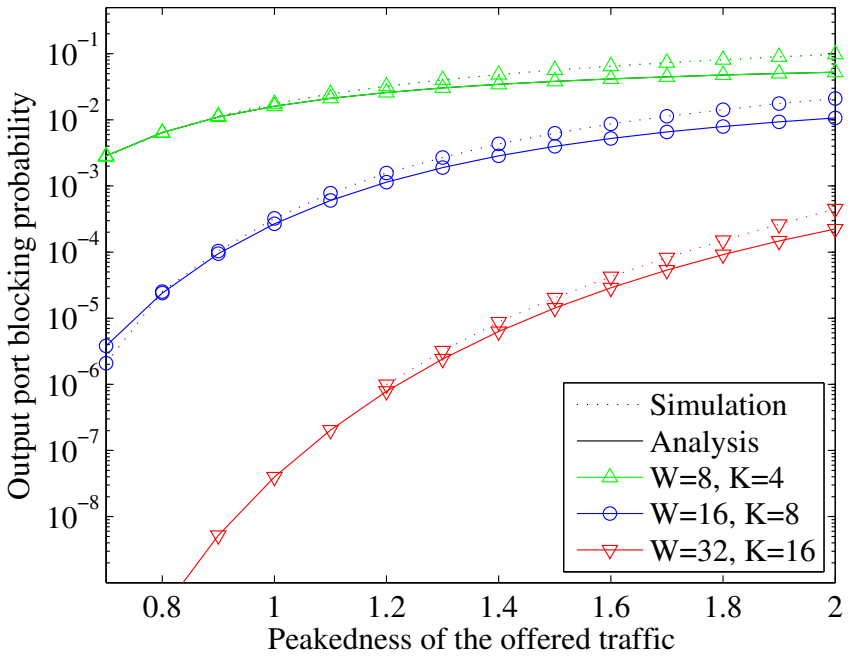

Figure 3.25: Burst blocking probability versus peakedness of the offered traffic for a 4-port OBS switch with offered load of mean intensity equal to 0.6 Erlangs per channel.

times of the E-BPP method to a level of accuracy $\epsilon = 10^{-8}$ have been observed to be $\approx$ 11ms for $4 \leq W \leq 128$ and $0 \leq K \leq W/2$ on a 1.83 GHz general-purpose PC. The time complexity of the method substantially increases when applying the FMM procedure for refining the burst loss estimates. Figure 3.26 depicts an example of the average time (in seconds) necessary to solve a 4-ports TAS-shFDL model for different values of W and with $K = W/2$ by jointly performing the E-BPP and the FMM methods. We remark that the time complexity is mainly dominated by the approximately quadratic behaviour of the FMM analysis. Nevertheless, convergence and numerical stability of the FMM analysis have also

Table 3.5: Maximum allowable Poisson offered load for $B \leq 10^{-4}$.

W=8	K=2	K=4	K=8	K=16	K=32
% full load - simulation	28.0%	37.6%	49.6%	61.7%	71.0%
% full load - analysis	28.0%	37.7%	50.5%	63.4%	75.7%
W=16	K=4	K=8	K=16	K=32	K=64
% full load - simulation	47.2%	56.9%	66.3%	71.5%	76.3%
% full load - analysis	47.3%	57.3%	67.8%	77.4%	85.2%

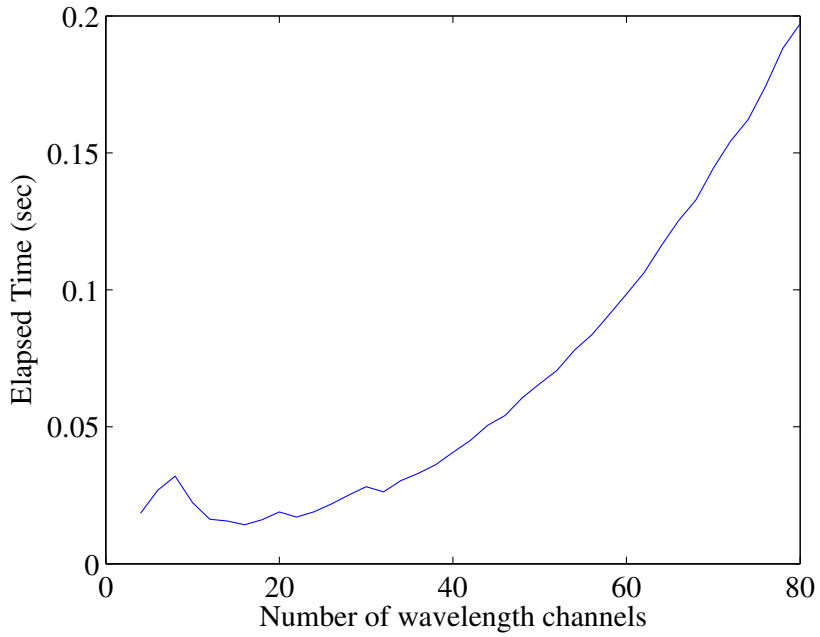

Figure 3.26: Average time required to solve the OBS node model (E-BPP + FMM) for increasing number of wavelength channels (Matlab^{TM}implementation).

been verified with a more time-efficient implementation of the model in the C language for $\approx 10^6$ test cases over the parameter range $W = 1, \ldots, 200$, $K = 1, \ldots, 100, K \leq 2W$, $P = 2, \ldots, 16$ and $0.5 < Z \leq 10$. Beyond these ranges of W and K, overflow in standard 64-bit (double) precision calculations can occur. Convergence times to 0.1% error, over the stated range, is observed to be $\approx$ 61ms maximum, $\approx$ 5ms average, on a 2.4 GHz general-purpose PC.

3.4 Conclusions

A method to evaluate the performance of an OBS TAS-shFDL node in terms of burst loss probability has been presented and validated by comparison with simulation data. The method shows good accuracy for a broad range of testing scenarios. Evidence from the presented results suggests that loss performance is highly sensitive to the offered traffic load and peakedness, thus it is essential to keep track of this aspect for dimensioning purposes. The analytic method successfully satisfies this requirement by following the shape of blocking curves at an acceptable level of accuracy for different configurations of channels and

traffic characteristics. Furthermore, it has been shown that a number of virtual buffers equal or less than the number of channels per output port may be sufficient to achieve substantial gains in maximum allowable offered loads.

Chapter 4

Modelling of the Optical Burst Switched Network

In this chapter an approximate analytic model of an FDL-buffered OBS network is presented. The model is built on the basis of the OBS TAS-shFDL node model derived in Chapter 3 and is provided to quantify the performance of an OBS network in terms of end-to-end burst blocking probability. The chapter is organised as follows. In Section 4.1 a brief background on network modelling applied to OBS is presented, focusing on the Reduced Load Approximation (RLA) and the Erlang Fixed Point Approximation (EFPA). Section 4.2 presents the analytic model of a buffered OBS network where burst contentions are resolved with the joint employment of TWCs in a full wavelength conversion strategy and shared FDLs in a feedback configuration. A method to evaluate end-to-end burst blocking probabilities is derived on the basis of the OBS TAS-shFDL node analysis conducted in Chapter 3. In Section 4.3 the streamline effect is introduced and its impact on the loss performance of OBS networks is discussed. Section 4.4 illustrates the validation of the network model by comparison with end-to-end burst loss results obtained with a discrete-event simulation of the network in Opnet Modeler ^{TM} [85]. Conclusions are presented in Section 4.5.

4.1 The Reduced Load and the Erlang Fixed Point Approximations

This section provides a brief background on a well-known technique used for performance evaluation of OBS networks as presented in [54] and [105]. Note that the main goal of the analysis is on determining the quality of service of the OBS network in terms of *end-to-end blocking probability*, that is the blocking probability experienced by bursts sent from a source node to a destination node over a specific network path. Although the grade of service of a network can be also defined by other performance metrics such as, for example, maximum tolerable end-to-end delay or network robustness under component failures (network survivability) [42], their study is out of the scope of the present work. Progress in these directions for optical communications networks has been made for example in [55] and more recently in [115]. Hence, the grade of service of the OBS network under study is uniquely determined by its ability to carry burst traffic from sources to destinations using available capacity resources (namely, the employed link wavelength channels, TWCs and FDL virtual buffers).

Consider a generic OBS network topology defined by graph $\mathcal{G}(\mathcal{N}, \mathcal{L}, \mathcal{R})$ where $\mathcal{N}$ represents the set of network nodes, $\mathcal{L}$ the set of network links and $\mathcal{R}$ is the set comprising the paths of the network. Each path corresponds to a route connecting a specific source node with a destination node. Network customers (such as hosts, access networks, etc.) transmit data over the considered network paths. The total number of nodes of the network is denoted as $N = |\mathcal{N}|$; similarly, $L = |\mathcal{L}|$ is the total number of network links and $R = |\mathcal{R}|$ is the total number of network paths. The analysis presented in this chapter assumes that the routing of the network has already been determined and corresponds to the set of paths $\mathcal{R}$ and the traffic demands are known, defined by vectors $\boldsymbol{\rho}= [\rho_1, \rho_2, \ldots, \rho_R]$ and $\boldsymbol{\psi}= [\psi_1, \psi_2, \ldots, \psi_R]$ where elements ρ_r and ψ_r are respectively the mean intensity (in Erlangs) and the variance of the traffic stream offered to path $r \in \mathcal{R}$. The peakedness of the traffic stream offered to path r is defined by $Z_r = \psi_r/\rho_r$. The peakedness values associated with all the traffic flows are organised in vector $\mathbf{Z} = [Z_1, Z_2, \ldots, Z_R]$. Additionally, denote with $\mathcal{R}_l$ the set of paths crossing link l and with $\mathcal{L}_r$ the set of all links being traversed

by path r. To further simplify the description of the analytic model, a slight abuse of set notation is made by indicating that "$l \in n$" if "link l is connected to an output port of node n".

The aim of the overall network analysis is to derive expressions for the estimation of the end-to-end blocking probabilities associated with each path, which we denote as $\mathcal{P}_r$ for all $r \in \mathcal{R}$. End-to-end delay is assumed to be dominated by propagation delay and so processing delay at core nodes and the delay introduced by FDLs are not considered in the analysis. Finally, it is further assumed that the topology of the network is fixed and does not change over time. An exact analysis of such a network would generally be too complex to conduct. The associated state space would be large and described by a very complex joint state distribution due to correlations between traffic streams on different links in the network. To overcome this issue, it is common to rely on approximate methods that simplify the analysis that allow the derivation of tractable analytic network models. A common approach is to assume that each link is independent, thus allowing the overall network analysis to be decomposed into a set of independent problems associated with each link [42]. Then, on the basis of the performance parameters of interest associated with each link (in this case, the burst blocking probability) it is possible to evaluate the overall performance of the network. This technique is known as the *link-decomposition* method and has been extensively used in network analysis [42].

A well-established application of the link-decomposition method that allows evaluation of the link blocking probabilities of a network is the *Erlang Fixed Point Approximation* (EFPA) [54]. This technique has been used in research literature for a wide class of loss networks and for the analysis of OBS networks in [103, 122, 125]. The applicability of EFPA relies on three assumptions: the first assumption, as previously discussed, is that each link of the network is considered independent, thus the analysis of the network may be decomposed into multiple independent problems each one associated with a specific link. The second assumption is that burst inter-arrival times are negative exponentially distributed, therefore burst arrivals can be described according to a Poisson process. The final assumption is that the traffic offered to a network link over a specific path is "thinned" by the blocking experienced on the preceding link over the same path and that this thinned

traffic remains Poisson. A simple example of this last assumption is depicted in Figure 4.1 where a traffic stream of mean intensity m Erlangs is offered to path r traversing links 1 and 2. The traffic carried by link 1 and offered to link 2 is a portion of the traffic initially offered to link 1, that is the traffic carried by link 1 and offered to link 2 is thinned by the blocking probability B_1 of link 1. If link 1 is offered with Poisson traffic then the traffic offered to link 2 is assumed to also be Poisson. This assumption is known as the *Reduced Load Approximation* (RLA). On the basis of the above mentioned three assumptions, the EFPA applied to an OBS network as proposed in [105] allows estimation of the load Λ_l of the total traffic offered to link l as

$$\Lambda_l = \sum_{r \in \mathcal{R}_l} \rho_r \prod_{j \in \mathcal{L}_r^{(l)}} (1 - B_j) \tag{4.1}$$

with

$$B_j = E(\Lambda_j, W_j) \tag{4.2}$$

where $\mathcal{L}_r^{(l)} \subseteq \mathcal{L}_r$ represents the set of links preceding link l over path r and B_j is the burst blocking probability experienced by link j given by the Erlang-B formula [57]. Note that W_j expresses the number of wavelength channels employed by link j.

Although very simple and efficient, this technique may not always determine an accurate estimation of the blocking probabilities. First of all, as discussed and demonstrated in Chapter 3, assuming Poisson arrivals may result in an inaccurate characterisation of the traffic, especially for OBS networks. Additionally, the EFPA generally tends to overestimate the values of blocking probability. For example, in Figure 4.1, the traffic carried by link 2 is additionally thinned by blocking B_2, however, in a realistic situation, all traffic carried by link 1 is also carried by link 2, thus B_2 = 0. This subject is discussed in more detail

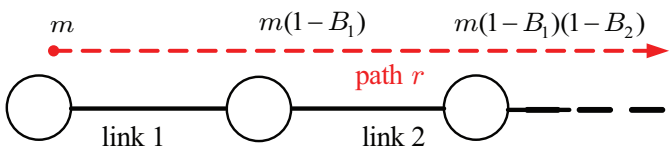

Figure 4.1: Example of Reduced Load Approximation.

in Section 4.4 when introducing the streamline effect. A final comment is on the "link-centric" approach adopted by the EFPA. Specifically, it is intrinsically assumed in Equation (4.1) that burst traffic flows of different paths traversing a common link experience the same level of blocking probability. This may not be an accurate assumption since traffic flows of the different paths are not exactly Poisson, but more accurately, characterised by different loads and peakednesses, experiencing different blocking probabilities. Hence, a modelling approach oriented on a multi-stream analysis for each link of the network should result in a more accurate estimation of the network performance metrics.

In this chapter, the EFPA is considered as a benchmark for comparison with the proposed analytic network model although the performance of several other network models can also be examined such as those proposed in [9, 125]; however, as stated in Chapter 1, the majority of models also assume Poisson burst arrivals and do not include the presence of FDLs at nodes, focusing more on OBS networks with full/partial wavelength conversion and deflection routing [125]. Exceptions can be found in [35, 62, 66, 95] where again burst inter-arrival times are assumed exponentially distributed. The authors in [107] model the network with the BPP model as presented in [28], but they examine the performance of deflection routing as opposed to the employment of FDLs. The next section deals with the derivation of an OBS network model where contention resolution is resolved with full wavelength conversion and shared FDLs.

4.2 The Analytic Model of the OBS Network: Shared-Buffer Network Model

The proposed model of the OBS network is constructed on the basis of the TAS-shFDL switch model described in the previous chapter and it will be referred as the *Shared-Buffer Network Model* (SBNM). A "path-centric" approach is adopted in the sense that the burst blocking probabilities are independently estimated for each path *separately*. This can be done by modelling the TAS-shFDL network nodes with the analytic description proposed in the previous chapter that allows computation of the values of blocking probabilities for each traffic flow. The ultimate goal of the analysis is to evaluate the end-to-end burst blocking

probability of each path of the OBS network.

The traffic offered to a generic link l can be of two types: (i) traffic that is offered from outside the core network (e.g., traffic generated from external sources such as access networks or hosts) and (ii) traffic carried by all the links that precede link l over the same path. Figure 4.2 depicts an example of this situation for a simple network of two links. Link l is offered with traffic that is carried by link l^- over the common path r and, additionally, is offered with traffic from external sources over path r'.

In the bufferless case, burst traffic flows offered to different outgoing links of a node do not contend amongst each other, allowing to estimate independently their experienced blocking probability. Hence, the evaluation of the moments of the traffic *carried* by link l depends only on the traffic *offered* to l; however, in the buffered case, the analysis is complicated by the *mixing* of traffic flows offered to different links of the node occurring in the shared FDL. In this case, the group of traffic flows contend amongst each other for available FDL virtual buffers, thus complicating the estimation of their blocking probabilities in the analysis. This means that, in the case of employment of an FDL in each node, the derivation of the moments of the traffic carried by a link $l \in n$ must be done by resolving the E-BPP + FMM method with respect to *all links* sharing the same FDL of node n. The situation is depicted in Figure 4.3: the traffic offered to link l along path r depends on the traffic carried by link l^- along path r and on the traffic offered to a link g along path r'. This is due to the fact that the traffic flows offered to link l and link g share the same FDL on node n. The network is solved by applying an iterative procedure where each iteration comprises two distinct phases. In Phase 1 the mean and the variance of the traffic flows offered to all links of the network are calculated. In Phase 2 the mean and the variance of the traffic flows

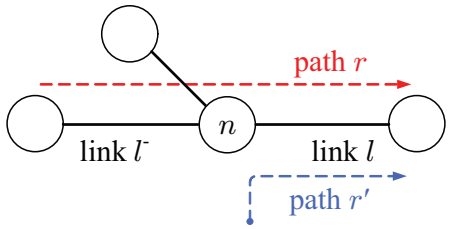

Figure 4.2: Traffic flows offered to an outgoing link: link $l \in n$ is offered carried traffic from link l^- on path r and external traffic on path r'.

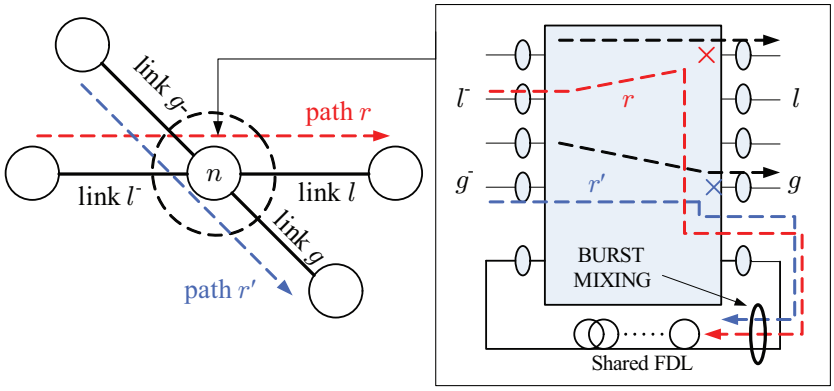

Figure 4.3: Example of interdependency between different traffic flows.

carried by all links are estimated resolving each OBS node with the E-BPP + FMM method described in Chapter 3. In the next iteration the moments of the traffic flows offered to all links are re-calculated by considering the contribution of the carried traffics computed at the previous iteration. Thus, the moments of the traffic carried by all links are computed once again resolving each node on the basis of the new estimates of the offered traffic moments obtained in the first phase. This recursion is repeated until convergence of the blocking probabilities is reached for all links. For simplicity, the overall procedure is illustrated in relation to a single node n:

- INITIALISATION: Define $\boldsymbol{\rho}= [\rho_1, \rho_2, \ldots, \rho_R]$ and $\boldsymbol{\psi}= [\psi_1, \psi_2, \ldots, \psi_R]$ as the vectors of the loads and the variances of the traffic flows offered to each path in the network. Additionally, denote with $m_{l,r}^{(k)}$ and $v_{l,r}^{(k)}$ respectively the mean and the variance of the traffic flow offered to link l along path r where k denotes the iteration index.

- PHASE 1: At iteration k, calculate the values of $m_{l,r}^{(k)}$ and $v_{l,r}^{(k)}$ as

$$m_{l,r}^{(k)} = \begin{cases} \rho_r, & \text{if } l \text{ is the first link of path } r \\ \bar{m}_{l_r^-,r}^{(k-1)}, & \text{if } l \text{ is not the first link of path } r \end{cases} \tag{4.3}$$

$$v_{l,r}^{(k)} = \begin{cases} \psi_r, & \text{if } l \text{ is the first link of path } r \\ \bar{v}_{l_r^-,r}^{(k-1)}, & \text{if } l \text{ is not the first link of path } r, \end{cases} \tag{4.4}$$

where l_r^- represents the link preceding l along path r and where $\bar{m}_{l_r^-,r}$ and $\bar{v}_{l_r^-,r}$ are respectively the mean and the variance of the traffic flow carried by link l_r^- over path r. Furthermore, note that at iteration $k = 0$

$$m_{l,r}^{(0)} = \begin{cases} \rho_r, & \text{if } l \text{ is the first link of path } r \\ 0, & \text{if } l \text{ is not the first link of path } r \end{cases} \tag{4.5}$$

$$v_{l,r}^{(0)} = \begin{cases} \psi_r, & \text{if } l \text{ is the first link of path } r \\ 0, & \text{if } l \text{ is not the first link of path } r. \end{cases} \tag{4.6}$$

- PHASE 2: in this phase the moments of the traffic flows carried by each link $l \in n$ are estimated on the basis of the method presented in Chapter 3 (E-BPP + FMM). First denote with $\mathbf{m}_l = [m_{l,1}, m_{l,2}, \ldots, m_{l,p_l}]$ and $\mathbf{v}_l = [v_{l,1}, v_{l,2}, \ldots, v_{l,p_l}]$ the vectors comprising the means and the variances of the traffic flows offered to all $r \in \mathcal{R}_l$, where p_l is the number of paths crossing link l and $\mathcal{R}_l$ denotes once again the set of paths traversing link l. Then, resolving node n with the E-BPP + FMM method yields

$$(\bar{\mathbf{m}}_l^{(k)}, \bar{\mathbf{v}}_l^{(k)}) = BPP(\mathbf{m}_l^{(k)}, \mathbf{v}_l^{(k)}, \mathbf{W}_n, K_n) \qquad \forall l \in n, \tag{4.7}$$

  where $\bar{\mathbf{m}}_l = [\bar{m}_{l,1}, \bar{m}_{l,2}, \ldots, \bar{m}_{l,p_l}]$, $\bar{\mathbf{v}}_l = [\bar{v}_{l,1}, \bar{v}_{l,2}, \ldots, \bar{v}_{l,p_l}]$ and function $BPP(\cdot)$ summarises the entire E-BPP + FMM procedure for resolving the OBS switch model presented in Chapter 3, $\mathbf{W}_n = [W_l]$ is a vector whose elements W_l correspond to the number of channels of link l for $l \in n$ and K_n denotes the number of FDL virtual buffers in node n. Note that the E-BPP + FMM procedure also allows derivation of vector $\hat{\mathbf{m}}_l^{(k)}$, that is the vector comprising the values of the means of the traffic streams overflowing from link $l \in n$. Thus, at the end of this phase, $\hat{\mathbf{m}}_l^{(k)}$ is used to compute the values of the blocking probability $B_{l,r}$ for link l over path $r \in \mathcal{R}_l$ on the basis of (3.30) $\forall r \in \mathcal{R}_l, \forall l \in n$. At the same time, burst loss probability B_l of link l is evaluated using (3.31) $\forall l \in n$.

Phases 1 and 2 are executed for all nodes $n = 1, \ldots, N$ of the network. Subsequently, the algorithm steps into the next k-th iteration. The recursion stops when convergence of

the blocking probabilities is reached, that is when

$$\Delta = \left| B_{l,r}^{(k)} - B_{l,r}^{(k-1)} \right| / B_{l,r}^{(k-1)} < \epsilon \quad \forall r \in \mathcal{R}_l, \forall l \in \mathcal{L}, \tag{4.8}$$

where the value of precision ϵ may be arbitrarily chosen. After convergence of the burst blocking probabilities, the end-to-end blocking probability of a generic path r can be finally computed as

$$\mathcal{P}_r = 1 - \prod_{\forall l \in \mathcal{L}_r} (1 - B_{l,r}). \tag{4.9}$$

Similarly to the case of the switch model, this work does not provide proof of uniqueness of the solution. Nevertheless, as shown in the Section 4.4, blocking results obtained from the analysis always converged to an observed value for all the scenarios under study.

4.3 The Streamline Effect

Consider a bufferless OBS network where contentions are resolved exclusively with TWCs, that is, no FDL is employed at any node. As briefly discussed in Section 4.1, the burst blocking probability experienced at each link depends on the interactions between bursts contending for a link wavelength channel. Specifically, two or more burst traffic streams merging on a common link over different paths will generally contend amongst each other for available link wavelength channels. If the next link over their paths is the same no burst contentions will happen unless:

- the next link comprises a number of wavelength channels less than the preceding link;
- one or more burst traffic streams from different paths are also offered to the next link.

This phenomenon is known as the *streamline effect* and may have a major impact in burst contention, either in OBS architectures providing full wavelength conversion capabilities or in OBS architectures without TWCs, under the wavelength continuity constraint [7]. This situation is depicted in more detail in Figure 4.4. Consider a simple network consisting of a link a and a link b. In case (a), burst traffic carried by link a over paths r and g is offered to link b; all contending bursts are removed from the streams at link a, thus the blocking

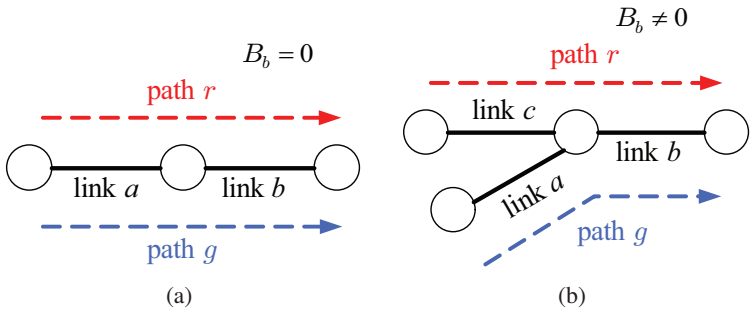

Figure 4.4: The streamline effect. Case (a): there is no blocking probability on link b due to streamline. Case (b): the burst traffic flows from path r and path g are offered to the same link b, producing a non-zero value of link blocking probability.

probability B_b is zero since no contention occurs at link b. In case (b), burst traffic carried by two different links over two different paths r and g is offered to link b. Contentions between the two traffic streams occur at link b, thus $B_b \neq 0$. An example of the application of the streamline effect can be found in [88] where the authors derive a load balancing scheme for OBS networks. The EFPA, as defined for the analysis of circuit-switched network in [54] or for OBS networks in [105], does not take into consideration the streamline effect and tends to overestimate the values of the link blocking probabilities. Thus, in order to obtain more accurate results, this work considers the impact of the streamline effect by ignoring from the analysis the contribution of the links whose blocking is zero because of streamlined traffic flows. This is done by applying a simple procedure as illustrated in Algorithm 2 before resolving the network. The output of the algorithm is the set of network links $\mathcal{L}_s$, that is the set of links where the streamline phenomenon occurs. Hence, the network model

Algorithm 2 Recursive procedure to remove streamlined links from $\mathcal{L}$

Input : $\mathcal{L}, \mathcal{R}_l, \mathcal{L}_r, \forall l \in \mathcal{L}, r \in \mathcal{R}$
Initialisation : $\mathcal{L}_s = \emptyset$
for all $l \in \mathcal{L}$ **do**
    if $\exists r \in \mathcal{R}_l : l$ is the first link of path r **then**
        break;
    else if $\exists r, g \in \mathcal{R}_l : l_r^- \neq l_g^-$ **then**
        break;
    else
        $\mathcal{L}_s \leftarrow \mathcal{L}_s \cup \{l\}$
    end if
end for
return $\mathcal{L}_s$

will be resolved by considering the updated set of network links $\mathcal{L}' = \mathcal{L} - \mathcal{L}_s$ where the streamlined links of set $\mathcal{L}_s$ are removed from the original set of network links $\mathcal{L}$. Algorithm 2 is applied for the presented analytic network model and also for the EFPA, resulting in an improved version simply referred to as the Erlang Fixed Point Approximation *with Streamline* (EFPA-S). Furthermore note that the streamline effect may occur also in the presence of FDLs. Streamlined burst traffic flows will not be offered to the FDL at all since they will not experience contention at their outgoing link.

4.4 Results

Similarly to the previous chapter, in this section the SBNM is validated by comparison with results obtained from a discrete-event simulation of an OBS network topology realised with Opnet Modeler ™. In Subsection 4.4.1 we introduce the OBS network topologies under study for the validation of the SBNM. Results for the bufferless case are presented in Subsection 4.4.2 whereas in Subsection 4.4.3 the accuracy of the network model is analysed when each node has a feedback FDL in a share-per node configuration.

4.4.1 The Network Topologies under Study

The first network topology is equivalent to the National Science Foundation Network Topology (NSFNET) depicted in Figure 4.5(a) as presented in [105] for a bufferless OBS network. Each node of the network is assumed to be designed according to a TAS-shFDL architecture, thus employing full wavelength conversion and a shared multi-channel FDL in a feedback configuration. The topology includes $N = 13$ network nodes and $L = 16$ bidirectional links each comprising the same number of wavelength channels W. The routing of the network is assumed to be already determined and is given by a set of $R = 12$ paths whose hops are shown in Table 4.1 as defined in [105].

For completeness, indicative results are presented for validating the accuracy of the network model with an additional network topology, that is the European Optical Network (EON) topology depicted in Figure 4.5(b). In this case, the network comprises $N = 15$ nodes, $L = 26$ bidirectional links and $R = 18$ paths whose hops are indicated in Table

4.2. The network performance is analysed in terms of end-to-end blocking probabilities $\mathcal{P}_r$ for all paths $r \in \mathcal{R}$. All paths are offered with burst traffic of the same load ρ and same variance ψ. The simulation of the network is realised on the basis of the simulator of the OBS node described in the previous chapter, thus the set-up is equivalent to the one already presented in Chapter 3. Similarly, BPP traffic is generated according to the same procedure described in the previous chapter. All simulated points are within 5% confidence intervals

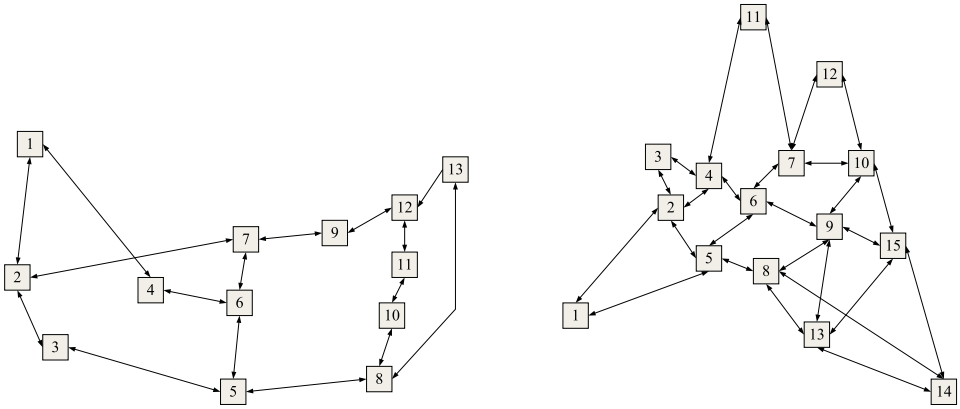

Figure 4.5: The NSF network backbone topology (a) and the EON network topology (b) under study.

Table 4.1: Paths of the NSF Network Topology.

Path	Path hops	Path	Path Hops
1	$1 \rightarrow 4 \rightarrow 6 \rightarrow 5 \rightarrow 8 \rightarrow 10$	7	$10 \rightarrow 8 \rightarrow 5 \rightarrow 6 \rightarrow 4 \rightarrow 1$
2	$2 \rightarrow 3 \rightarrow 5 \rightarrow 6 \rightarrow 7$	8	$7 \rightarrow 6 \rightarrow 5 \rightarrow 3 \rightarrow 2$
3	$2 \rightarrow 7 \rightarrow 9 \rightarrow 12 \rightarrow 13$	9	$13 \rightarrow 12 \rightarrow 9 \rightarrow 7 \rightarrow 2$
4	$3 \rightarrow 5 \rightarrow 8 \rightarrow 13$	10	$13 \rightarrow 8 \rightarrow 5 \rightarrow 3$
5	$5 \rightarrow 6 \rightarrow 7 \rightarrow 9 \rightarrow 12$	11	$12 \rightarrow 9 \rightarrow 7 \rightarrow 6 \rightarrow 5$
6	$8 \rightarrow 10 \rightarrow 11 \rightarrow 12 \rightarrow 13$	12	$13 \rightarrow 12 \rightarrow 11 \rightarrow 10 \rightarrow 8$

Table 4.2: Paths of the European Optical Network Topology.

Path	Path hops	Path	Path Hops
1	$1 \rightarrow 2 \rightarrow 4 \rightarrow 6 \rightarrow 7 \rightarrow 10$	10	$11 \rightarrow 7 \rightarrow 12$
2	$3 \rightarrow 4 \rightarrow 6$	11	$12 \rightarrow 10 \rightarrow 15 \rightarrow 14$
3	$13 \rightarrow 15 \rightarrow 10 \rightarrow 12$	12	$10 \rightarrow 7 \rightarrow 11$
4	$12 \rightarrow 7 \rightarrow 6 \rightarrow 4 \rightarrow 2$	13	$13 \rightarrow 9 \rightarrow 6 \rightarrow 4 \rightarrow 11$
5	$2 \rightarrow 4 \rightarrow 11$	14	$8 \rightarrow 5 \rightarrow 2 \rightarrow 3$
6	$11 \rightarrow 7 \rightarrow 6 \rightarrow 5 \rightarrow 8$	15	$4 \rightarrow 2 \rightarrow 1$
7	$12 \rightarrow 10 \rightarrow 9 \rightarrow 13$	16	$7 \rightarrow 10 \rightarrow 15$
8	$5 \rightarrow 8 \rightarrow 13 \rightarrow 14$	17	$13 \rightarrow 8 \rightarrow 5 \rightarrow 1$
9	$1 \rightarrow 5 \rightarrow 6 \rightarrow 7$	18	$14 \rightarrow 15 \rightarrow 10 \rightarrow 7 \rightarrow 11$

of 95 % level but they are not displayed to improve the clarity of the graphs. The results are firstly examined for the case with no FDLs and then for the case of employment of FDLs.

4.4.2 Bufferless Case: No FDLs

In this case there are no FDLs deployed in the network. This situation allows a direct comparison between the SBNM and the EFPA. The analytic model is further compared with the EFPA-S and validated against simulation results. Tables 4.3 and 4.4 illustrate the end-to-end blocking probability values of each path respectively for W=16 and for W=64 wavelength channels. Note that the EFPA performs quite well for both scenarios when the traffic is Poisson. The situation considerably improves when considering the streamline effect. In fact all the blocking values are substantially closer to simulation than in the the first case (e.g, note the blocking values of paths 3 and 11 in Table 4.3). First of all, even for the case of Poisson offered traffic, the application of the SBNM still yields an average end-to-end blocking slightly closer to simulation data than the EFPA-S. This is mainly due to two main factors: (i) in the EFPA-S the traffic carried by each link is assumed to be Poisson whereas in reality tends to be smoother and the proposed network model allows to better approximate its characteristics; (ii) the path-centric approach adopted in the

Table 4.3: Path blocking probabilities of the NSF network topology for $W = 16$ wavelength channels. Each path is offered with external traffic of mean load equal to 0.25 Erlangs per channel.

Path	Z=1				Z=0.8		Z=1.2	
	Simulation	SBNM	EFPA	EFPA-S	Simulation	SBNM	Simulation	SBNM
1	4.47E-03	4.53E-03	4.54E-03	4.53E-03	1.36E-03	1.17E-03	9.00E-03	1.02E-02
2	4.24E-03	4.32E-03	4.45E-03	4.45E-03	1.36E-03	1.14E-03	8.28E-03	9.47E-03
3	7.96E-03	8.32E-03	1.29E-02	8.81E-03	2.53E-03	2.25E-03	1.51E-02	1.78E-02
4	1.19E-02	1.25E-02	1.74E-02	1.33E-02	3.86E-03	3.39E-03	2.24E-02	2.65E-02
5	7.93E-03	8.32E-03	1.31E-02	8.80E-03	2.52E-03	2.25E-03	1.51E-02	1.78E-02
6	7.82E-03	8.12E-03	1.28E-02	8.72E-03	2.53E-03	2.22E-03	1.43E-02	1.72E-02
7	1.18E-02	1.23E-02	1.32E-02	1.32E-02	3.82E-03	3.36E-03	2.20E-02	2.59E-02
8	7.86E-03	8.30E-03	1.28E-02	8.80E-03	2.66E-03	2.25E-03	1.49E-02	1.77E-02
9	8.49E-03	8.68E-03	1.32E-02	8.96E-03	2.72E-03	2.30E-03	1.61E-02	1.88E-02
10	7.98E-03	8.30E-03	8.73E-03	8.80E-03	2.60E-03	2.25E-03	1.49E-02	1.77E-02
11	8.10E-03	8.49E-03	1.72E-02	8.88E-03	2.69E-03	2.27E-03	1.54E-02	1.82E-02
12	8.54E-03	8.68E-03	8.96E-03	8.96E-03	2.71E-03	2.30E-03	1.63E-02	1.88E-02
Average	8.09E-03	8.41E-03	1.16E-02	8.85E-03	2.61E-03	2.26E-03	1.53E-02	1.80E-02

Table 4.4: Path blocking probabilities of the NSF network topology for $W = 64$ wavelength channels. Each path is offered with external traffic of mean load equal to 0.3 Erlangs per channel.

Path	Z=1				Z=0.8		Z=1.4	
	Simulation	SBNM	EFPA	EFPA-S	Simulation	SBNM	Simulation	SBNM
1	4.26E-05	4.14E-05	4.14E-05	4.14E-05	4.02E-06	3.52E-06	1.60E-04	1.89E-04
2	2.90E-05	4.13E-05	4.14E-05	4.14E-05	4.45E-06	3.51E-06	1.31E-04	1.87E-04
3	9.24E-05	8.25E-05	1.24E-04	8.27E-05	8.90E-06	1.05E-05	3.44E-04	3.72E-04
4	1.04E-04	1.24E-04	1.65E-04	1.24E-04	1.56E-05	1.41E-05	4.46E-04	5.59E-04
5	8.90E-05	8.25E-05	1.24E-04	8.27E-05	9.61E-06	1.05E-05	3.67E-04	3.72E-04
6	8.72E-05	8.25E-05	1.24E-04	8.27E-05	7.61E-06	1.05E-05	3.29E-04	3.71E-04
7	1.21E-04	1.24E-04	1.24E-04	1.24E-04	1.91E-05	1.05E-05	4.87E-04	5.58E-04
8	7.66E-05	8.24E-05	1.24E-04	8.27E-05	7.90E-06	1.05E-05	3.06E-04	3.72E-04
9	8.56E-05	8.26E-05	1.24E-04	8.28E-05	8.33E-06	1.05E-05	3.26E-04	3.75E-04
10	7.80E-05	8.24E-05	8.27E-05	8.27E-05	8.19E-06	7.03E-06	3.05E-04	3.72E-04
11	8.28E-05	8.25E-05	1.65E-04	8.27E-05	8.32E-06	1.40E-05	3.26E-04	3.74E-04
12	8.28E-05	8.26E-05	8.28E-05	8.28E-05	8.89E-06	7.03E-06	3.33E-04	3.75E-04
Average	8.09E-05	8.25E-05	1.10E-04	8.27E-05	9.25E-06	9.37E-06	3.22E-04	3.73E-04

analysis determines better estimates of the blocking probabilities as opposed to the link-centric approach of the EFPA where all streams offered to a link are assumed to experience the same link blocking probability. This last feature may not be evident in a network scenario where all streams are offered with Poisson traffic of the same load but it can be shown that it substantially improves accuracy in the case where each path is offered with streams of different values of peakednesses. A simple example is illustrated in Figure 4.6 where a network link l is offered with two streams of the same load and different peakedness values. In case (a) a path-centric approach is adopted by using the BPP method as presented in [28] and described in Chapter 3, thus evaluating the blocking probability associated with each path separately. In case (b) a link-centric approach is considered like in the EFPA, where the blocking probability experienced by the two streams is equal to the link blocking.

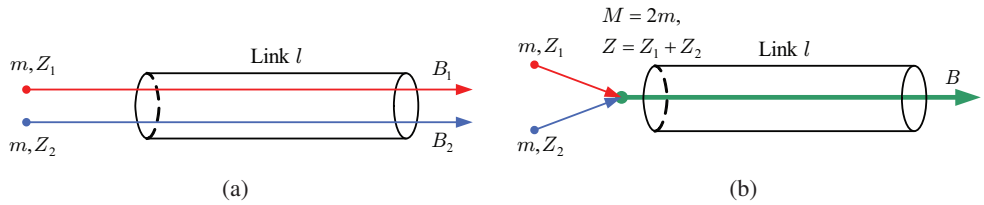

Figure 4.6: Path-centric approach (a) vs link centric approach (b).

In this case the link is offered with a traffic stream resulting from the aggregation of the two streams, with a total load equal to $M = 2m$ and a total peakedness equal to $Z = Z_1 + Z_2$. The blocking probability B can be calculated by applying once again the BPP method which, for the single offered stream case, is reduced to the following formula

$$B = T\left[1 + \frac{W}{M}(Z-1)\right], \tag{4.10}$$

where T and W are respectively the time congestion and the number of wavelength channels of link l. The time congestion T can be evaluated with the following recursion

$$T^{(k)} = \frac{q(w+k-1)T^{(k-1)}}{k + q(w+k-1)T^{(k-1)}} \qquad k = 1, \ldots, W, \tag{4.11}$$

with $T^{(0)} = 1$ and where $q = 1 - 1/Z$, $w = M/(Z-1)$.

For example, let us assume that link l comprises $W = 32$ wavelength channels being offered with two streams of same mean intensity $m = 0.3$ Erlangs and with peakedness given by $Z_1 = 2$ and $Z_2 = 0.8$. In a link-centric approach, by applying (4.10) we obtain the same blocking $B = 0.0083$ for both streams; however, using the BPP method for each stream separately we obtain two different values of blocking probability, that is $B_1 = 0.0159$ and $B_2 = 0.0039$. This feature is particularly advantageous when considering FDLs in the node model as illustrated in in the examples of Figures 3.22 and 3.23. In this case the FDL is offered with multiple streams overflowing from the outgoing links of the node, each one with different load and peakedness. Clearly, in this situation a path-centric approach would be preferable than a link-centric one which would yield a single value of blocking for all streams.

Although significant for the accuracy of the obtained results, this is not yet the major advantage of the proposed network model which instead is illustrated when traffic is not Poisson. In this case, the EFPA-S can not be applied as the traffic is not Poisson whereas the SBNM allows accurate estimation of the values of blocking probabilities for smooth and peaked burst traffic conditions. For example, the average relative error in Table 4.4 for peaked traffic is respectively ≈ 15 % for the SBNM and ≈ 74 % if applying the EFPA-S;

additionally, for smooth traffic the relative error of the analysis is ≈ 1.3 % as opposite to the EFPA-S where the error reaches almost an order of magnitude.

4.4.3 Buffered Case: Employment of FDLs

In this case each node is employed with an FDL comprising a number of virtual buffers ranging within the interval $[0, K_{max}]$ with $K_{max} = W/2$ virtual buffers. Similarly to the node analysis presented in Chapter 3, a comparison with a Poisson model of the FDL-buffered network has been made by using again the model proposed in [66]. Particularly, the blocking probability B_l associated with link l is approximated by using Equation (3.53) similarly to the evaluation of the blocking probability B_p of output port p made in Chapter 3 for the multi-port switch analysis. Once B_l is evaluated for all $l \in \mathcal{L}$, the EFPA-S can be finally applied to estimate end-to-end blocking probabilities by using the calculated values of link blocking probabilities in Equation (4.1) where Equation (4.2) is replaced by Equation (3.53). Figures 4.7 and 4.8 illustrate the accuracy of the proposed network model compared with simulation results and with the modified version of the EFPA discussed above. Note how the analytic model performs quite favourably when compared with simulation data for all traffic peakednesses. For the Poisson case the proposed network model substantially outperforms the $M/M/W/W + K$ model for increasing number of FDL channels (note that both analyses yield to almost the same performance when the number of virtual buffers is low). This is particularly evident in Figure 4.8 where, for a number of virtual buffers greater than 10, the error introduced by the modified EFPA-S is approximately of an order of magnitude. Conversely, the SBNM successfully follows the shape of the blocking curves, yielding a maximum relative error of ≈ 26.5 % for $W = 16$ and $K = 8$ as opposed to a ≈ 300 % relative error introduced by the modified EFPA-S for the same case. Furthermore, note that the analytic network model accurately estimates the value of blocking probabilities for different peakedness, an advantage that can not be offered with the application of the EFPA.

Figures 4.9-4.14 illustrate the average end-to-end blocking probability of the network for increasing numbers of virtual buffers and different offered loads, whereas Figures 4.15 and 4.16 give a detailed insight into the isolated blocking probability values experienced by

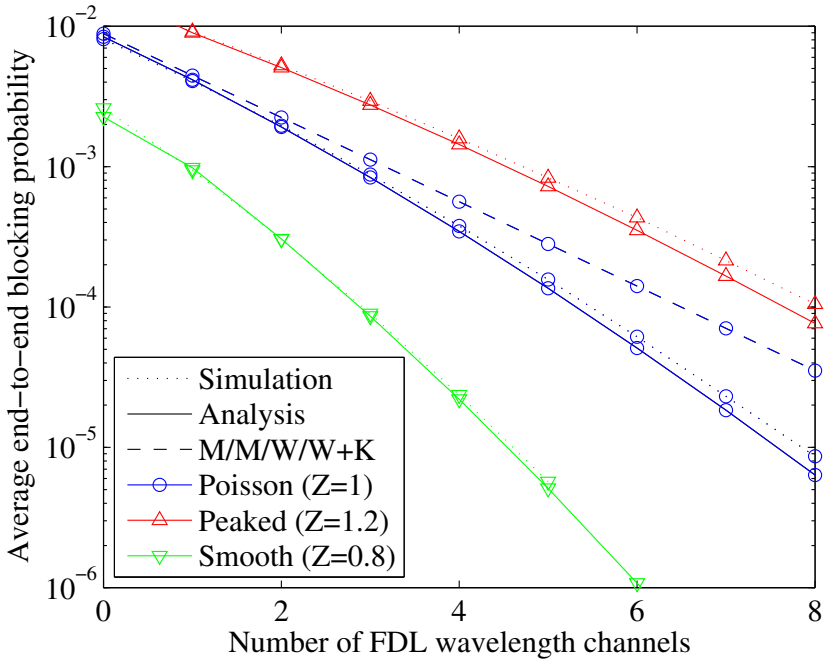

Figure 4.7: Average end-to-end burst blocking probability vs number of FDL wavelength channels for $W = 16$. Each path is offered Poisson traffic with $\rho = 0.25$ Erlangs per channel.

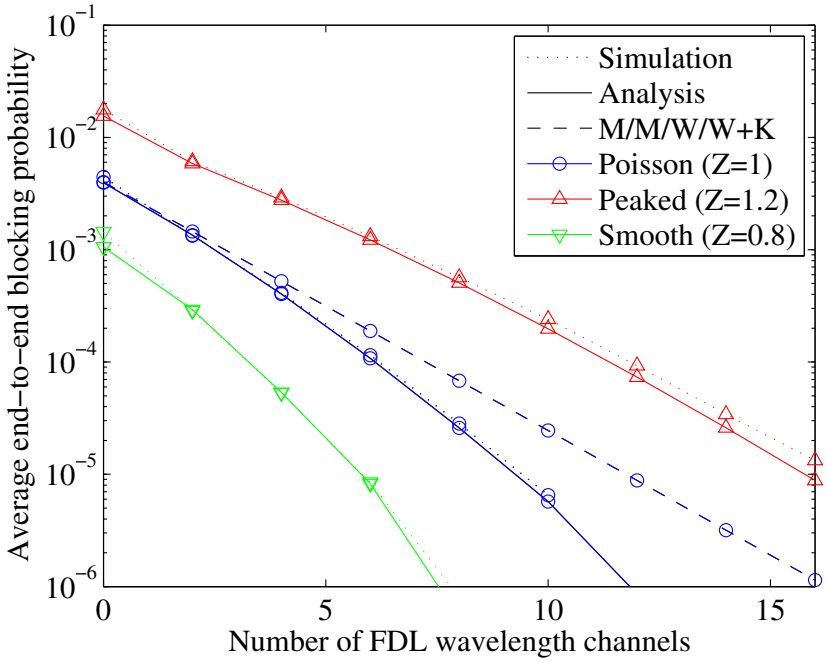

Figure 4.8: Average end-to-end burst blocking probability vs number of FDL wavelength channels for $W = 32$. Each path is offered Poisson traffic with $\rho = 0.3$ Erlangs per channel.

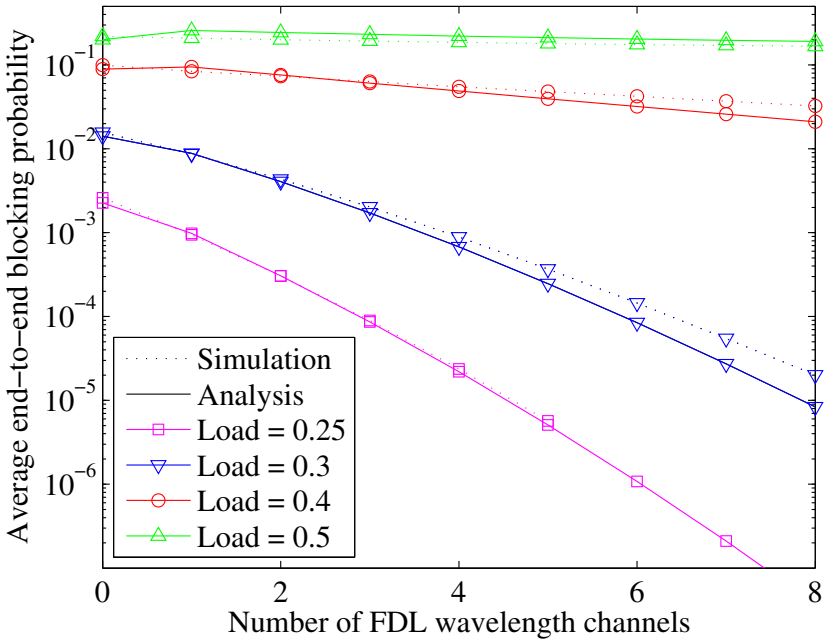

Figure 4.9: Average end-to-end burst blocking probability vs number of FDL wavelength channels for $W = 16$ and $Z = 0.8$. Normalised loads per path are in Erlangs.

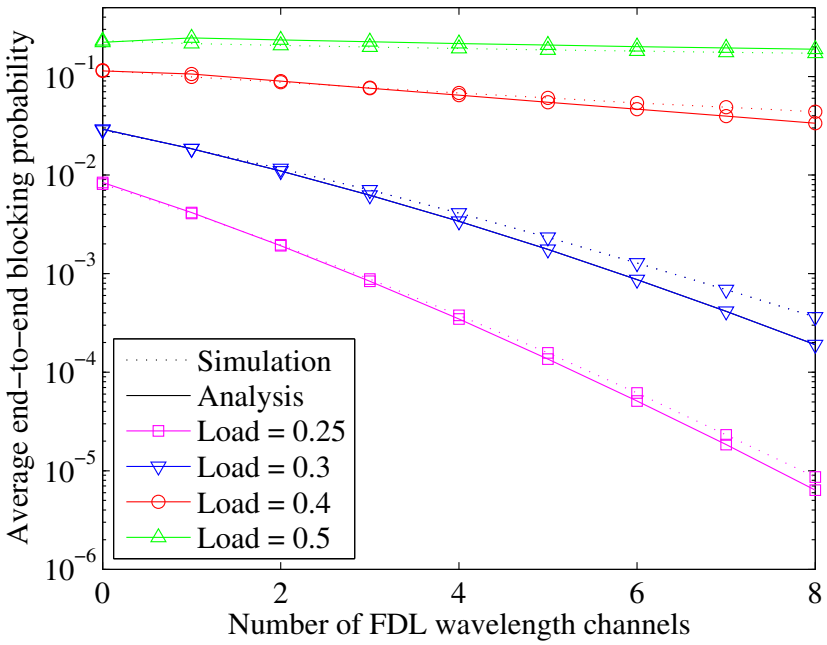

Figure 4.10: Average end-to-end burst blocking probability vs number of FDL wavelength channels for $W = 16$ and $Z = 1$. Normalised loads per path are in Erlangs.

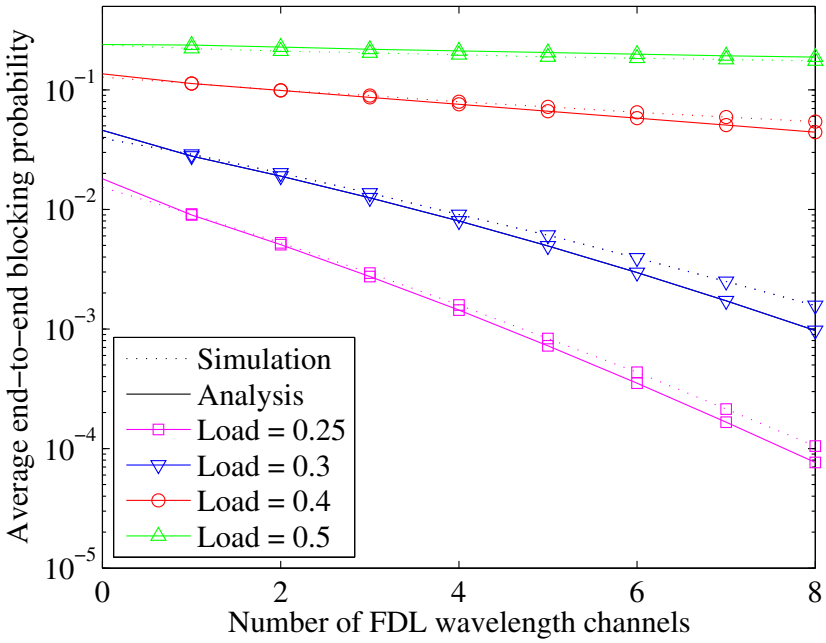

Figure 4.11: Average end-to-end burst blocking probability vs number of FDL wavelength channels for $W = 16$ and $Z = 1.2$. Normalised loads per path are in Erlangs.

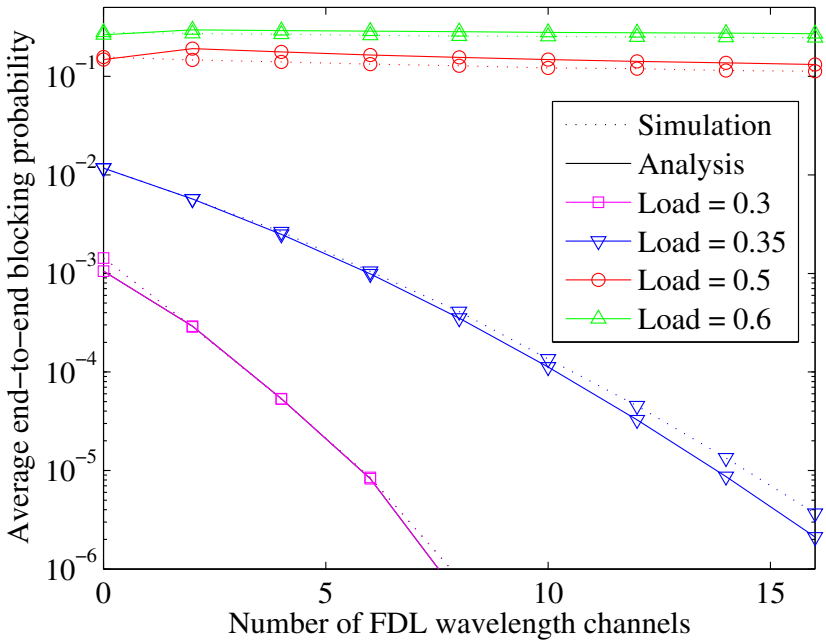

Figure 4.12: Average end-to-end burst blocking probability vs number of FDL wavelength channels for $W = 32$ and $Z = 0.8$. Normalised loads per path are in Erlangs.

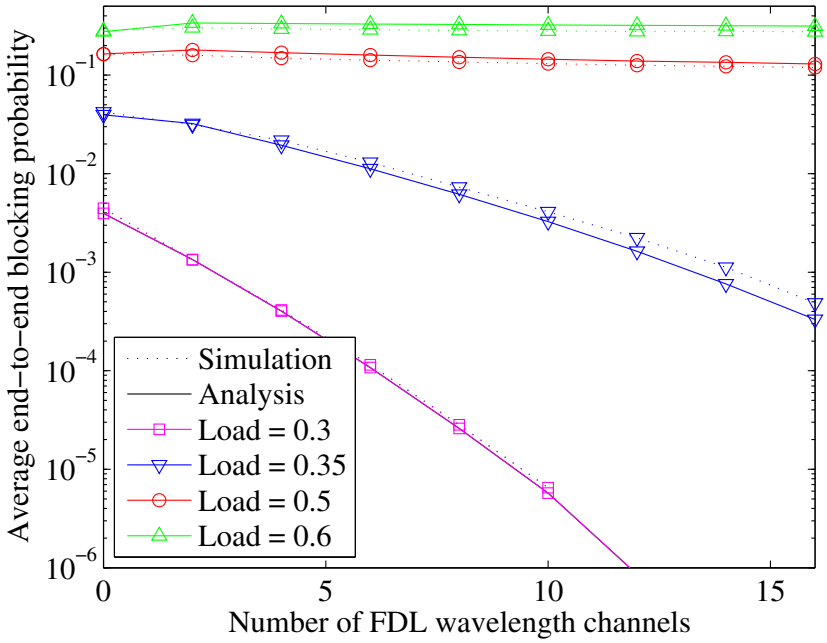

Figure 4.13: Average end-to-end burst blocking probability vs number of FDL wavelength channels for $W = 32$ and $Z = 1$. Normalised loads per path are in Erlangs.

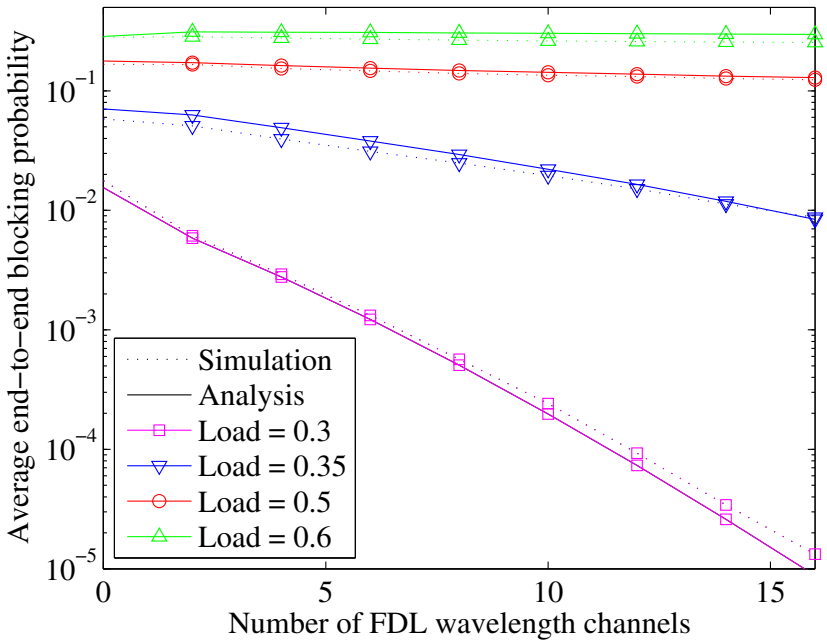

Figure 4.14: Average end-to-end burst blocking probability vs number of FDL wavelength channels for $W = 32$ and $Z = 1.4$. Normalised loads per path are in Erlangs.

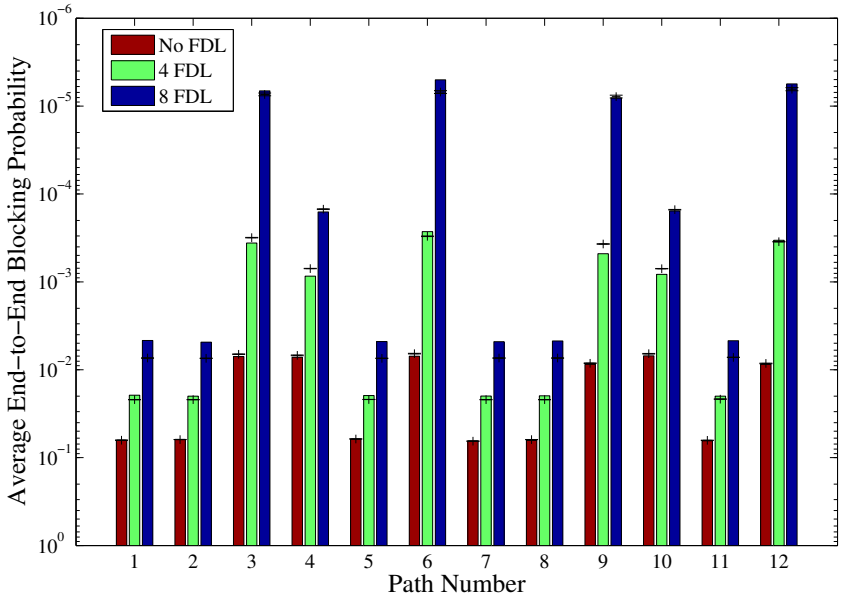

Figure 4.15: NSF network end-to-end blocking probabilities for $W = 16$. Each path is offered with Poisson traffic of load equal to 0.25 Erlangs per wavelength channel. Simulation data is depicted with error bars representing 95% level confidence intervals.

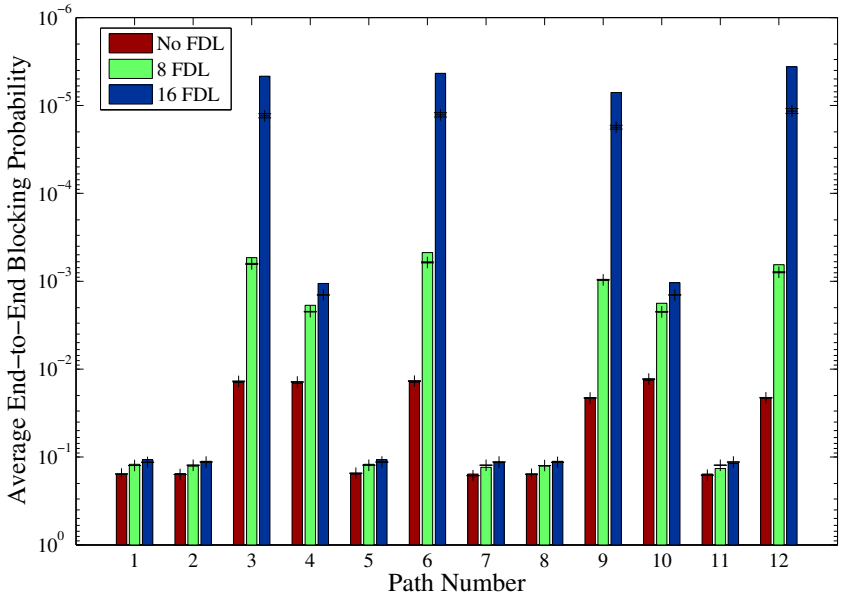

Figure 4.16: NSF network end-to-end blocking probabilities for $W = 32$. Each path is offered with Poisson traffic of load equal to 0.35 Erlangs per wavelength channel. Simulation data is depicted with error bars representing 95% level confidence intervals.

each path for Poisson offered traffic and for 3 different buffer allocation scenarios. Once again, the analytic model generally compares favourably against the obtained simulation data. Particularly, note that even in the less favourable scenario the model can still successfully track the high sensitivity of the blocking probability to the load and to the peakedness of the offered traffic, a feature that is not possible for a one-moment (Poisson) traffic analysis as demonstrated in Figures 4.7-4.8. Figures 4.17 and 4.18 show the average end-to-end blocking probabilities for increasing numbers of FDL virtual buffers and different peakedness values for the case of the EON network topology. The same conclusions on the accuracy of the model made for the NSF network topology can be drawn for this case. Once again, note how the model allows to track successfully the sensitivity of the blocking probability to the peakedness of the offered traffic. This is probably the most important advantage offered by the proposed network model that makes it suitable for OBS network dimensioning; however note that the accuracy of the method tends to diminish for increasing number of virtual buffers. For example, note that in Figure 4.16 the relative error of the blocking probabilities for paths 3, 6, 9, 12 is ≈ 55 %. This is mainly due to the fact that, when the number of channels in the FDL is high, the amount of traffic that is re-offered to the output port increases and it challenges the assumption of independence between the flows made in the adoption of Equation (3.27). Even if this source of error is small within the node analysis (as shown in Chapter 3), it can substantially increase the inaccuracy in the network model. This is probably the major limitation of the proposed network analysis, since it may be difficult to accurately model networks with FDLs comprising a very high number of virtual buffers. An improvement in this direction may be achieved by conducting a detailed analysis of the FDL behaviour within the node model but it would yield to a much more complex analysis, most likely resulting in the derivation of an intractable network model. For example, the accuracy of the network could be improved (in principle) by modelling each buffered node as a queuing system with multiple preemptive priority streams where the arrival process is assumed to be generally distributed. This may be a very difficult challenge to resolve and, to the knowledge of the author, progress in this direction has been made only for a queuing system with Poisson arrival processes. Nevertheless, the network model, even for limited numbers of FDL virtual buffers, can still prove to be useful for per-

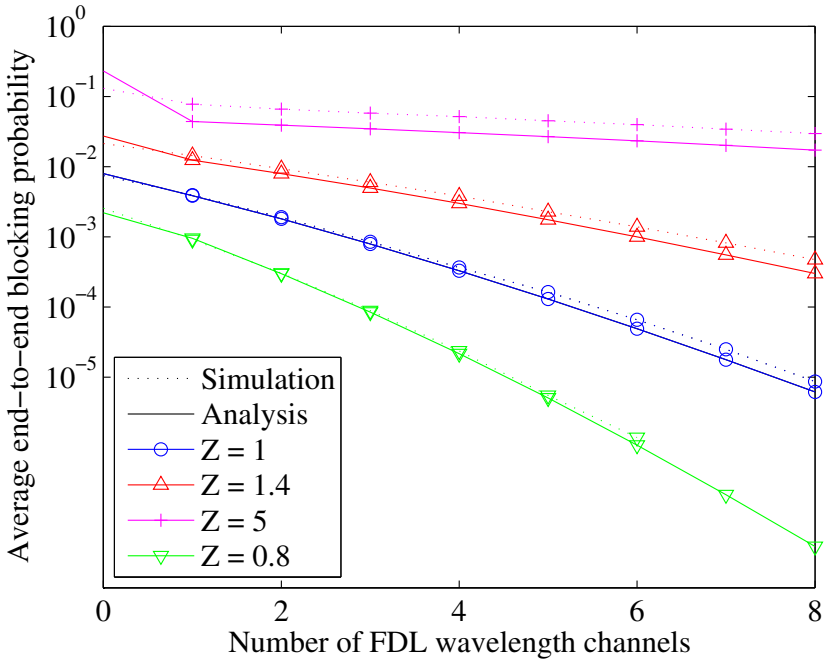

Figure 4.17: Average end-to-end blocking probability of the EON topology where $W = 16$ and each path is offered with $\rho = 0.25$ Erlangs per channel.

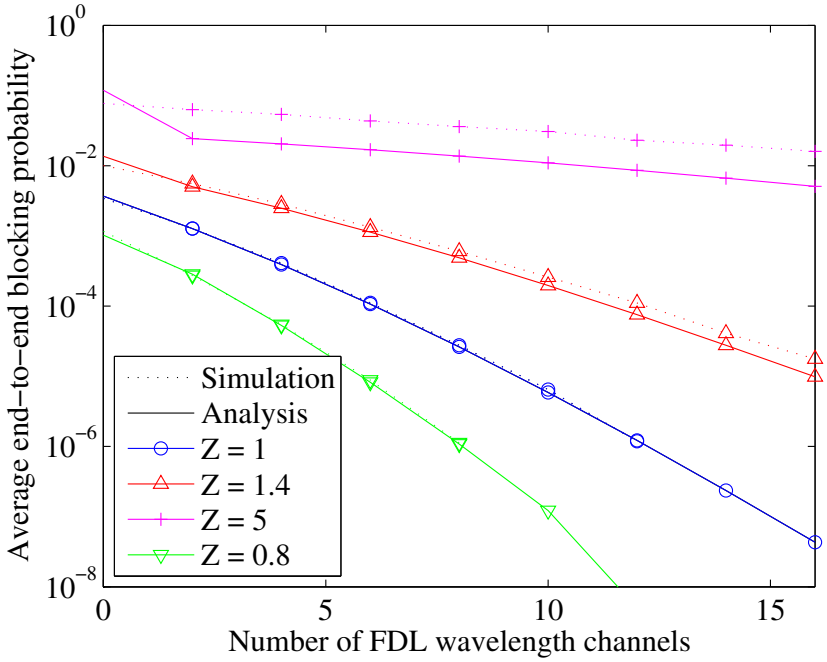

Figure 4.18: Average end-to-end blocking probability of the EON topology where $W = 32$ and each path is offered with $\rho = 0.3$ Erlangs per channel.

formance evaluation of OBS networks. In fact as shown in [40] and discussed in Chapter 3, the effectiveness of FDLs becomes lower when increasing the number of virtual buffers (see Table 3.5), thus suggesting that for network planning it would be more cost-effective to use FDLs with low numbers of virtual buffers. Additionally, the channel efficiency of an OBS network is already considerably high when network links comprise a very high number of wavelength channels, so that FDLs may not be cost-effective or be required at all. Furthermore note that targeting operating loads with FDLs in these situations may be disadvantageous since the sensitivity of blocking to small variations in load may become unmanageable. Finally, the complexity of OBS channel scheduling may not scale very well with increasing number of channels, particularly with void filling scheduling. So all in all, it would be the opinion of the author that the FDL-buffered switch architecture presented is in itself most likely limited to low number of virtual buffers (an example of a state-of-the-art OBS testbed for a similar OBS node architecture is presented in [63]). Note also that, for some paths, the addition of the same number of FDLs is not equally effective (e.g., paths 3 and 4 on Figure 4.16). This suggests that it would be advantageous to optimise the number of FDLs allocated at each node in order to balance and improve the network performance for a given outlay on FDL hardware, a subject that will be investigated in the next chapter.

Figure 4.19 illustrate the behaviour of the average and maximum link utilisation for increasing values of target blocking probabilities. We consider again the EON topology where each link comprises 32 wavelength channels. These graphs give an insight of the effectiveness of the FDLs in increasing the offered load required to operate the network at a desired performance level defined by a specific value of burst loss. For example, note that in order to operate the network at a burst blocking probability equal to 10^{-5} for Poisson traffic, the average link utilisation for the bufferless case is about 25%. If instead an FDL containing 32 virtual buffers is employed at each network node, the utilisation increases up to approximately more than 50%. Note once again how the peakedness of the offered traffic has a considerable impact on both the average and maximum utilisation. Particularly, when $Z = 4$, the average link utilisation is only about 30% (more than 20% less than in the Poisson case) for target blocking of 10^{-5} when $K = 32$ FDL wavelength channels. In the bufferless case, for the same value of link utilisation, the maximum performance achievable

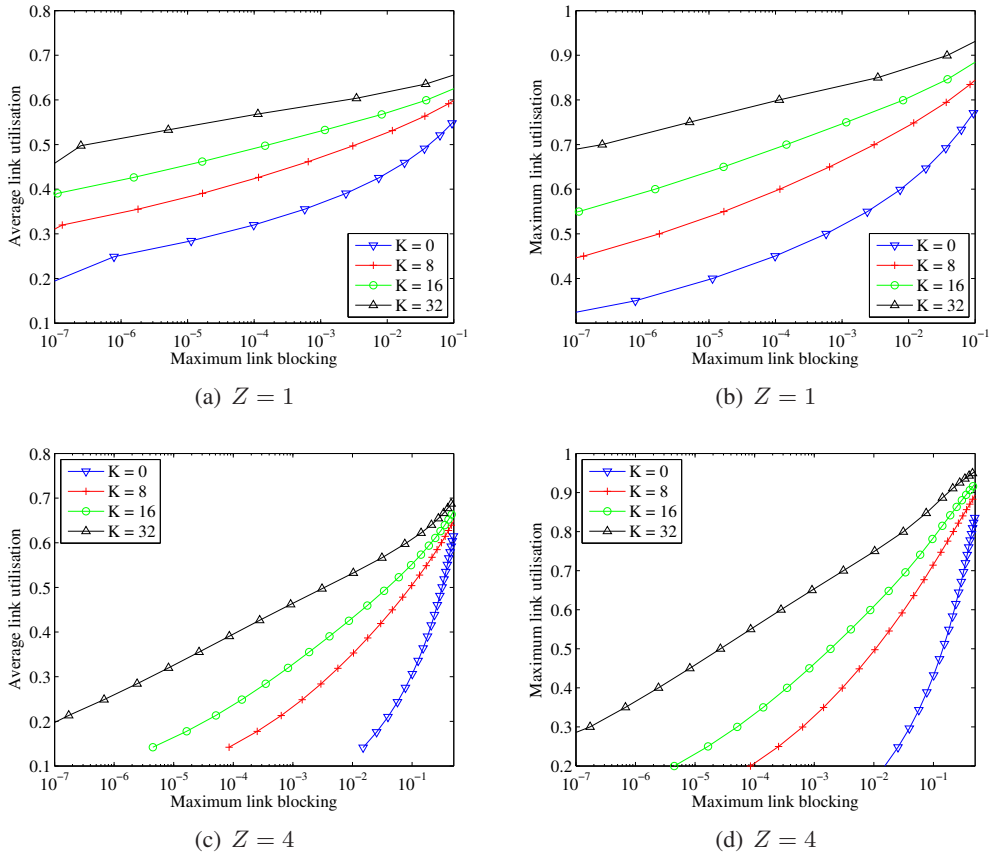

(a) $Z = 1$ (b) $Z = 1$

(c) $Z = 4$ (d) $Z = 4$

Figure 4.19: Average and maximum link utilisation vs maximum target burst blocking probability for the EON topology with $W = 32$ wavelength channels.

is no less than 10^{-1}.

The accuracy of the model is challenged for the mesh network topology depicted in Figure 4.20 where the average node degree is between 3 and 4. The network is defined by $N = 20$ nodes and $L = 32$ bidirectional links all comprising $W = 64$ wavelength channels. Burst traffic is offered to $R = 100$ randomly selected routes amongst the set of source-destination shortest paths calculated with the Dijkstra algorithm. Once again the peakedness values range from 0.8 to 1.4. Each FDL is equipped with $K = 32$ virtual buffers for each node of the network. Figure 4.21 illustrates the end-to-end blocking probabilities of selected paths for different values of offered load. The paths have been chosen in order to show the behaviour of the model for different values of burst blocking probability. They also give an insight of the accuracy of the model at very high values of burst blocking probabilities. Note that in this case the error is higher than in the previously illustrated scenarios. As discussed

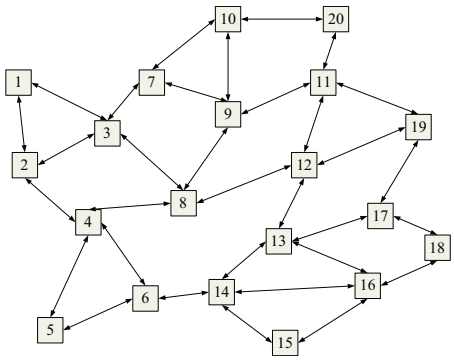

Figure 4.20: Mesh network topology under study.

before this mainly depends on the fact that the amount of burst traffic carried back from the FDLs is increased, challenging the assumption of independence between traffic flows made in the derivation of the node model. Nevertheless the model still compares quite favourably for high loads and approximately follows the shape of the blocking curves.

4.5 Conclusions

This chapter dealt with the derivation of a buffered OBS network model where contentions are resolved with the employment of a share-per-node FDL. The analysis has been built on the basis of the OBS node model derived in Chapter 3 and allows evaluation of the performance of an OBS network in terms of end-to-end and link blocking probabilities. The accuracy of the method has been validated by comparing the analytic results with results obtained from discrete-event simulations of a NSF and a EON network topologies. The proposed technique outperforms well-known OBS network models proposed in literature and generally compares quite favourably with simulation data for a broad range of parameters of interest such as link wavelength channels, number of virtual buffers, offered load and peakedness. The main drawback of the proposed methodology consists in a lower accuracy when increasing the number of FDL virtual buffers employed at each node, however the model is still applicable for a considerable variety of realistic network scenarios, thus proving itself suitable for resolving OBS resource dimensioning problems as shown in the next chapter.

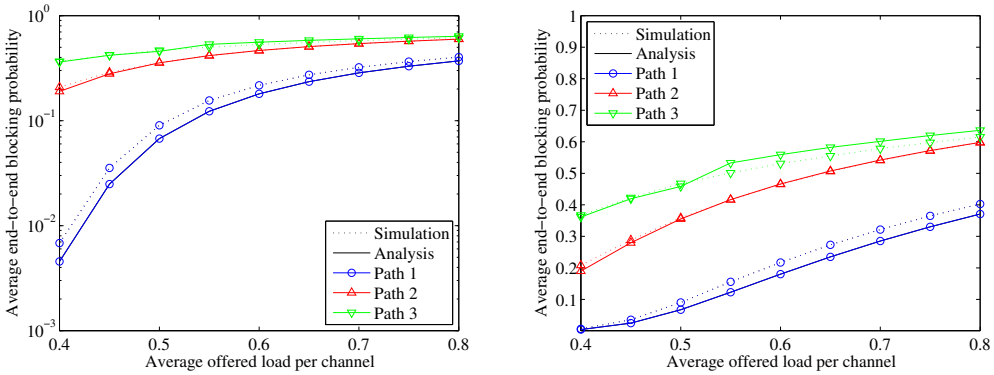

(a) Logarithmic scale, $Z = 1$

(b) Linear scale, $Z = 1$

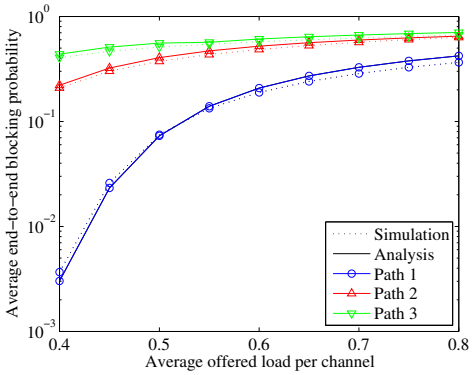

(c) Logarithmic scale, $Z = 1.4$

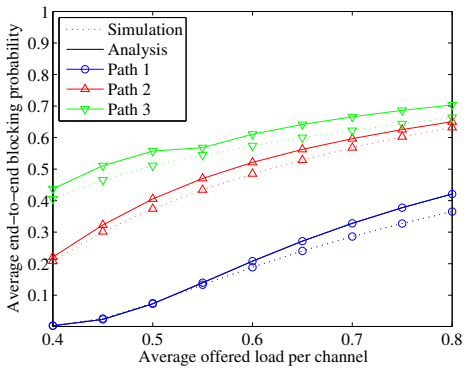

(d) Linear scale, $Z = 1.4$

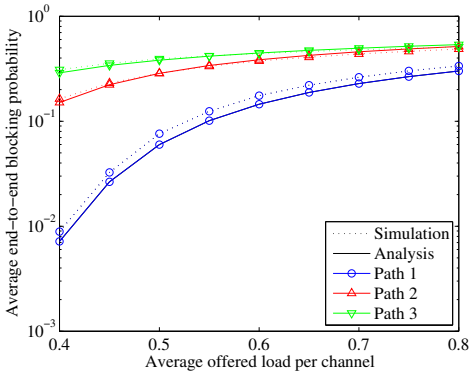

(e) Logarithmic scale, $Z = 0.8$

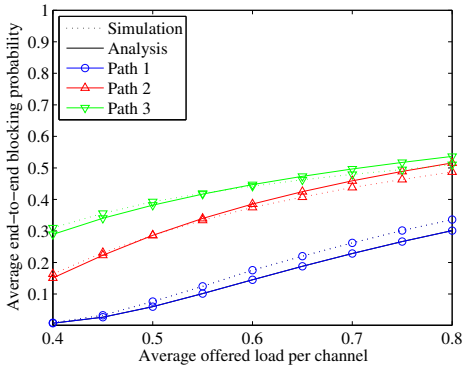

(f) Linear scale, $Z = 0.8$

Figure 4.21: Average end-to-end blocking probability of selected network paths for the mesh network topology, with $W = 64$ wavelength channels and $K = 32$ FDL virtual buffers.

Chapter 5

Resource Dimensioning of the OBS Network

This chapter studies the dimensioning of OBS network resources in terms of optimal allocation of link channels and virtual buffers. A general overview of this subject and the main motivation for resource optimisation are discussed in Section 5.1. The definition of four resource allocation problems is presented in Section 5.2 on the basis of cost functions quantifying the total network hardware expenditures and on the OBS network model derived in Chapter 4. The defined problems are then resolved by means of a single/multi-objective genetic algorithm as described in Section 5.3 where the main properties of the algorithm are shown. Results obtained with the presented optimisation techniques are illustrated and commented on in Section 5.4. Conclusions are finally drawn in Section 5.5.

5.1 Why Optimise?

The optimal design of a network is critical for the realisation of cost-efficient network infrastructure that guarantees a desired grade of performance at minimal hardware cost. This applies not only to OBS networks but to any general network. The process of planning a cost-efficient network is defined by several phases that can be iteratively solved as illustrated in [42]. Some examples of such operations include, but are not limited to, (i) determining the network topology, (ii) deciding the switching equipment, (iii) routing the traffic and (iv)

optimally allocating the network resources. The study of the entire planning process is very broad and it may be challenging to conduct an overall detailed analysis of all its aspects. Typically, researchers focus their attention only on one or a few of these activities and this thesis is no exception. Particularly, this chapter deals with the problem of finding an optimal allocation and capacity of network resources necessary to meet performance requirements at minimal cost. This fundamental question in relation to OBS networks can be stated in the following way.

Define a specific OBS network topology represented by graph $\mathcal{G}(\mathcal{N}, \mathcal{L}, \mathcal{R})$ where, similarly to Chapter 4, N is the number of nodes, L the number of links and R the number of paths. Additionally, assume burst traffic demands for each path represented by mean and variance vectors $\boldsymbol{\rho}$ and $\boldsymbol{\psi}$. Given these inputs, the goal is to determining an optimal allocation of link wavelength channels and of FDL virtual buffers in order to guarantee a pre-defined level of performance in terms of end-to-end burst blocking probability and to minimise the total hardware cost associated with the deployment of the network. The following example illustrates the importance of determine an optimal resource dimensioning of the network. Consider the buffered OBS EON network topology of the previous chapter where each link comprises $W = 32$ wavelength channels and each path is offered with Poisson traffic of mean intensity equal to 0.35 Erlangs. Assume that the maximum tolerable end-to-end blocking value for each path is given by $\mathcal{P}_{max} = 10^{-3}$. Figure 5.1 illustrates the end-to-end blocking probabilities in the bufferless case, where the maximum tolerable blocking probability is indicated with a dashed red line. Note that the performance level requirements are not met for any paths. The situation is different for the case depicted in Figure 5.2 where each node is equipped with a shared FDL offering 10 virtual buffers. In this case all end-to-end blocking probabilities are below the maximum tolerable value $\mathcal{P}_{max} = 10^{-3}$ at a total hardware cost corresponding to 180 FDL virtual buffers. Figure 5.3 illustrates the same scenario where this time the allocation of FDL virtual buffers is represented by vector K=[0 10 0 10 9 10 8 6 0 8 8 8 0 0 10], where each element K_n corresponds to the number of virtual buffers at node n. In this case the total number of virtual buffers is lower than the previous case, resulting in a total hardware cost corresponding to the employment of 87 FDL virtual buffers, however each individual end-to-end blocking

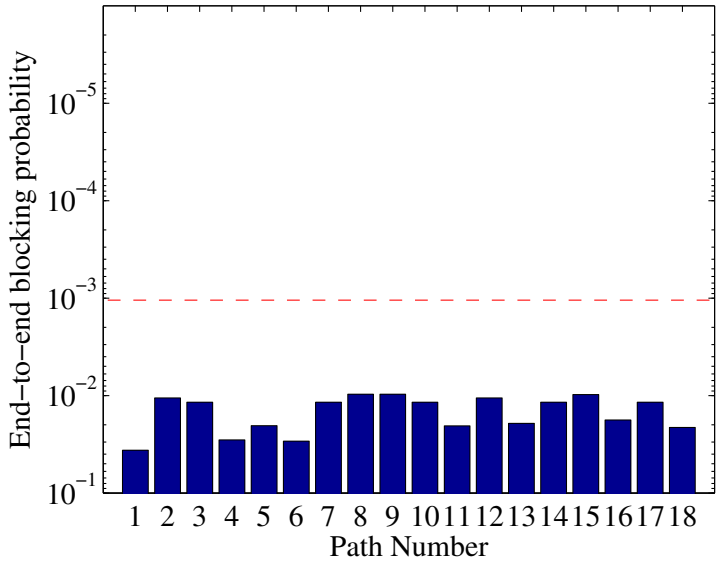

Figure 5.1: End-to-end blocking probabilities of the EON OBS network with no FDL virtual buffers.

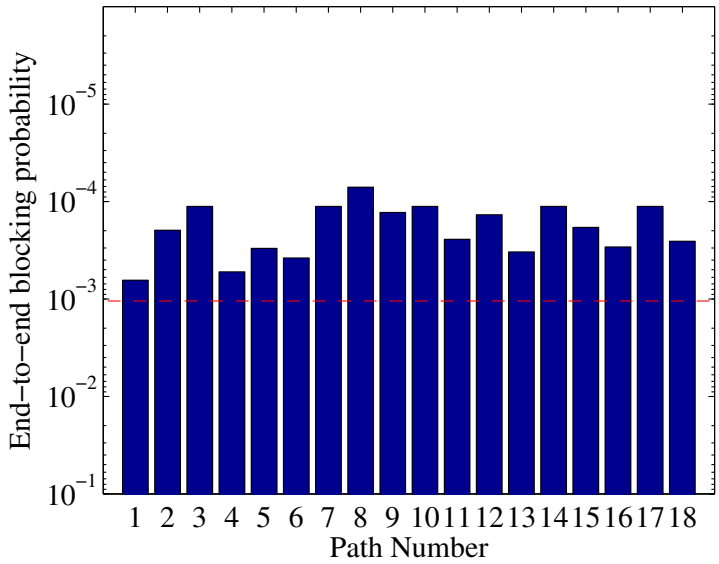

Figure 5.2: End-to-end blocking probabilities of the EON OBS network with 10 FDL virtual buffers per node.

probability still meets the performance level requirements. This suggests that it may be possible to further minimise the total hardware cost of the network and still meet the same loss performance levels of a uniform virtual buffer allocation by finding an optimal **K**. This chapter deals with this problem.

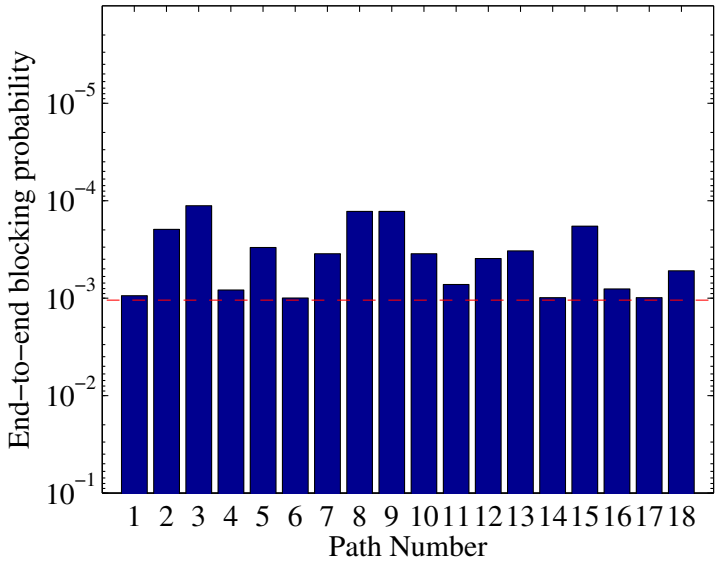

Figure 5.3: End-to-end blocking probabilities of the EON OBS network with FDL allocation **K** = [0 10 0 10 9 10 8 6 0 8 8 8 0 0 10].

The optimisation of optical networks is a topic that has been extensively investigated by the research community, mainly in relation to the *Routing and Wavelength Assignment* (RWA) problem. Although several works have been proposed on OBS network optimisation, little attention has been devoted to the problem of the optimal allocation of resources such as link wavelength channels and FDL virtual buffers dimensioning. Notable exceptions have been proposed in [29] where genetic algorithms are used to jointly derive optimal routing and link channel allocation for bufferless OBS networks. Castro et al. presents in [19] a method to optimise the number of FDLs in a buffered OBS network where the analytic model of the node is based on the one derived in [66] and the optimal solution is found by means of Tabu Search. This is probably the work that is most similar to the optimisation process proposed in this chapter. Nevertheless, the network model is capable of handling only Poisson offered traffic and all network links are simply modelled as $M/M/W/W+K$ queues (where W is the number of wavelength channels per link and K the number of shared FDLs per port), resulting in a less accurate analysis when compared to the one presented in the previous chapter. This chapter deals with the use of genetic algorithms to jointly determine the optimal allocation of link wavelength channels and FDL virtual buffers for minimising the hardware cost of an OBS network under a maximum tol-

erable end-to-end burst loss. The architecture of each node is based on the TAS-shFDL configuration as described in Chapters 3 and 4.

5.2 Definition of the Optimisation Problems

In this section we introduce four optimisation problems based on the analytic model of the OBS network described and validated in Chapter 4. We start by introducing a cost function that will be used to define the objectives of the optimisation problems. Following [40] and on the basis of the TAS-shFDL architecture analysis described in Chapter 3, we determine the total equipment cost arising from the employment of a feedback FDL in an OBS node. Once again we indicate with W_l the number of wavelength channels of link l for $l = 1, \ldots, L$ and with K_n the number of FDL virtual buffers at node n for $n = 1, \ldots, N$. Furthermore we indicate with P_n the number of output ports of node n.

As discussed in Chapter 3, for the TAS-shFDL architecture, the installation of an extra input/output port dedicated to the FDL requires one additional EDFA. Furthermore, since we are assuming full wavelength conversion, each wavelength channel of the FDL must have a dedicated TWC, for a total of K_n TWCs. Finally, in order to send burst packets to the FDL, each wavelength channel on each output port requires an additional SOA, for a total of $\sum_{\forall l \in n} W_l$ SOAs. Note that, similarly to Chapter 4, we have made an abuse of notation by indicating with $l \in n$ that a link l is connected to an output port of node n. Similarly, in order to send packets to the output ports, each wavelength channel of the FDL requires P_n SOAs for a total of $P_n \cdot K_n$ SOAs. Under these premises, we define the total cost associated with allocation of an FDL to node n as

$$C_n^{FDL} = c_E + c_T K_n + c_S \left(\sum_{l \in n} W_l + P_n K_n \right), \tag{5.1}$$

where we have denoted with c_E, c_T and c_S respectively the unit cost of an EDFA, of a TWC and of a SOA. Furthermore, each link connected to an output port of node n requires at least 2 EDFAs, W_l TWCs and $P_n \cdot W_l$ SOAs. Thus, the hardware cost associated with

the output ports of node n can be determined as

$$C_n^{links} = 2P_n c_E + c_T \sum_{l \in n} W_l + c_S P_n \sum_{l \in n} W_l. \tag{5.2}$$

Therefore, the total hardware cost of node n is expressed as

$$\begin{aligned} C_n &= C_n^{links} + C_n^{FDL} = \\ &= 2\left(P_n + 1\right) c_E + c_T \left(\sum_{l \in n} W_l + K_n \right) + c_S \left[(P_n + 1) \sum_{l \in n} W_l + P_n K_n \right]. \end{aligned} \tag{5.3}$$

We can rewrite function C_n as $C_n = C_n^{fix} + C_n^{var}$ where $C_n^{fix} = 2(P_n + 1)c_E$ is the fixed part of the total cost depending exclusively on the installation of the output links and of the FDL whereas $C_n^{var} = c_T(\sum_{l \in n} W_l + K_n) + c_S[(P_n + 1)\sum_{l \in n} W_l + P_n K_n]$ is the variable part of the total cost depending on how many wavelength channels and how many virtual buffers are employed for node n. Note that $C_n^{fix} = 2(P_n + 1)c_E$ when $K_n > 0$ and $C_n^{fix} = 2P_n \cdot c_E$ if $K_n = 0$. Finally, the total hardware cost of the network can be defined as

$$C(\mathbf{W}, \mathbf{K}) = \sum_{\forall n} C_n = \sum_{\forall n} (C_n^{fix} + C_n^{var}), \tag{5.4}$$

where $\mathbf{W} = [W_1, \ldots, W_L]$ and $\mathbf{K} = [K_1, \ldots, K_N]$ are vectors representing respectively the link wavelength channels allocation and the FDL virtual buffers allocation of the network. Under these premises, the following problems can be defined:

5.2.1 Problem 1

Given an OBS network defined by graph $\mathcal{G}(\mathcal{N}, \mathcal{L}, \mathcal{R})$ where each link l comprises the same number of wavelength channels W and where the traffic demands are quantified by vectors

$\boldsymbol{\rho}$ and $\boldsymbol{\psi}$, minimise the network cost function C as follows,

$$\begin{aligned} \underset{\mathbf{K}}{\text{minimise}} \quad & C(\mathbf{K}) \\ \text{subject to} \quad & \mathcal{P}_r(\mathbf{K}) \leq \mathcal{P}_{max}, && r = 1, \ldots, R, \\ & K_{min} \leq K_n \leq K_{max}, && n = 1, \ldots, N, \\ & K_n \in \mathbb{N}_0, \end{aligned} \tag{5.5}$$

where we have indicated with $\mathcal{P}_r(\mathbf{K})$ the end-to-end blocking probability on route r for a given allocation $\mathbf{K}$ of FDLs to network nodes. Furthermore, $\mathcal{P}_{max}$ the maximum tolerable end-to-end blocking probability and with K_{min} and K_{max} respectively the minimum and the maximum number of virtual buffers that can be allocated in a network node. Note that two types of constraints are considered in this problem:

- a *performance level* constraint given by $\mathcal{P}_r(\mathbf{K}) \leq \mathcal{P}_{max}$ for $r = 1, \ldots, R$. This constraint is used to reflect situations in which the maximum tolerable level of burst loss experienced by all customers over every path of the network must be lower or equal to $\mathcal{P}_{max}$.

- a *physical* constraint given by $K_{min} \leq K_n \leq K_{max}$ for $n = 1, \ldots, N$. The number of FDL virtual buffers employed in the node influences the architectural complexity of the node itself; in fact, it yields an increase of the number of SOAs to be employed at each link and at the FDL, thus potentially limiting the physical (and economical) realisation of the switch. Hence, limits on the maximum and minimum value of K_n are considered in order to reflect more realistic scenarios.

The problem defined above falls into the category of mixed integer nonlinear programming problems, a branch of NP-hard problems that is particularly challenging to solve. Several methods can be found in the literature that attempt to overcome the complexity in solving the issues related to this class of problem, such as Lagrangian relaxation, decomposition methods, branch and bound algorithms etc. [83]. This thesis relies on the application of genetic algorithms to solve the proposed problems as it will be discussed in Section 5.3.

5.2.2 Problem 2

Given an OBS network defined by graph $\mathcal{G}(\mathcal{N}, \mathcal{L}, \mathcal{R})$ where the traffic demands are quantified by vectors $\boldsymbol{\rho}$ and $\boldsymbol{\psi}$, minimise the network cost function C as follows,

$$\begin{aligned} \underset{\mathbf{W},\mathbf{K}}{\text{minimise}} \quad & C(\mathbf{W}, \mathbf{K}) \\ \text{subject to} \quad & \mathcal{P}_r(\mathbf{W}, \mathbf{K}) \leq \mathcal{P}_{max}, && r = 1, \ldots, R, \\ & K_{min} \leq K_n \leq K_{max}, && n = 1, \ldots, N, \\ & W_{min} \leq W_l \leq W_{max}, && l = 1, \ldots, L, \\ & K_n \in \mathbb{N}_0, \\ & W_l \in \mathbb{N}, \end{aligned} \tag{5.6}$$

where we have indicated with W_{min} and W_{max} respectively the minimum and the maximum number of wavelength channels that can be allocated in each network link. This problem is equivalent to Problem 1 but in this case the aim is to jointly determine an optimal allocation of link wavelength channels $\mathbf{W}$ and of FDL virtual buffers $\mathbf{K}$ that minimise $C(\mathbf{W}, \mathbf{K})$ under performance level and physical constraints similar to the ones discussed in Problem 1.

5.2.3 Problem 3

Given an OBS network defined by graph $\mathcal{G}(\mathcal{N}, \mathcal{L}, \mathcal{R})$ where each link l comprises the same number of wavelength channels W and where the traffic demands are quantified by vectors $\boldsymbol{\rho}$ and $\boldsymbol{\psi}$, simultaneously minimise the maximum end-to-end loss probability $max(\mathcal{P}_r)$ for $r = 1, \ldots, R$ and minimise the total hardware cost of the network C, that is

$$\begin{aligned} \underset{\mathbf{K}}{\text{minimise}} \quad & max[\mathcal{P}_r(\mathbf{K})] \\ \underset{\mathbf{K}}{\text{minimise}} \quad & C(\mathbf{K}) \\ \text{subject to} \quad & K_{min} \leq K_n \leq K_{max}, \quad n = 1, \ldots, N, \\ & K_n \in \mathbb{N}_0. \end{aligned} \tag{5.7}$$

As opposed to the first two problems, Problem 3 represents an example of a *multi-objective optimisation problem*. In this particular type of problems the concept of optimality of a solution is somewhat weak since the objective functions may be conflicting. For example, a given allocation of FDLs may provide a low maximum end-to-end burst loss but a high hardware cost C whereas another allocation may yield to higher burst loss but lower hardware cost, thus it is difficult to decide which solution is better between the two since it is unclear how to define optimality. Hence, for this particular class of problem it is common to determine not only a unique optimal solution but to select a set of feasible solutions on the basis of their trade-off between the two objective functions. In this case, in order to define optimality, it is necessary to introduce the concept of *dominance* of a solution. Particularly, for a multiple-objective minimisation problem with t objective functions denoted as $f_i(\cdot)$, $i = 1, \ldots, t$, a solution $\mathbf{x}$ is said to *dominate* another solution $\mathbf{y}$ if

$$\forall i : f_i(\mathbf{x}) \leq f_i(\mathbf{y}) \tag{5.8}$$

$$\exists\, j : f_j(\mathbf{x}) < f_j(\mathbf{y}). \tag{5.9}$$

In this case, $\mathbf{y}$ is said to be *dominated* by $\mathbf{x}$ and we denote this relationship as $\mathbf{x} \succ \mathbf{y}$. A solution that is not dominated by any other solution is said to be *Pareto-optimal*.

Figure 5.4 illustrates an example of a set of potential Pareto-optimal solutions for Problem 3, where each solution is represented as a point in the graph. We note that all points in set I are dominated by solution $\mathbf{K}^*$ since they all provide values of end-to-end loss and of total network cost higher than the ones given by $\mathbf{K}^*$. On the contrary, all the points contained in set II are dominating $\mathbf{K}^*$ as they yield values of burst loss and network cost lower than the ones provided by $\mathbf{K}^*$ (if they exist). The set of all Pareto-optimal solutions, that is all the points of the graph that are not dominated by any other point constitute the so-called *Pareto-front*. Typically, the purpose of solving these kind of multi-objective optimisation problems is to determine a good estimate of such a front by finding as many Pareto solutions as possible. These solutions can then be used as available solutions for decision-making problems in realistic network planning scenarios. Thus, the more solutions are available the better it is (ideally all Pareto-optimal solutions would be found).

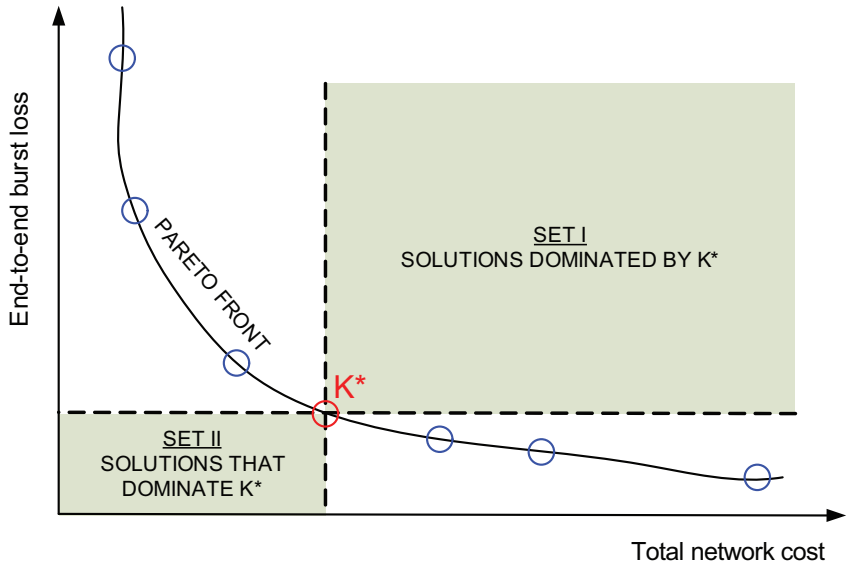

Figure 5.4: Example of Pareto-front.

5.2.4 Problem 4

Given an OBS network defined by graph $\mathcal{G}(\mathcal{N}, \mathcal{L}, \mathcal{R})$ where the traffic demands are quantified by vectors $\boldsymbol{\rho}$ and ψ, simultaneously minimise the maximum end-to-end loss probability $max(\mathcal{P}_r)$ for $r = 1, \ldots, R$ and minimise the total hardware cost of the network C, that is

$$\begin{aligned}
&\underset{\mathbf{W},\mathbf{K}}{\text{minimise}} && max[\mathcal{P}_r(\mathbf{W}, \mathbf{K})] \\
&\underset{\mathbf{W},\mathbf{K}}{\text{minimise}} && C(\mathbf{W}, \mathbf{K}) \\
&\text{subject to} && K_{min} \leq K_n \leq K_{max}, \quad n = 1, \ldots, N, \\
& && W_{min} \leq W_l \leq W_{max}, \quad l = 1, \ldots, L, \\
& && K_n \in \mathbb{N}_0, \\
& && W_l \in \mathbb{N}.
\end{aligned} \tag{5.10}$$

This multi-objective optimisation problem is an extension of Problem 3 where, similarly to Problem 2, the joint optimisation of link wavelength channels and FDL virtual buffers is considered.

5.3 Resolving the Optimisation Problems: Single and Multi-Objective Genetic Algorithm

Genetic algorithms (GAs) [25, 44] are a branch of *evolutionary* algorithms, a family of search heuristics that mimics the process of evolution to find *near-optimal* solutions for optimisation problems. Candidate solutions are classified as near-optimal because, being search heuristics, GAs cannot guarantee global optimality. In a GA, each candidate solution is represented by a string of decision variables called an *individual* (or *chromosome*) where each decision variable corresponds to a *gene*. The algorithm starts by generating an initial random population of individuals. A set of individuals is selected from the population to form a new generation on the basis of "how suitable" they are as solutions of the optimisation problem. The "goodness" of the selected individuals is evaluated by a specific *fitness* function which is typically defined as a combination of the objective functions of the optimisation problem in question. In this way, the better individuals (*parents*) have more chances to "reproduce" and transfer their "good" genes to their children (*offspring*) that will form a better new generation, mimicking the evolution process. The algorithm normally ends when a user-defined maximum number of generations is reached or when some conditions on the improvement achieved by the best individuals are met. Due to their approach based on a search within a given population, GAs allow simultaneous search of different regions of the solutions space and potentially find multiple candidate near-optimal solutions of an optimisation problem in a single run [44]. Figure 5.5 illustrates the main steps defining a genetic algorithm. Each step is described in the next sections in relation to the above defined optimisation problems.

5.3.1 Population and Encoding of the Individuals

The GA is typically initialised by randomly generating a first population of $PopSize$ individuals. The decision on the size of the initial population and on the nature of its individuals is considerably important for finding near-optimal solutions. Generally, the bigger the population, the higher is the diversity of the generated individuals. Preserving a certain degree of diversity in the population is important as it increases the chances of finding near-optimal

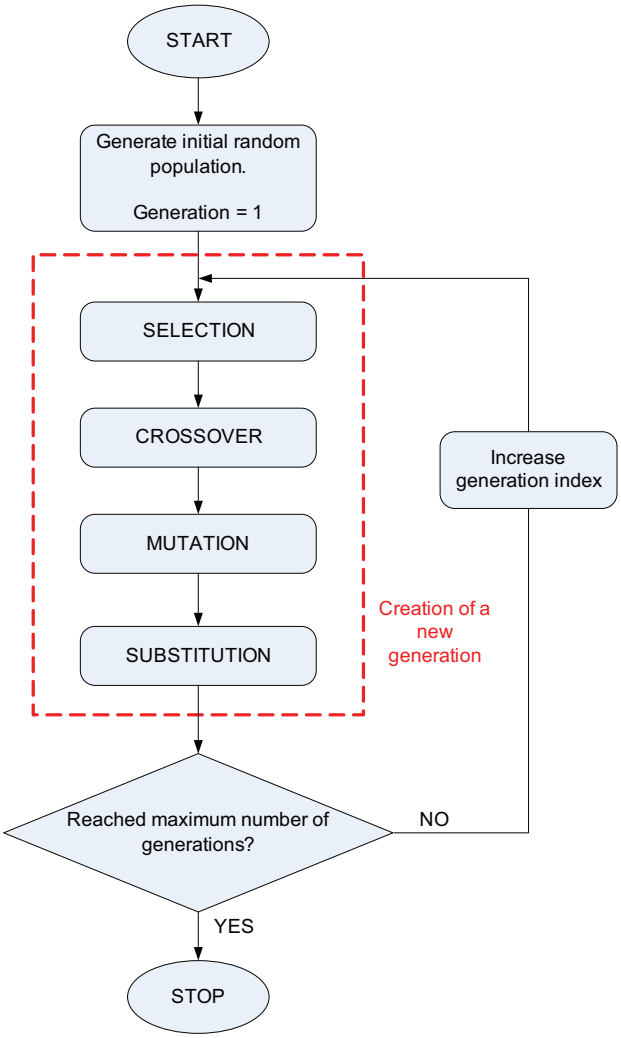

Figure 5.5: Basic structure of a genetic algorithm.

solutions; conversely, if the population size is too big, the algorithm may converge slowly.

Each individual corresponds to a specific allocation of network resources, that is of link wavelength channels and FDL virtual buffers. Specifically, for Problems 1 and 3 an individual is represented by an allocation of FDLs **K**. Each element of **K** is the number of wavelength channels of an FDL at a given node and represents a gene of the individual. Thus, all individuals are encoded directly into strings of integer numbers with values in the range $[K_{min}, K_{max}]$. Note that the encoding process forces the potential solutions to be integrals and within the interval $[K_{min}, K_{max}]$. Hence, the physical and integrality constraints present in all the optimisation problems are already satisfied by the process of encoding of the individuals. The same encoding process is applied for Problems 2 and

4 with the only difference that the first part of an individual corresponds to the vector of network links $\mathbf{W} = [W_1, W_2, \ldots, W_L]$ whereas the second and last part is given by the vector of FDL virtual buffers $\mathbf{K} = [K_1, K_2, \ldots, K_N]$. Hence, for Problems 2 and 4 an individual is finally encoded as vector $\mathbf{X} = [\mathbf{W}\,\mathbf{K}]$. Figure 5.6 illustrates the encoding process for all four optimisation problems.

5.3.2 Fitness Function

After generating a random population, the "goodness" of each individual is determined by evaluating a fitness function. The greater is the fitness value of an individual, the higher is the probability that the individual will be selected for "reproduction". Generally, for non-constrained minimisation problems, the fitness function may correspond to the opposite of the objective function, that is $-C(\mathbf{K})$ for the FDL allocation problems and $-C(\mathbf{W}, \mathbf{K})$ for the joint allocation of link and FDL problems; however, the situation considerably complicates when adding constraints to the optimisation problems. In this case issues may arise when considering individuals that do not satisfy the constraints and are considered *unfeasible* (conversely, all individuals that do satisfy the constraints are termed *feasible*). In fact, it may be difficult to decide how to handle unfeasible individuals. A possible solution may be to *a-priori* discard all individuals that do not satisfy the constraints (*death-penalty*) [60]; however, in this way, the algorithm risks elimination of unfeasible individuals that are close to the optimal solution and, thus, may provoke a slower (or no) convergence to the optimum. Another way is to modify the fitness function of each individual by introducing a non-zero *penalty function* for all the unfeasible solutions. The problem of defining an appropriate penalty function has stimulated the interest of many researchers and several methods have been proposed on this topic. A good overview can be found in [77] where the performances of different constraint-handling techniques are analysed and compared. This thesis adopts

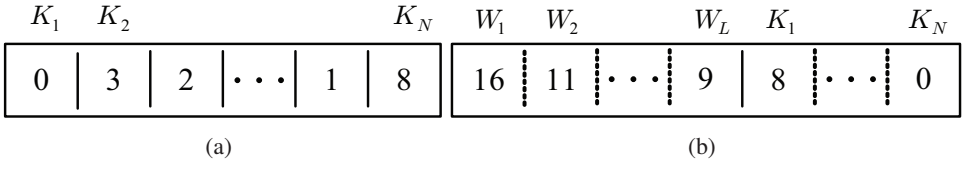

Figure 5.6: Encoding of individuals for Problems 1 and 3 (a) and Problems 2 and 4 (b).

a simple yet very efficient method inspired by Deb in [25] where the penalty function corresponds to the sum of all the *constraint violations* of an unfeasible individual. Particularly, for an unfeasible solution $\mathbf{x}$ of a constrained optimisation problem where the i-th constraint is denoted as $c_i(\mathbf{x}) \leq C_{MAX}$, the constraint violation of $\mathbf{x}$ for the i-th constraint is defined as $g_i(\mathbf{x}) = |c_i(\mathbf{x}) - C_{MAX}|$. Therefore, for a solution $\mathbf{x}$, its fitness $f(\mathbf{x})$ is evaluated as

$$f(\mathbf{x}) = \begin{cases} o(\mathbf{x}) & \text{if } \mathbf{x} \text{ is feasible} \\ o(\mathbf{x}^-) - \sum_{\forall i} G_i g_i(\mathbf{x}) & \text{if } \mathbf{x} \text{ is unfeasible,} \end{cases} \tag{5.11}$$

where we have indicated with $o(\mathbf{x})$ the objective function value of $\mathbf{x}$, with $o(\mathbf{x}^-)$ the objective value of $\mathbf{x}^-$, that is the feasible solution with the lowest fitness in the population, and with $\sum_{\forall i} G_i g_i(\mathbf{x})$ the sum of all the constraint violations of $\mathbf{x}$. Constant G_i is defined as the *penalty parameter* of the i-th constraint and its purpose is to keep the constraint violation of the same order of magnitude as the value of the objective function. Under these premises, for Problem 1 the fitness function f of an individual $\mathbf{K}$ can be written as

$$f(\mathbf{K}) = \begin{cases} -C(\mathbf{K}) & \text{if } \mathbf{K} \text{ is feasible,} \\ -C(\mathbf{K}^-) - G\,|max[\mathcal{P}_r(\mathbf{K})] - \mathcal{P}_{max}| & \text{if } \mathbf{K} \text{ is unfeasible,} \end{cases} \tag{5.12}$$

where we have indicated with $\mathbf{K}^-$ the feasible FDL allocation with the lowest fitness in the population and G is the penalty parameter (note that we have only one penalty parameter as there can be only violations on one constraint). Similarly, the fitness function of an individual for Problem 2 is given by

$$f(\mathbf{X}) = \begin{cases} -C(\mathbf{X}) & \text{if } \mathbf{X} \text{ is feasible,} \\ -C(\mathbf{X}^-) - G\,|max[\mathcal{P}_r(\mathbf{X})] - \mathcal{P}_{max}| & \text{if } \mathbf{X} \text{ is unfeasible,} \end{cases} \tag{5.13}$$

where again $\mathbf{X}^-$ represents the feasible allocation of links wavelength channels and FDL with the lowest fitness in the population.

The constraints included in Problems 3 and 4 are already satisfied from the process of encoding of the individuals, thus, in these cases there is no need to rely on constraint-

handling techniques; however, it is necessary to determine an appropriate fitness function that takes into consideration the contribution of both the conflicting objective functions to be minimised. A typical approach is to combine linearly the objective functions in order to define the fitness, assigning different weights to each objective. The weights associated with the objective functions determine the search direction of the algorithm within the Pareto solution space. If the values of the weights are fixed, the search direction is fixed as well; in this case, it is difficult to extensively explore the search space and it may happen that some candidate Pareto solutions cannot be found. On the other hand, if the weights' values are randomly generated, the GA looks for solutions through different search directions, increasing the probability to find more Pareto solutions. GAs using this approach are called *Random Weighted Genetic Algorithms* (RWGAs) [47] and we will use them to solve the multi-objective optimisation problems defined in the previous section. Particularly, for Problem 3 the fitness function of an individual is defined as

$$f(\mathbf{K}) = -\epsilon C(\mathbf{K}) - (1-\epsilon) max[\mathcal{P}_r(\mathbf{K})], \tag{5.14}$$

where ϵ is a randomly generated number uniformly distributed within the interval (0,1). Note that a different value of ϵ is generated each time the fitness function of an individual is calculated. A graphical interpretation of the RWGA is depicted in Figure 5.7. If we fix $\epsilon = 0.5$ the GA will explore the solution space only in one fixed direction (denoted in the example by the red arrow); this means that it may discover solutions represented by points A and B but is very unlikely to find points C, D and E. Conversely, if we randomly change ϵ for each individual's fitness evaluation, the search will be performed through multiple directions (green arrows) and the chances to find points C, D and E will increase. Note also that the fitness function is overall negative since we are considering a minimisation problem. Similarly to Problem 3, the fitness of an individual for Problem 4 is evaluated as

$$f(\mathbf{X}) = -\epsilon C(\mathbf{X}) - (1-\epsilon) max[\mathcal{P}_r(\mathbf{X})], \tag{5.15}$$

where once again vector $\mathbf{X}$ represents a joint allocation of link wavelength channels and

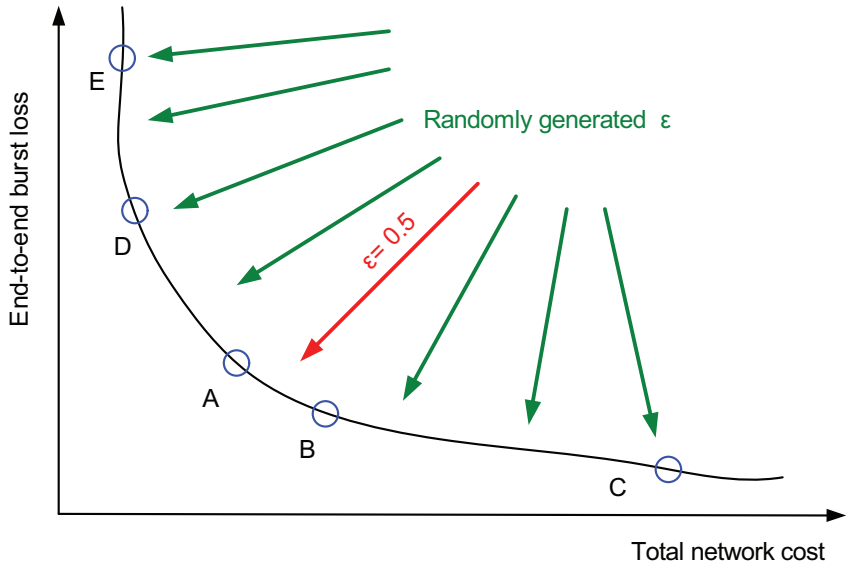

Figure 5.7: Example of the application of the Random Weight Genetic Algorithm for Problems 3 and 4.

FDL virtual buffers in the network under study.

5.3.3 Selection

At each generation, the fitness of all individuals is evaluated and then a set of "good" candidate solutions are selected to "reproduce" (*parents*). The *selection* process is a key operation in genetic algorithms and there are several mechanisms to perform it. In this thesis, individuals are selected according to the *roulette wheel technique* [44] where fittest individuals have more chances to be chosen for reproduction. First of all the fitness value of all the individuals of the population is normalised as follows

$$f_i^* = f_i / \sum_{j=1}^{popSize} f_j \qquad i = 1, \ldots, popSize, \tag{5.16}$$

where f_j is the fitness of individual j. Then, all fitness values are sorted in ascending order (denoting them with t_i^*). The selection of two parents is performed as follows: a random number δ uniformly distributed within the interval [0,1] is generated. If $\delta < t_1^*$, individual 1 is selected as a parent for reproduction. If $\delta > t_1^*$, a comparison between δ and the cumulative sum $s_1 = t_1^* + t_2^*$ is performed. If $\delta < s_1$, individual 2 is selected as a parent

otherwise we recursively re-calculate the cumulative sum $s_2 = s_1 + t_3^*$ and proceed with the next comparison in a similar manner until two individuals will be selected as parents. The main risk in using the roulette wheel technique is that individuals with high values of fitness may be selected too frequently for reproduction and the resulting future generations of individuals will be too similar to each other. This may be a considerable issue for resolving optimisation problems with GAs where keeping the diversity of the individuals is essential in order to find the optimal solution. Hence, we attempt to overcome this issue by adopting also a *tournament* selection [78]. In this case, a "pool" of randomly selected individuals is chosen for playing a tournament. The individuals of the pool with the highest fitness win the tournament and are further selected for reproduction. In this way, the diversity of the population is better preserved since individuals with low fitness values have more chances to be selected for reproduction. Nevertheless, in this case the price to pay corresponds to a slower convergence of the algorithm. Additionally, the size of the pool must be carefully decided when running the GA (e.g., if it is too high, individuals with low fitness values will have less chances to be selected for reproduction). Both selection methods are adopted for the resolution of the proposed optimisation problems.

5.3.4 Crossover

Once two individuals have been selected as parents, they reproduce to generate offspring. The generation of new offspring is performed with a GA operator called *crossover* with a user-defined probability $Prob_c$. Once again, research literature is rich with different proposals for the crossover operation [25, 44]. In this thesis a *two-point* crossover operation is applied, as follows. Firstly, two crossover points are randomly defined. From the beginning of the sequence to the first crossover point, the offspring will inherit the genes of one parent; then, from the first crossover point to the second crossover point, the offspring will obtain the genes of the other parent; finally, from the second crossover point until the end, the offspring will receive the genes of the first parent once again. The second offspring will be generated with the same procedure but with the opposite order of parents. This procedure is performed to generate new individuals for all the optimisation problems. An example of this operation is illustrated in Figure 5.8 for the case of Problems 1 and 3 where each indi-

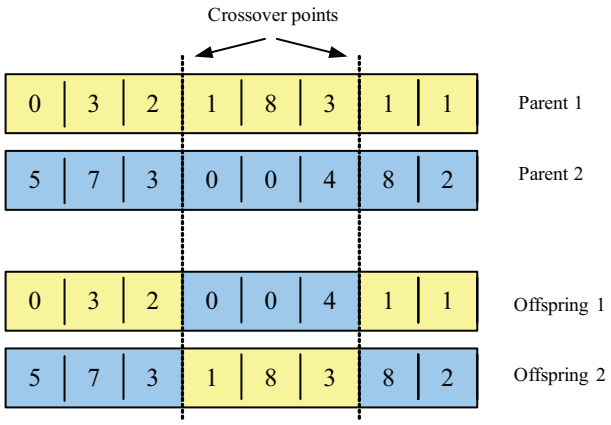

Figure 5.8: Example of a two-point crossover operation.

vidual corresponds to an allocation of FDL virtual buffers. In order to preserve diversity, we also consider in the algorithm a *random* crossover. With this method, an offspring will be generated by randomly swapping the genes of the parents.

5.3.5 Mutation

Once the two offspring are generated, we *mutate* them by randomly changing one of their genes with a predefined mutation probability $Prob_m$. The mutation is an essential step in GAs that helps preserve the diversity in the population and prevents the GA getting stuck in a local minimum. All problems adopt the same mutation scheme but with different ranges of mutated genes. Specifically, in Problems 1 and 3 a gene can randomly change with a value within the interval $[K_{min}, K_{max}]$ whereas for Problems 2 and 4 a gene can mutate within intervals $[W_{min}, W_{max}]$ if it represents the wavelength channels of a link and within $[K_{min}, K_{max}]$ if it represents FDL virtual buffers. The mutation of the individuals complete the process of generation of new offspring that will replace their parents in the new generation.

5.3.6 Elitism

A drawback of creating a new generation according to the above described operations is that good individuals in terms of fitness may be lost while running the algorithm because they are substituted with children that may have lower fitness. To overcome this problem,

typically a subset of the individuals with the highest values of fitness are selected and included in the new generation. This final step is known as *elitism* and the set of E chosen individuals is called the *elite* [78]. This procedure keeps the best E individuals in the population as the algorithm continues its search for fitter solutions and, compared to non-elitistic strategies, increases considerably the speed of convergence of the algorithm. Elitism is applied for all the optimisation problems under study as described in the following overview of the applied GAs.

5.3.7 Summary of the Single and Multi-objective GAs

The last part of this section presents an overview of the GAs applied for resolving the optimisation problems under study. Problems 1 and 2 are resolved with the single objective GA defined by the following steps:

1. Set a maximum number of generations $maxGen$, a crossover probability $Prob_c$ and a mutation probability $Prob_m$.

2. At iteration 1 randomly generate an initial population of $popSize$ individuals where each individual is encoded as **K** for Problem 1 and **X** for Problem 2.

3. Repeat the following steps until the maximum number of generations $maxGen$ is reached:

    - Evaluate the fitness of each individual with Equation (5.12) for Problem 1 and with Equation (5.13) for Problem 2.
    - Repeat the following steps until a new population of size $popSize$ is created:
        - select two parents with the roulette wheel technique or with the tournament method.
        - perform a two-point or random crossover for determining the offspring with probability $Prob_c$.
        - perform a gene mutation of the generated offspring with probability $Prob_m$.
        - substitute the parents with their children in the new generation.

- Include in the new generation E individuals amongst the fittest ones of the previous generation.

4. Stop the algorithm.

Problems 3 and 4 are resolved with a multi-objective GA based on the above described GA. The main differences are in the way of structuring the population and in the way of including the elite. Particularly, inspired by the work proposed in [47, 132], the population is divided into three sets: the *elite set* of maximum size $maxEliteSize$, the *reproduction set* of size $repSize$ and the *random set* of size $randSize$. At generation g, Pareto-optimal solutions discovered at generation $g-1$ are included in the elite set. If the size of the Pareto front $paretoSize$ is lower than $maxEliteSize$ then all Pareto-optimal solutions are included in the elite set. If vice versa, $maxEliteSize$ Pareto-optimal solutions are randomly selected and included in the elite set. Note that $popSize = eliteSize + repSize + randSize$. The random set simply contains $randSize$ randomly generated individuals. The presence of this set helps to avoid getting stuck in a local minimum [132]. Finally, the reproduction set comprises $repSize$ individuals generated by the usual steps of selection, crossover and mutation. Note that $repSize = popSize - randSize - min(paretoSize, maxEliteSize)$. All individuals of the population are eligible for reproduction. The algorithm ends when a maximum number of generations $maxGen$ is reached.

The steps of the multi-objective GA used to resolve Problems 3 and 4 are summarised as follows:

1. Set $maxGen$, $Prob_c$, $Prob_m$ $maxEliteSize$, $repSize$ and $randSize$.

2. At iteration 1 randomly generate an initial population of $popSize = maxEliteSize + repSize + randSize$ individuals where each individual is encoded as **K** for Problem 3 and **X** for Problem 4.

3. Repeat the following steps until the maximum number of generations $maxGen$ is reached:

   - Evaluate the fitness of each individual with Equation (5.14) for Problem 3 and with Equation (5.15) for Problem 4.

- Include in the new generation $E = min(paretoSize, maxEliteSize)$ individuals corresponding to potential Pareto-optimal solutions selected amongst all the individuals on the basis of (5.9). Update the values of $repSize$ on the basis of the obtained value of E.
- Repeat the following steps until $repSize$ individuals are created and included in the new generation:
  - select two parents with the roulette wheel technique or with the tournament method.
  - perform a two-point or random crossover for determining the offspring with probability $Prob_c$.
  - perform a gene mutation of the generated offspring with probability $Prob_m$.
  - substitute the parents with their children in the new generation.
- Randomly generate $randSize$ individuals and include them in the new generation.

4. Stop the algorithm.

Results obtained from resolving the optimisation problems under study are presented and commented in the next section.

5.4 Results

The optimisation problems are resolved for the NSF and the EON OBS topologies presented in the previous chapter. The configuration settings of the genetic algorithm are shown in Tables 5.1 and 5.2 for all 4 optimisation problems. The decision on the hardware unit costs c_S, c_E and c_T is quite difficult to make as real costs for these devices vary considerably on the basis of their manufacturer and their specifications. Based on studies proposed in papers such as [33, 94, 118] all unit costs are related to that of a SOA, the SOA being currently less expensive than an EDFA or a TWC. Thus, the unit cost of a SOA is set as h_S = 1 and the unit costs of an EDFA and a TWCs are fixed respectively at $3h_S$ and at $15h_S$. All end-to-

Table 5.1: GA configuration for Problems 1 and 2

$maxGen$	100 (Problem 1), 200 (Problem 2)
$popSize$	100 (Problem 1), 300 (Problem 2)
Elite size (E)	20 (Problem 1), 30 (Problem 2)
Encoding	Integer **K** (Problem 1), Integer **X** (Problem 2)
Selection	Roulette Wheel (Problem 1), Tournament (Problem 2)
Crossover	Two-point (Problem 1), Random (Problem 2)
$Prob_c$	0.9
$Prob_m$	0.05

Table 5.2: GA configuration for Problems 3 and 4

$maxGen$	500
$popSize$	300
$randSize$	100
$maxEliteSize$	30
Encoding	Integer **K** (Problem 3), Integer **X** (Problem 4)
Selection	Tournament
Crossover	Random
$Prob_c$	0.9
$Prob_m$	0.05

end blocking probabilities $\mathcal{P}_r$ for $r = 1, \ldots, R$ are estimated by using the analytic method described in Chapter 4.

5.4.1 Resolving Problem 1

In this case, the goal is to determine an optimal allocation of FDL virtual buffers that minimises the total hardware network cost under performance and physical constraints respectively defined by maximum tolerable end-to-end burst loss and maximum and minimum values of FDL virtual buffers. Problem 1 is solved by using the single-objective GA described at the end of the previous section for both network topologies. In the NSF topology, each network link comprises the same number of wavelength channels $W = 16$ and each path is offered with burst traffic of mean intensity $\rho = 0.25$ Erlangs per channel. For the EON topology case, each network link includes $W = 32$ wavelength channels and each path is offered with burst traffic of load $\rho = 0.35$ Erlangs per channel. In both scenarios, the offered traffic peakedness Z is included in the interval [0.8,1.4]. Finally, the physical constraints for the NSF network topology are set as $K_{min} = 0$, $K_{max} = 8$ whereas for

the EON topology $K_{min} = 0$, $K_{max} = 16$. Tables 5.3 and 5.4 illustrate the benefits introduced by the optimisation of FDL virtual buffers in terms of cost savings subject to different values of $\mathcal{P}_{max}$.

We generally note how the cost varies considerably with Z, an occurrence that justifies the choice of modelling the OBS network with the analytic method proposed in Chapter 4. We compare the total hardware cost resulting from the optimisation of the network resources (C_{OPT}) with the total cost resulting from the minimum uniform allocation of FDLs that satisfies the requirements in terms of $\mathcal{P}_{max}$ (C_{UNI}). Due to the small size of the solution space in the uniform allocation case, all uniform solutions are determined via exhaustive search by using the OBS network analytic model of Chapter 4. For example, in Table 5.4, to reach a maximum tolerable blocking probability $\mathcal{P}_{max} = 10^{-2}$ on all paths for $Z = 1.4$, the optimal allocation of FDL virtual buffers is found to be **K**=[0 8 0 10 4 6 10 4 0 10 10 4 0 0 4], resulting in a total cost of $C_{OPT} = 24092$. The same performance requirements can be satisfied with a uniform allocation of no less than 10 buffers for each

Table 5.3: Cost comparison between optimal (OPT) and uniform (UNI) virtual buffers allocation: NSFNET topology. $K_{max} = 8$ buffers, $W = 16$, $\rho = 0.25$ Erlangs per channel. 'NF' stands for 'Not Feasible'.

	$\mathcal{P}_{max}$	10^{-1}	10^{-2}	10^{-3}	10^{-4}	10^{-5}
Z = 0.8	C_{OPT}	8270	8270	8980	9235	9475
	C_{UNI}	8270	8270	9358	9748	9943
Z = 1	C_{OPT}	8270	8647	9160	9490	NF
	C_{UNI}	8270	9163	9553	10138	NF
Z = 1.4	C_{OPT}	8270	9090	9569	NF	NF
	C_{UNI}	8270	9553	10138	NF	NF

Table 5.4: Cost comparison between optimal (OPT) and uniform (UNI) virtual buffers allocation: EON topology. $K_{max} = 16$ buffers, $W = 32$, $\rho = 0.35$ Erlangs per channel. 'NF' stands for 'Not Feasible'.

	$\mathcal{P}_{max}$	10^{-1}	10^{-2}	10^{-3}	10^{-4}	10^{-5}
Z = 0.8	C_{OPT}	22116	22806	23882	24467	24842
	C_{UNI}	22116	24277	25177	25852	26302
Z = 1	C_{OPT}	22116	23552	24347	24962	NF
	C_{UNI}	22116	24952	25627	26527	NF
Z = 1.4	C_{OPT}	22116	24092	25187	NF	NF
	C_{UNI}	22116	25627	26977	NF	NF

node, resulting in a total cost of $C_{UNI} = 25627$. Thus, for this particular case, the optimisation process yields an $\approx 6\%$ reduction in total hardware cost of the network. Considering only the cost associated with the employment of FDL virtual buffers without considering the expenses related to the installment of links, the corresponding cost savings yielded by the found optimal allocation are of $\approx 43.7\%$. We also note that for some scenarios it is not possible to find an optimal (or uniform) allocation of the FDLs (e.g., Table 5.3 for $Z = 1.4$ and $\mathcal{P}_{max} = 10^{-4}$). This is because all the solutions found are unfeasible, that is there is no FDL virtual buffer allocation that can satisfy the performance and requirements under the constraints defined by the optimisation problem.

Figures 5.9 illustrates an example of an optimal solution corresponding to a distribution of the FDL virtual buffers in the OBS network. We observe that the FDL distribution changes considerably with Z, since congestion at nodes increases when traffic becomes peaked. Note that some nodes are not assigned with FDLs, regardless of the peakedness of their offered traffic demands. Hence, the GA is able to identify the nodes of the network for which adding an FDL does not contribute to lowering the end-to-end blocking probability value. In fact, although the offered load may be generally considered low in all the cases of

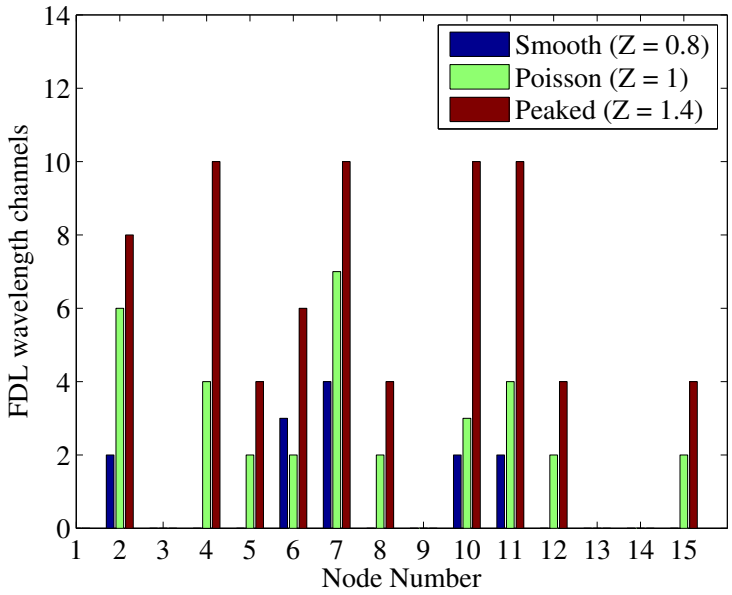

Figure 5.9: Optimal allocation of the FDLs in the EON topology scenario for $W = 32$, $\rho = 0.35$ Erlang and $\mathcal{P}_{max} = 10^{-2}$.

study (0.25-0.35 Erlangs), this is not the case for congested links in the core network, where the load can reach values of 0.5 Erlangs per wavelength channel. The proposed GA allows determination of the optimal number of FDL buffers required for nodes with such congested links, a number that is higher than the one determined for the less congested links at the edges of the network. For example, note that in Figure 5.9 nodes 1,3,9,13 and 14 do not contribute in lowering the blocking if equipped with FDLs, thus they are not assigned with FDLs. This feature considerably decreases the FDL cost compared to an uniform allocation as shown in the example of Figure 5.10. In this particular case, the optimal allocation of FDL virtual buffers is found to be **K**=[0 2 0 0 0 3 4 0 0 2 2 0 0 0 0]. Note that in order to meet the performance level requirements, at least 4 FDL buffers must be employed to node 7. This means that, in an uniform allocation, we must employ at least 4 FDL buffers for each node of the network, resulting in a considerably increased FDL cost per network node compared to the optimal scenario.

End-to-end blocking probabilities for each path are shown in Figures 5.11 and 5.12 and compared to simulation results obtained from the same discrete-event network simulator de-

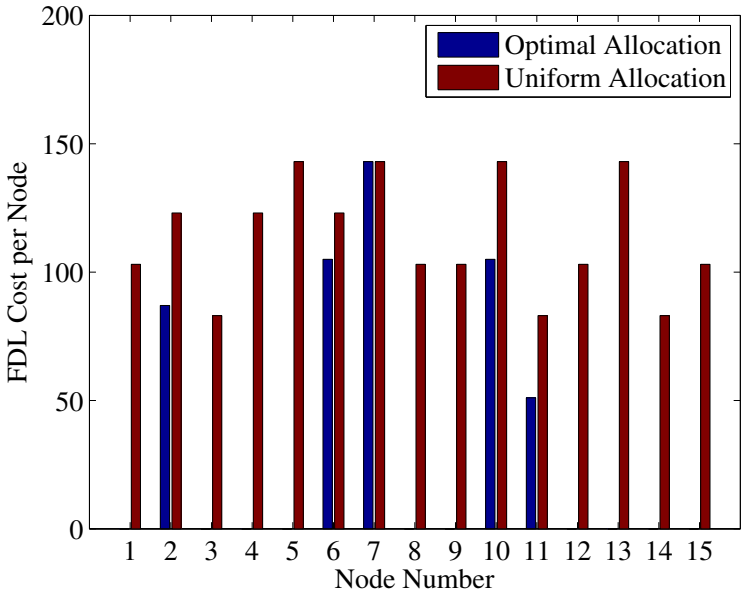

Figure 5.10: Comparison of the FDL cost per node C_n^{FDL} between optimal and uniform FDL allocation in the EON topology scenario, for $W = 32$, $\rho = 0.35$ Erlangs, $Z = 0.8$ and $\mathcal{P}_{max} = 10^{-2}$.

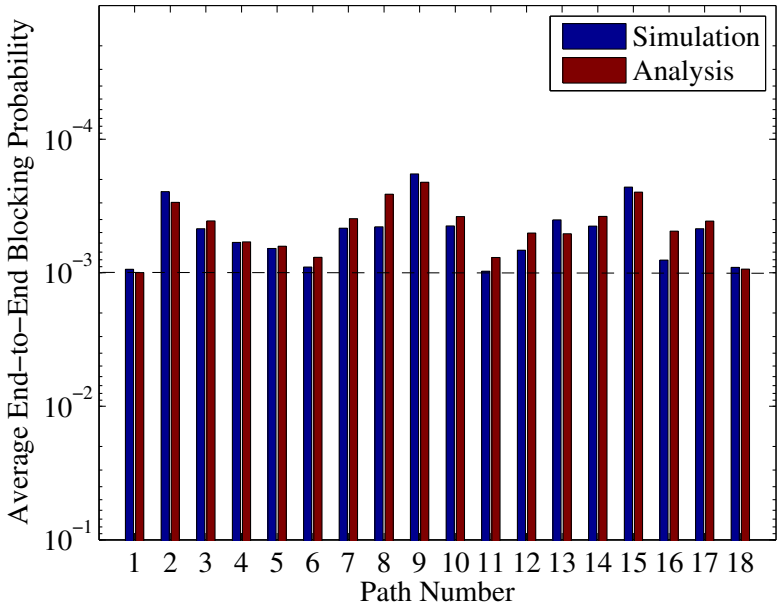

Figure 5.11: Path blocking probabilities of the EON scenario for $W = 16$, $\rho = 0.3$ Erlangs per channel, $Z = 1$ and $\mathcal{P}_{max} = 10^{-3}$. The optimal FDL allocation is found to be **K**=[0 6 0 7 6 7 8 6 0 6 6 6 0 0 6].

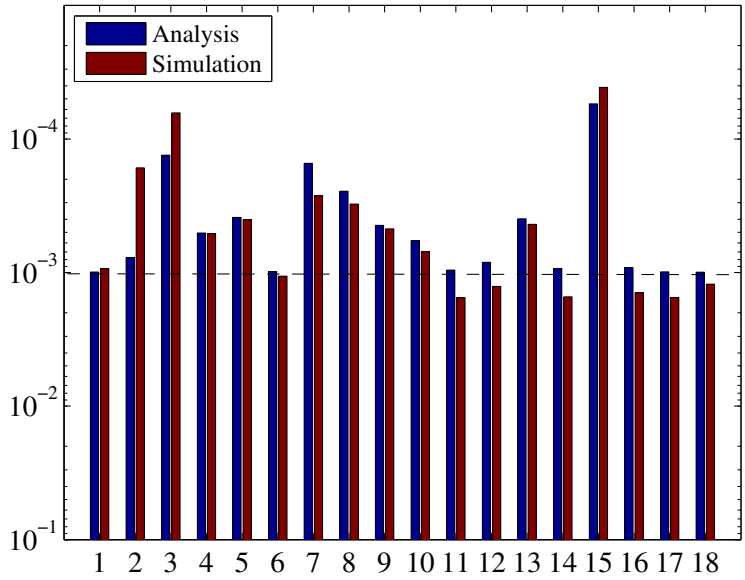

Figure 5.12: Path blocking probabilities of the EON scenario for $W = 32$, $\rho = 0.2$ Erlangs per channel, $Z = 3$ and $\mathcal{P}_{max} = 10^{-3}$. The optimal FDL allocation is found to be **K**=[0 10 0 16 10 10 13 6 0 6 8 13 5 7 15].

scribed in Chapter 4. Observe that the analytic method provides a quite accurate estimate of the blocking probability at the optimal point compared to simulation data. The graph in Figure 5.11 additionally shows that each path blocking is below the maximum tolerable value given by $\mathcal{P}_{max}$, thus satisfying the performance constraint of both optimisation problems. This further validates the network model proposed in the previous chapter, demonstrating its usefulness when applied for resolving optimisation problems. In Figure 5.12 the the optimal solution obtained by analysis is validated for $W = 32$ channels, $\rho = 0.2$ Erlang and $Z = 3$. Note that in this case the peakedness is very high, hence the two-moment matching analysis of the network may not be accurate enough. In fact, the average deviation from simulation is higher than in Figure 5.11 and the FDL optimal allocation does not satisfy the performance constraints (e.g., paths 6,11,12,14, 16,17 and 18 have simulated burst blocking values higher than the maximum tolerable one).

5.4.2 Resolving Problem 2

In this case the single-objective GA is applied in order to find an optimal joint allocation of link wavelength channels and FDL virtual buffers that minimises the total hardware cost and meets the performance requirements under the defined physical constraints of the problem. Similarly to Problem 1, the problem is solved for both network topologies with the same scenarios. The only difference is in the addition of the extra constraint regarding the minimum and maximum allowable number of wavelength channels per link, that is $W_{min} = 8$, $W_{max} = 16$ for the NSFN topology and $W_{min} = 16$, $W_{max} = 32$ for the EON topology.

For this problem, challenges arise that are more complex to resolve compared to Problem 1. The main issue here is given by the size of the solutions space. In fact, note that each individual is encoded in a string of $L + N$ integers resulting in a total number of potential solutions equal to $(W_{max} - W_{min} + 1)^L \cdot (K_{max} - K_{min} + 1)^N$ as opposed to the $(K_{max} - K_{min} + 1)^N$ individuals of the solution space associated with Problem 1. This is particularly evident for the EON topology scenario where, for example, resolving Problem 2 corresponds to finding an optimal solution within a space of $\approx 2.8 \cdot 10^{50}$ individuals as opposed to the $\approx 2 \cdot 10^{14}$ individuals of Problem 1. In this case, in order to let

the GA efficiently explore the solution space, the number of individuals of the population must be high enough to guarantee a level of diversity such that the optimal solution can be ultimately found. Nevertheless, the higher the number of individuals, the slower the GA will converge to the solution, mainly due to the time spent in computing the fitness function. This is probably the main drawback when using the GA for the proposed optimisation problems, especially in a multi-objective optimisation scenario as we will see for Problems 3 and 4. Another main difficulty in converging to the optimal solution is given by the particular nature of the solution space defined by the optimisation problem. In fact, in this case the individuals are not uniformly distributed in the search space and it may happen that the algorithm fails to discover solutions in regions of the space with lower population "density" [26]. This phenomenon is known as *genetic drift* [26] and several methods attempting to resolve it have been proposed in the literature. The interested reader can find a detailed summary of the most popular ones in [60]. In this case, we are still able to find the optimal solution of the problem for different performance requirements by including in the initial population at least one feasible solution. This can be easily done by applying the network model and finding a uniform allocation of link and FDL wavelength channels that satisfies the performance constraints. Hence, the feasible individual corresponding to the obtained uniform allocation is included in the population while the rest of the individuals are randomly generated. The population size is set to $popSize = 300$ individuals and the GA is run for $maxGen$ = 200 generations. An additional attempt to keep diversity between individuals is made by adopting a tournament selection strategy along with a random crossover operation. In this regard, the tournament pool size is set at 80.

Results for the minimum cost offered by the optimal solutions are displayed in Tables 5.5 and 5.6 respectively for the NSFN and the EON topologies. Minimum costs obtained by optimal individuals are once again compared with minimum costs resulting from uniform allocations of link wavelength channels and FDL virtual buffers, similarly to what has been presented in Problem 1. Optimum uniform allocations of link/FDL wavelength channels are determined by exhaustive search over the set of all possible feasible solutions. As expected, the optimal costs are all lower than the correspondent ones of Problem 1, since the number of link wavelength channels has been optimised as well; the improvements in terms of cost

savings are also quite relevant. Note for example that, in Table 5.3, the minimum cost to meet a performance level of $\mathcal{P}_{max} < 10^{-5}$ over all paths for smooth traffic is $C_{OPT}(\mathbf{K}) = 9475$ whereas in Table 5.5 it is $C_{OPT}(\mathbf{X}) = 7785$, resulting in a cost saving percentage of $\approx 17.8\%$. Additionally, similarly to Problem 1, all optimal solutions achieve costs lower than the ones obtained with uniform allocations. Note that this is also true for optimal solutions meeting performance levels of 10^{-1} as opposed to Problem 1 where optimal and uniform allocation may be equivalent. For example, note that in Table 5.5 a maximum tolerable end-to-end burst loss of $\mathcal{P}_{max} = 10^{-4}$ for Poisson traffic is obtained with a minimum cost of $C_{OPT} = 7880$ associated with an optimal allocation **X** = [**W F**] given by vectors **W** = [9 10 16 16 9 13 16 8 16 16 13 16 10 9 16 16 14 11 16 9 16 16 16 16 8 9 11 8 9] and **F** = [7 2 6 2 7 1 7 7 0 7 0 7 7]; to meet the same performance constraint, a uniform allocation of $W = 16$ wavelength channels per link and $K = 7$ virtual buffers per FDL must be adopted,

Table 5.5: Cost comparison between optimal (OPT) and uniform (UNI) link/FDL wavelength channels allocation: NSFNET topology. $K \in$ [0,8], $W \in$ [8,16], $\rho = 4$ Erlangs per path. 'NF' stands for 'Not Feasible'.

	$\mathcal{P}_{max}$	10^{-1}	10^{-2}	10^{-3}	10^{-4}	10^{-5}
Z = 0.8	C_{OPT}	5064	6278	6901	7348	7785
	C_{UNI}	6488	7803	8678	9408	10138
Z = 1	C_{OPT}	5705	6601	7280	7880	NF
	C_{UNI}	6878	8143	9068	10138	NF
Z = 1.4	C_{OPT}	6056	6908	8023	NF	NF
	C_{UNI}	7413	8873	10333	NF	NF

Table 5.6: Cost comparison between optimal (OPT) and uniform (UNI) link/FDL wavelength channels allocation: EON topology. $K \in$ [0,16], $W \in$ [16,32], $\rho = 11.2$ Erlangs per path. 'NF' stands for 'Not Feasible'.

	$\mathcal{P}_{max}$	10^{-1}	10^{-2}	10^{-3}	10^{-4}	10^{-5}
Z = 0.8	C_{OPT}	13283	18323	18238	19359	20120
	C_{UNI}	18696	22964	24183	25083	26030
Z = 1	C_{OPT}	15305	18386	19187	20460	NF
	C_{UNI}	21117	24361	25083	26527	NF
Z = 1.4	C_{OPT}	16174	19225	21036	NF	NF
	C_{UNI}	21792	24858	26977	NF	NF

yielding a minimum cost of $C_{UNI} = 10138$. Hence, in this case the optimisation process reduces the total hardware cost by $\approx 22.2\%$.

Probably the most important observation is on the sensitivity of the total minimum cost to the peakedness of the offered traffic. Specifically, similarly to Problem 1, the obtained results justify once again the importance of approximating non-Poisson traffic characteristics in the network model when resolving resource dimensioning problems. Note for example that the total hardware optimum cost required to meet the performance constraints is incrementing by an average of $\approx 5.5\%$ when changing Z from 0.8 to 1.

An example of an optimal solution is depicted in Figure 5.13 for the EON topology scenario, with performance constraints given by $\mathcal{P}_{max} = 10^{-2}$ and for different values of peakedness. First of all note how in all three cases the GA is able to identify the most congested links by keeping the highest number of wavelength channels. The situation is different when analysing the part of the individual dedicated to the FDL virtual buffer allocation (in this case, the last 15 genes of the individual). Particularly, note that the configuration of FDL virtual buffers is different from the corresponding optimal allocation found in Problem 1. In fact, FDLs that are ineffective and discarded for Problem 1 become effective for Problem 2 due to the different dimensioning of the link wavelength channels and generally comprise more virtual buffers. For a clearer picture compare Figure 5.9 with the FDL allocation of Figure 5.13. It can be observed that discarded FDLs for Problem 1 (e.g, FDLs at nodes 13 and 14) are instead employed with medium-to-high numbers of virtual buffers (e.g, from a minimum of 4 to a maximum of 12 virtual buffers). Figure 5.14 illustrates this aspect from another perspective by showing the total number of link wavelength channels and of FDL virtual buffers employed for Problem 1 and Problem 2 in the NSFN network scenario. Note that in case (a) the number of FDL virtual buffers employed in Problem 1 monotonically increases and is always below the values determined by the optimisation process in Problem 2. Furthermore, note that in Problem 2 the total number of FDL virtual buffers is not monotonic due to the different configuration of link wavelength channels (whose total number is depicted in Figure 5.14(b)). Once again, an example of the accuracy and validity of the solution for the optimisation problem is shown by comparing the obtained values of path blocking probabilities with simulation data in Figure 5.15.

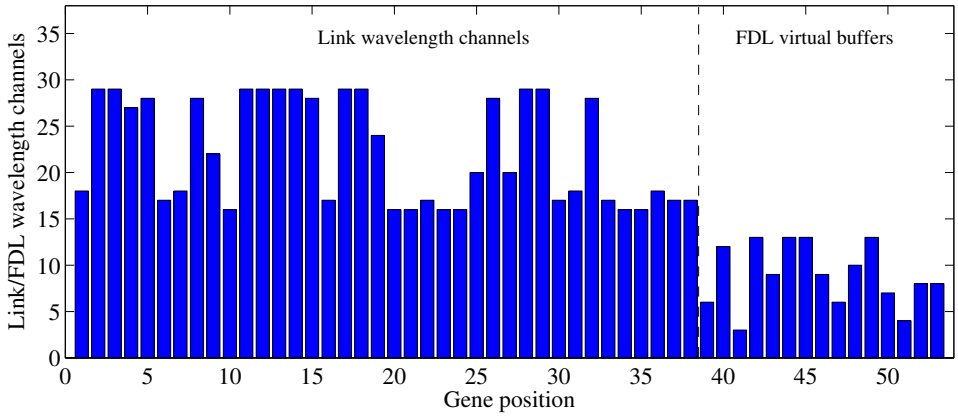

(a)

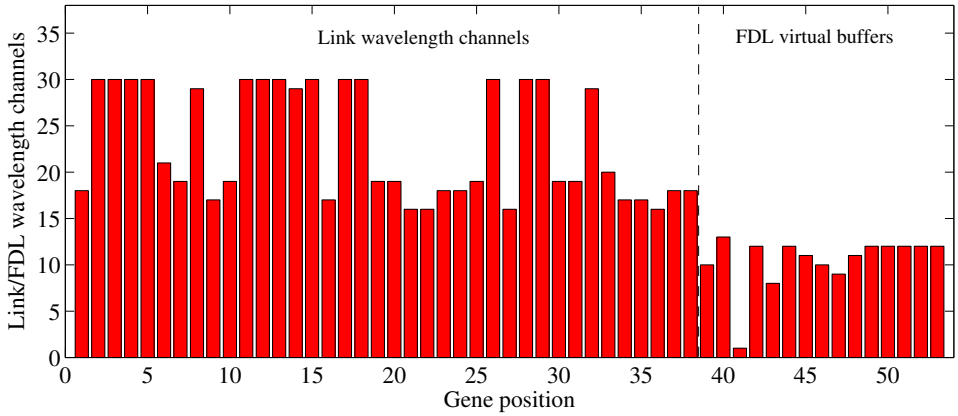

(b)

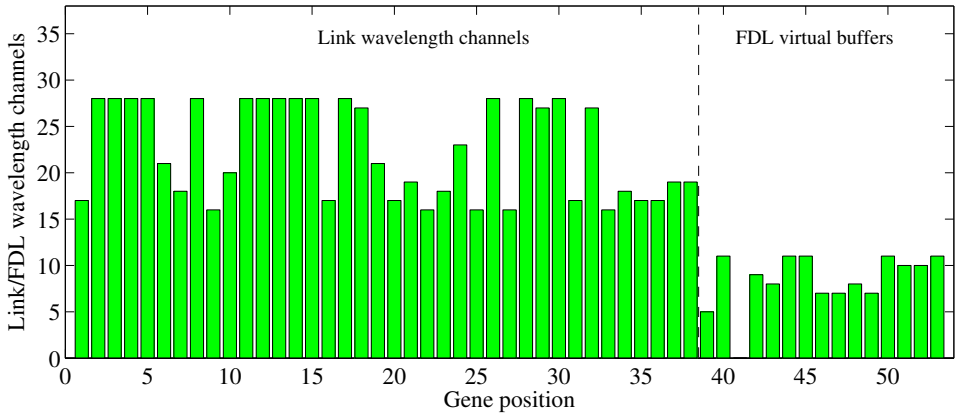

(c)

Figure 5.13: Configuration of the optimal solution corresponding to the allocation of link and FDL wavelength channels for the EON topology scenario, with $\mathcal{P}_{max} = 10^{-2}$: (a) Poisson case, (b) peaked case with $Z = 1.4$ and (c) smooth case with $Z = 0.8$.

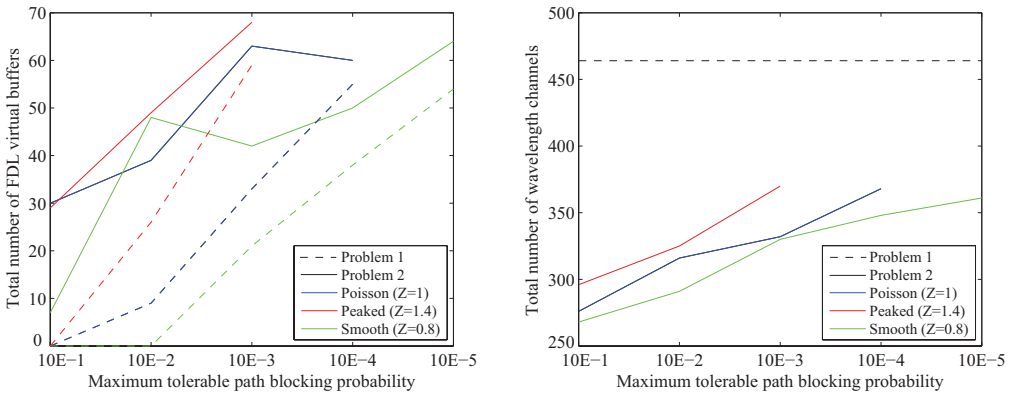

Figure 5.14: Total number of required wavelength channels for the NSFN topology scenario in order to achieve the maximum tolerable end-to-end burst loss. Total FDL virtual buffers (a) and total link channels (b).

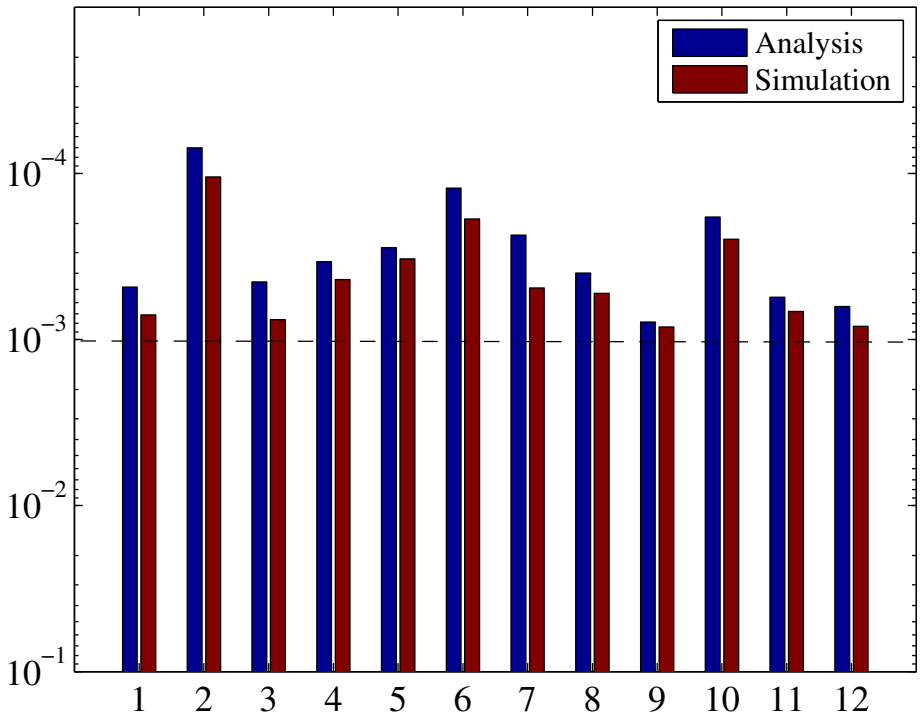

Figure 5.15: Path blocking probabilities of the NSFN topology scenario for $W = 16$, $\rho = 0.25$ Erlangs per channel, $Z = 1.4$ and $\mathcal{P}_{max} = 10^{-3}$. The optimal link/FDL channel allocation is **X**=[8 8 16 16 8 12 16 9 16 16 16 16 10 11 16 16 8 12 15 11 16 13 16 16 8 11 15 11 8 8 3 7 5 8 0 7 8 0 8 1 8 5].

Figure 5.16(a) is an additional illustrative example of the performance of the applied GA for the NSF topology scenario, where the absolute value of the fitness of the best individual in the population is shown for increasing number of generations. It can be observed that the fitness value begins to stabilise after 100 generations and settles to the minimum value after $\approx$ 180 generations. The same cannot be said for the EON topology scenario in Figure 5.16(b) where the absolute value of fitness is stabilising after $\approx$ 300 generations. This is mainly due to the size and nature of the solution space which requires the GA to run on a bigger population and for a higher number of generations compared to the NSF topology case.

5.4.3 Resolving Problem 3

In this case we want to find an optimal allocation of FDL virtual buffers that simultaneously minimises the maximum end-to-end burst loss probability and the total network hardware cost. We adopt the multi-objective GA presented in the previous section in order to resolve the optimisation problem. The analysis is once again conducted for both the NSF and the EON network topologies with the same configuration settings as in Problem 1. The population size $popSize$ is set at 300 individuals. The maximum number of elite individuals is set to $maxEliteSize = 30$, whereas the size of the random set is

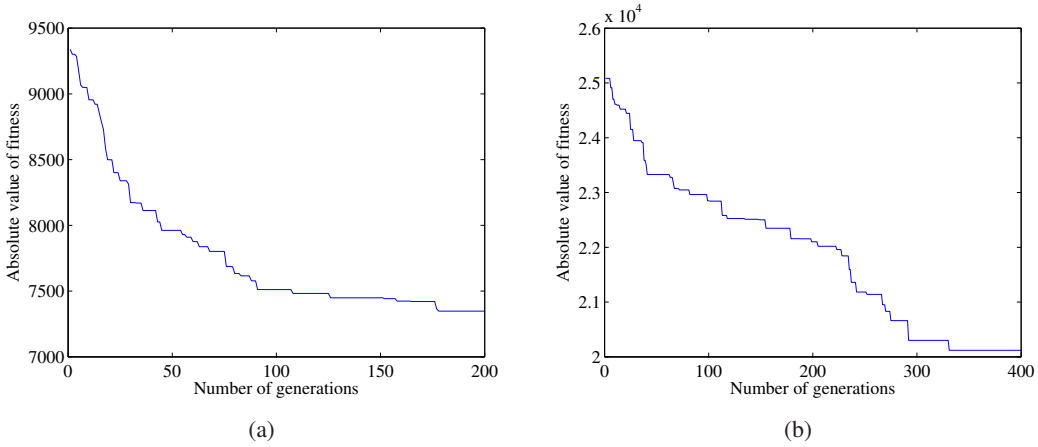

Figure 5.16: Absolute fitness value of the best individual in the population: case (a) NSFN topology scenario, with $Z = 0.8$ and $\mathcal{P}_{max} = 10^{-4}$. Case (b) EON topology scenario, with $Z = 0.8$ and $\mathcal{P}_{max} = 10^{-5}$.

$randSize = 100$ individuals. Thus, the reproduction set size is dynamically defined by $repSize = popSize - randSize - min(paretoSize, maxEliteSize)$. The GA selects individuals according to the tournament selection strategy and generates offspring by adopting a random crossover operator. The optimisation process ends after a maximum number of generations $maxGen = 500$ has been reached. Results obtained for the NSF case are depicted in Figures 5.17 and 5.18. The curves represent estimates of the Pareto-fronts, that is the values of achievable end-to-end burst loss at different optimum hardware cost determined by the obtained Pareto-optimal solutions. Each curve is associated with a specific value of peakedness. Once again, note how the achievable performance determined by each Pareto-optimal solution is considerably sensitive to the peakedness of the offered traffic. Similarly to the results of Problems 1 and 2, the obtained graphs give an insight to the problematics arising from the resource dimensioning of an OBS network with non-Poissonian offered traffic characteristics. For example, note that in Figure 5.18 the difference in terms of network cost in order to achieve a maximum end-to-end burst loss of 10^{-4} from smooth to peaked traffic is more than 500 SOA unit costs. Note also that the optimum solutions

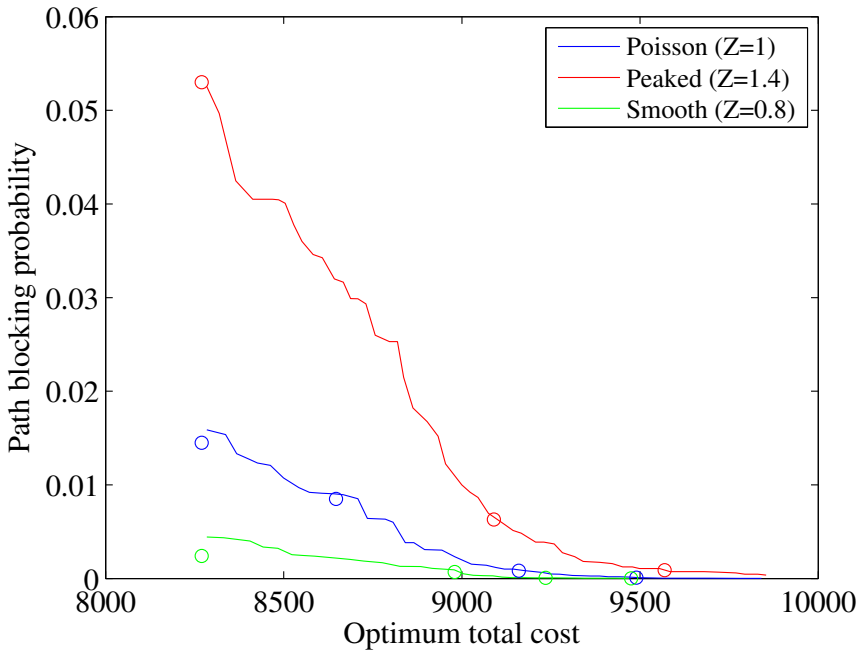

Figure 5.17: Pareto Front for the NSFN scenario for 3 different values of peakedness. Circles represent optimal solutions determined in Problem 1.

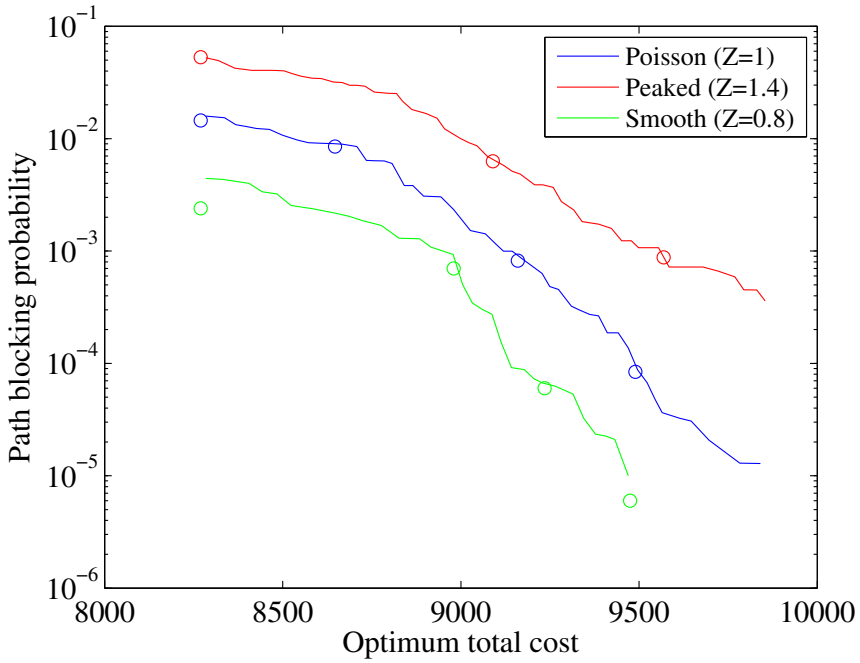

Figure 5.18: Pareto Front for the NSFN scenario for 3 different values of peakedness. End-to-end burst loss are represented in logarithmic scale. Circles represent optimal solutions determined in Problem 1.

determined for Problem 1 are either part of the curves or very close, showing that the GA is capable of successfully determining a good estimate of the Pareto fronts. Even though it can not be guaranteed that all Pareto-optimal solutions have been found, the obtained curves still provide useful information for pertinent resource dimensioning of the network under different offered peakedness values. The same conclusions can be drawn for the EON topology as illustrated in Figures 5.19 and 5.20, although in this case the shape of the curves may indicate that the GA was not able to fully explore the solution space (e.g., note the shape of the Pareto front for peaked traffic and for values of burst blocking greater than 10^{-2}). As discussed for Problem 2, this is mainly due to the fact that the solution space is bigger than in the NSF network case, thus the GA may be required to run on a bigger population and for a higher number of generations in order to guarantee an efficient exploration of the solution space. Nevertheless, in this particular example the algorithm is still able to find an acceptable estimate of the Pareto front as depicted in Figure 5.20. In fact, once again note how the curves are quite close to the expected optimal solutions determined in Problem 1. Figure 5.21 illustrates an example of the number of Pareto-optimal solutions found at each

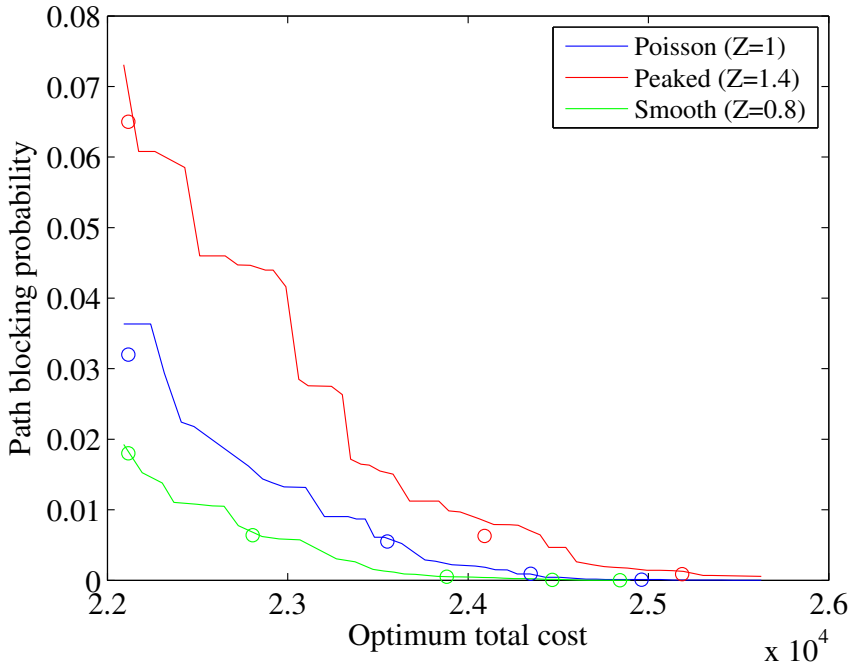

Figure 5.19: Pareto Front for the EON scenario for 3 different values of peakedness. Circles represent optimal solutions determined in Problem 1.

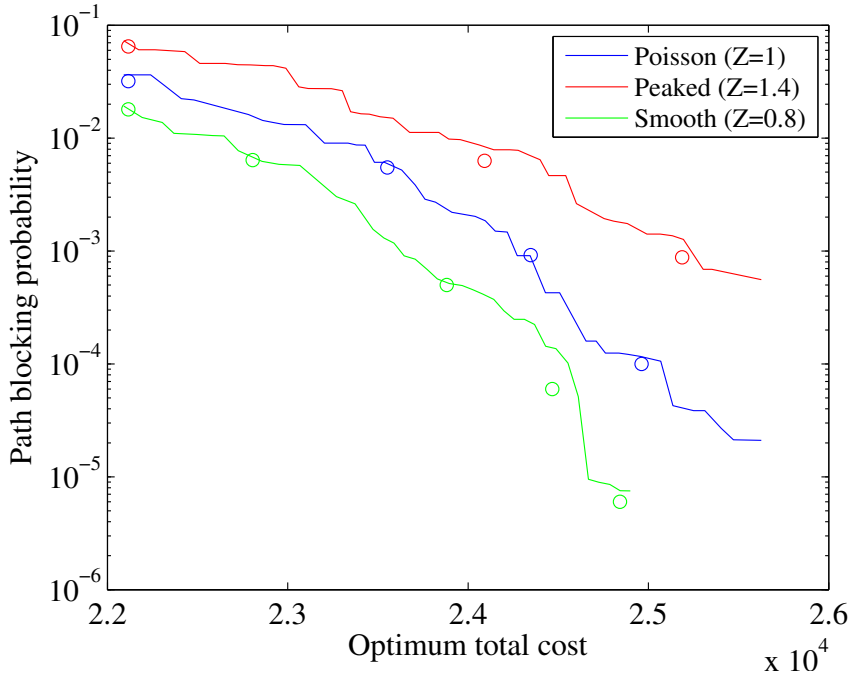

Figure 5.20: Pareto Front for the EON scenario for 3 different values of peakedness. End-to-end burst loss are represented in logarithmic scale. Circles represent optimal solutions determined in Problem 1.

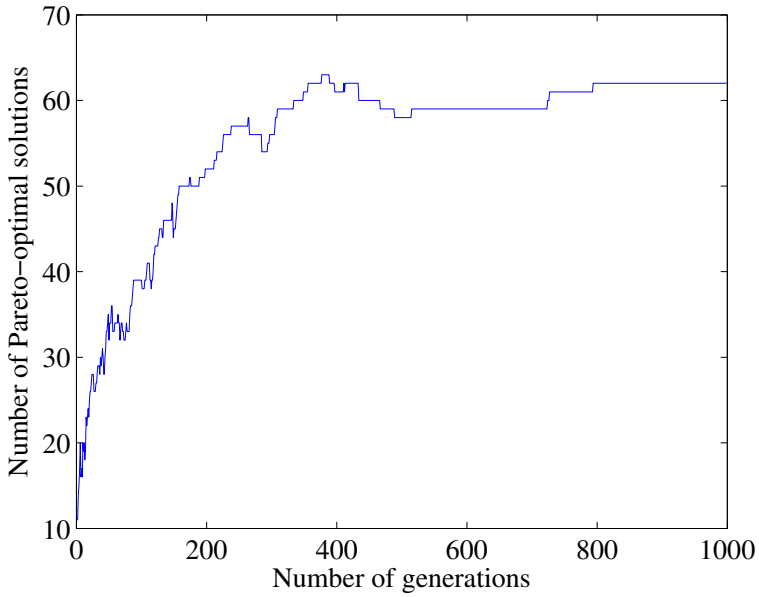

Figure 5.21: Number of Pareto-optimal solutions found for the EON topology scenario and $Z = 1.4$.

generation for the EON topology. Note that the number may also decrease since it may happen that a just found Pareto-optimal solution dominates several solutions comprised in the estimated Pareto front. After some generations, the number of solutions settles around a fixed value of 61 solutions and does not vary anymore (note that we must wait at least 200 generations before observing a stabilisation of the Pareto-front size).

5.4.4 Resolving Problem 4

In this case, the aim is to jointly optimise the number of link wavelength channels and of FDL virtual buffers in order to simultaneously minimise the end-to-end burst loss probability and the total network hardware cost. Once again, both network topologies are examined for 3 different values of peakedness. This last optimisation problem is the most challenging to solve due to the nature and the size of the solution space. Particularly, as discussed for the resolution of Problem 2, the GA is not able to determine a good estimate of the Pareto front due to the genetic drift. In fact, the presence of high density regions of the solution space prevents the algorithm from finding Pareto-optimal solutions in other regions with lower densities of individuals. This phenomenon is depicted in Figure 5.22 for the case of

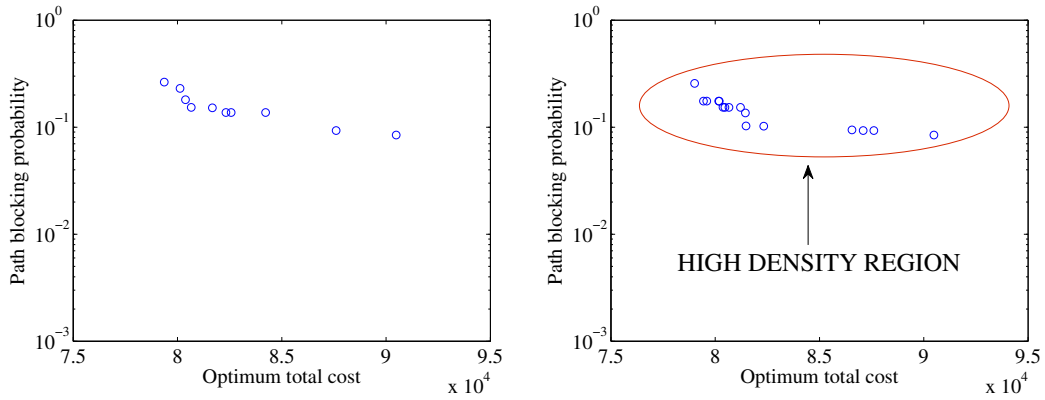

Figure 5.22: Evolution of the Pareto front for the NSFN topology: after 10 generations (a) and after 50 generations (b).

the NSFN topology. Note that after 50 generations the algorithm is only capable of finding Pareto-optimal solutions in the region of the solutions space delimited by a blocking probability value greater than 10^{-1}. In order to resolve this issue a strategy similar to the one adopted for Problem 2 is considered for the proposed optimisation problem. Specifically, the solution space is divided into different subsets $\mathcal{S}_i$ and the multi-objective GA is run independently for each subset. For this particular problem, all subsets are delimited by values of blocking probabilities of interests such that $\mathcal{S}_i = \mathbf{X}_i : \mathcal{P}_{max}(\mathbf{X}_i) < 10^{-i}$. Thus, for example $\mathcal{S}_1$ includes all the individuals that give a maximum end-to-end loss lower than 10^{-1}, S_2 includes all the individuals that give a maximum end-to-end loss lower than 10^{-2}, etc. The initial population is once again randomly generated but, similarly to Problem 2, a feasible individual with uniform allocation (determined with the analytic network model) is also included. The GA is then normally applied for each subset with the configuration settings defined in Table 5.2. Note that the discovered candidate Pareto-solutions are included in the estimate Pareto front only if they are within the bounds defined by the corresponding subset. For example, assume that the GA is running for subset $\mathcal{S}_4$ and two solutions $\mathbf{X}_1$ and $\mathbf{X}_2$ are discovered, yielding respectively values of end-to-end blocking probability equal to 0.00003 and 0.023. In this case only the first solution will be considered Pareto-optimal and included in the estimated Pareto front (unless the latter already contains solutions that dominate $\mathbf{X}_1$).

Results obtained with the proposed modification of the GA are presented in Figures 5.23 and 5.24, showing the estimated Pareto fronts for different values of offered traffic peakedness. In this case it can be observed that the estimation of the Pareto front is certainly poorer than the ones obtained for the previous optimisation problem. In fact, note that for smooth traffic it is not possible to determine the expected true shape of the curve for values of blocking probability in proximity of 10^{-1}. Nevertheless, with the proposed strategy it is possible to better explore the solution space and find candidate Pareto optimal solutions in less populated areas. Furthermore note that the estimated Pareto front is still quite close to the optimum points found in Problem 2 for the NSFN topology.

The proposed strategy does not provide the expected Pareto fronts for the EON topology case, thus it has not been possible to resolve the same multi-objective optimisation problem for this particular network scenario. The author believes that this is due mainly to the increased size and nature of the solution space which do not allow the GA to discover individuals closer to the Pareto front. Indeed, this is quite an interesting and challenging subject and is a topic for future work.

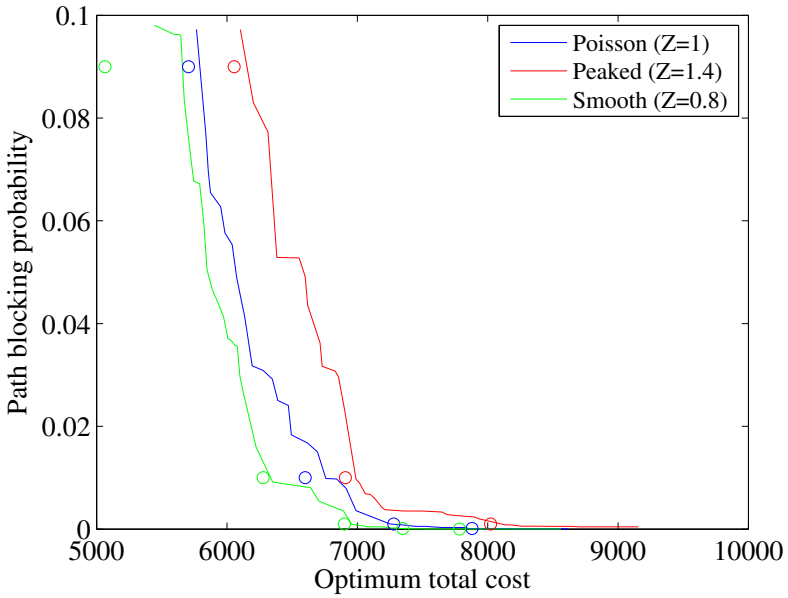

Figure 5.23: Pareto Front for the NSFN scenario for 3 different values of peakedness. Circles represent optimal solutions determined in Problem 2.

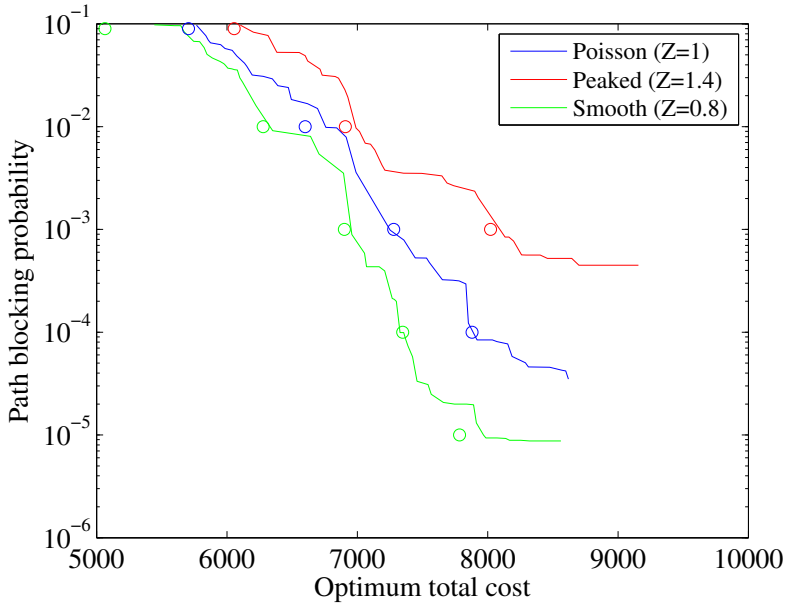

Figure 5.24: Pareto Front for the NSFN scenario for 3 different values of peakedness. End-to-end burst loss are represented in logarithmic scale. Circles represent optimal solutions determined in Problem 2.

5.5 Conclusions

This chapter dealt with the definition and solution of four resource dimensioning problems for an FDL-buffered OBS network. The analysis has been made on the basis of the analytic network model derived in the previous chapter and the optimisation problems have been resolved with the application of single/multi-objective genetic algorithms. Results highlight the usefulness of the analytic network model when applied for resolving OBS network optimisation problems, mainly in relation to its capability of approximating non-Poissonian traffic characteristics. Optimal allocations of link/FDL wavelength channels are found to be highly sensitive to the peakedness of the offered traffic, causing substantial variations of the minimum required total network hardware costs for relatively small variations in peakedness values.

Chapter 6

Conclusions

This thesis dealt with the analytic modelling and the resource optimisation of FDL-buffered OBS networks. The work has been motivated by the necessity of deriving analytic tools that can be used for OBS performance analysis and optimisation with the purpose of designing networks subject to a desired grade of service and physical constraints. This last chapter presents the conclusions of the thesis. In Section 6.1, the reader can find a summary of the thesis main contributions whereas Section 6.2 proposes suggestions for future investigations toward the same research direction pursued by the author.

6.1 Main Contributions

The main contributions of the work presented in this thesis can be listed as follows:

- The first contribution is the derivation of an analytic model of a buffered OBS node where contentions amongst bursts are resolved with full wavelength conversion and with FDLs, that is the E-BPP+FMM method. Particularly, an OBS TAS-shFDL architecture has been considered for the analysis, where the output ports share a multi-channel FDL in a feedback configuration. The system has been studied by conducting a flow analysis with the aim of estimating burst blocking probabilities associated with each traffic flow. All traffic flows have been characterised in terms of their average load and of their peakedness by means of two-moment matching techniques, resulting in the realisation of an accurate approximate model of the switch. The analysis

has been validated by comparing the estimated values of burst blocking probability with results obtained from a discrete-event simulator of the OBS node. It has been demonstrated that the model is accurate when compared to simulation for a broad range of values of blocking probabilities, burst traffic characteristics and resource capacities. Furthermore the model always outperformed state-of-the-art one-moment node models, where burst traffic arrivals are assumed to be Poisson. The results presented in Chapter I further showed the high sensitivity of the blocking probability to the load of the offered traffic and especially to its peakedness, a phenomenon that the proposed model was successfully able to track.

- The second contribution is the realisation of an FDL-buffered OBS network model based on the E-BPP+FMM analysis derived in Chapter 3, that is the Shared-Buffer Network Model (SBNM). The analytic model has been realised with the link decomposition method and with a two-moment description of the traffic streams within the network, allowing the estimation of end-to-end burst loss for performance evaluation of the OBS network. The method follows a path-centric approach in the sense that each blocking probability is calculated separately for each path. Additionally, the results have been further refined by eliminating from the analysis the links whose burst blocking probability is zero due to the streamline effect. Results showed good accuracy when compared with simulation data for two different network scenarios and for a broad range of blocking probability values, traffic characteristics and resource capacities. Similarly to the node model, the analysis outperformed one-moment Poisson network models in terms of accuracy, further demonstrating the importance of considering the peakedness of the traffic when conducting performance evaluation of the OBS network. As in the node model, results illustrated a strong sensitivity of the blocking probability to the load and the peakedness of the offered traffic, especially under low load regime. Overall, the proposed analytic method proved to be useful for modelling OBS networks in the definition and resolution of optimisation problems.

- The third and final contribution of this thesis is related to resource dimensioning of FDL-buffered OBS networks. Specifically, a network cost function has been intro-

duced as an indicative estimation of the expenses associated with the TAS-shFDL architecture components. Then, four optimisation problems have been defined, modelling the OBS network with the methodology presented in Chapter 4. All problems consisted of identifying an optimal allocation of network resources (link/FDL wavelength channels) that minimises the total hardware costs under grade of service and physical constraints. Single and multi-objective GAs have been developed and used to solve the problems. Results showed once again the importance of considering the sensitivity of blocking to the peakedness of the offered traffic when dimensioning the network. Particularly, it has been observed an $\approx 7\%$ difference in total network cost savings when reducing the peakedness value by $\approx 20\%$, which may be translated into several hundreds of SOA unit costs in terms of total hardware expenses. The main purpose of this chapter has been to illustrate a potential application of the proposed network model, demonstrating its effectiveness when used for determining optimal link/FDL wavelength channels allocation for buffered OBS networks.

6.2 Future Works

The research community has devoted great effort to performance evaluation of OBS in the past decade, particularly to switch modelling and simulation studies of OBS networks. This thesis attempted to provide contributions toward areas of study that did not received the same level of attention, as discussed in the previous section. Nevertheless, further investigations are still required in order to realise and deploy commercially viable OBS-based technologies. In relation to the work proposed in this thesis, there is certainly still space for substantial improvements, especially for OBS node modelling.

First of all, it would be desirable to realise an analytic model of the OBS TAS-shFDL node architecture when multiple FDLs are employed for resolving contentions. The author already investigated this subject in [74] but neglecting the case where burst offered traffic is smooth. Hence, the realisation of a more general model including a shared pool of FDLs that can handle different traffic peakedness values would yield a more comprehensive and accurate performance analysis of the TAS-shFDL architecture. The author believes that the

E-BPP+FMM analysis proposed in this thesis can be extended and serve as a building block for the derivation of such a model.

More effort should be devoted to OBS performance analysis when the number of wavelength converters is limited, that is under partial wavelength conversion capability. Like in the majority of the research literature, the proposed analytic model assumes full wavelength conversion, that is, each wavelength channel is equipped with a TWC; however, wavelength converters are expensive devices and, in order to deploy realistic OBS-based network architectures, it is believed that their total number will be most likely limited and organised in a pool shared between the output ports of a node. Furthermore, it has already been proven that OBS nodes employing partial wavelength conversion configurations may achieve the similar performance to nodes with full wavelength conversion capability in terms of reducing burst loss probability. Hence, inclusion of partial wavelength conversion in the proposed analysis would result in a more complete and realistic TAS-shFDL node model, allowing study of the performance of the switch under different configurations of TWCs and FDLs.

Finally, further improvements can be made for the optimisation process of the OBS network. This thesis dealt only with OBS resource dimensioning problems, particularly focusing on solving link/FDL allocation problems using single/multi-objective genetic algorithms. Clearly there is a great variety of scenarios that can be analysed and several different methodologies applied when resolving these kind of problems. It has been further illustrated that the complexity of the optimisation problem depends on the size and nature of the solution space (e.g., note that it has not been possible to resolve Problem 4 for the EON topology scenario). More sophisticated population-based algorithms should be considered for the resolution of the problem, such as cell-based GAs [60]. Nevertheless, the purpose of Chapter 5 was primarily to illustrate the usefulness of the derived analytic OBS network model when applied to optimisation problems. It is the hope of the author that the work presented in this thesis would provide useful information to other researchers working in the area, helping them in the derivation of more accurate and efficient OBS analytic models.

List of Publications

- **D. Tafani**, C. McArdle, L. P. Barry, "Resource Dimensioning of Optical Burst Switched Networks with Genetic Algorithms," *IEEE/OSA Journal of Optical Communications and Networking*, to be submitted.

- C. McArdle, **D. Tafani**, L. P. Barry, "Overflow Traffic Moments in Channel Groups Offered Bernoulli-Poisson-Pascal (BPP) Load," *Proc. of IEEE Globecom 2012*, pending review.

- **D. Tafani**, B. Kantarci, H. Mouftah, C. McArdle, L. P. Barry, "Distributed Management of Energy-Efficient Lightpaths for Computational Grids," *Proc. of IEEE Globecom 2012*, pending review.

- **D. Tafani**, B. Kantarci, H. Mouftah, C. McArdle, L. P. Barry, "Energy-Efficient Ligthpaths for Computational Grids," *Proc. of ICTON 2012*, 2 - 5 July 2012, Coventry, UK.

- **D. Tafani**, C. McArdle, L. P. Barry, "Cost Minimisation for Optical Burst Switched Networks with Share-per-Node Fibre Delay Lines," *IEEE Communications Letters*, in press.

- **D. Tafani**, C. McArdle, L. P. Barry, "A Two-Moment Performance Analysis of Optical Burst Switched Networks with Shared Fibre Delay Lines in a Feedback Configuration," *Elsevier Optical Switching and Networking*, in press.

- **D. Tafani**, C. McArdle, L. P. Barry, "Optimal Allocation of Fibre Delay Lines in Optical Burst Switched Networks," *Proc. of IARIA 8th Advanced International Conference on Telecommunications 2012 (AICT 2012)*, Stuttgart, Germany, 27 May - 01 June 2012.

- **D. Tafani**, C. McArdle, L. P. Barry, "Analytical Model of Optical Burst Switched Networks with Share-per-Node Buffers," *Proc. of the Sixteenth IEEE Symposium on*

Computers and Communications (ISCC 2011), 28 June 2011-1 July 2011, Kerkyra, Corfu, Greece.

- C. McArdle, **D. Tafani**, T. Curran, A. Holohan, L. P. Barry, "Renewal Model of a Buffered Optical Burst Switch," *IEEE Communications Letters*, vol. 15, no. 1, January 2011.

- **D. Tafani**, C. McArdle, L. P. Barry, "An Analytic Model of a Buffered Multi-Port Optical Burst Switch using Two Moments Traffic Approximation," *Proc. 2010 China-Ireland International Conference on Information and Communications Technologies (CIICT 2010)*, Wuhan, China, October 2010.

- C. McArdle, **D. Tafani**, L. P. Barry, "Analysis of a Buffered Optical Switch with General Interarrival Times," *Selected Papers of The International Symposium on Performance Evaluation of Computer and Telecommunication Systems (SPECTS 2009), Journal of Networks*, vol. 6, no. 4, pp. 536-548, April 2011.

- C. McArdle, **D. Tafani**, L. P. Barry, "Simplified Overflow Analysis of an Optical Burst Switch with Fibre Delay Lines," *Proc. Sixth International Conference on Broadband Communications Networks and Systems (BROADNETS 2009)*, Madrid, Spain, September 14-16 2009.

- **D. Tafani**, C. McArdle, "Approximate Analysis of Fibre Delay Lines and Wavelength Converters in an Optical Burst Switch," *Proc. 2009 China-Ireland International Conference on Information and Communications Technologies (CIICT 2009)*, Maynooth, Ireland, August 19-21 2009.

- C. McArdle, **D. Tafani**, L. P. Barry, "Equivalent Random Analysis of a Buffered Optical Switch with General Interarrival Times," *Proc. 2009 International Symposium on Performance Evaluation of Computer and Telecommunications Systems (SPECTS 2009)*, Istanbul, Turkey, July 13-16 2009.

Bibliography

[1] A. Al Amin, K. Nishimura, K. Shimizu, M. Takenaka, T. Tanemura, H. Onaka, T. Hatta, A. Kasukawa, S. Tsuji, Y. Kondo, Y. Urino, H. Uetsuka, Y. Nakano, "Development of an Optical-Burst Switching Node Testbed and Demonstration of Multibit Rate Optical Burst Forwarding," *IEEE/OSA Journal of Lightwave Technology*, vol. 27, no. 16, pp. 3466-3475, 2009. 3, 8, 58

[2] R. C. Jr. Almeida, J. U. Pelegrini, H. Waldman, "A Generic-Traffic Optical Buffer Modeling for Asynchronous Optical Switching networks," *IEEE Communications Letters*, vol. 9, no. 2, September 2005. 20

[3] N. Akar, E. Karasan, G. Muretto, C. Raffaelli, "Performance Analysis of an Optical Packet Switch Employing Full/Limited Range Share Per Node Wavelength Conversion," *Proceedings of the IEEE Global Telecommunications Conference, 2007 (GLOBECOM 2007)*, pp. 2369-2373, Washington DC, USA, 26-30 November 2007. 20, 24

[4] S. Azodolmolky, A. Tzanakaki, I. Tomkos, "Study of the Impact of Burst Assembly Algorithms in Optical Burst Switched Networks with Self-Similar Input Traffic," *Proceedings of the International Conference on Optical Transparent Networks, ICTON 2006*, vol. 3, pp. 35-40, 2006. 10, 21

[5] I. Baldine, G. N. Rouskas, H. G. Perros, D. Stevenson, 'JumpStart: a Just-In-Time Signaling Architecture for WDM Burst-Switched Networks ," *IEEE Communications Magazine*, vol. 40, no. 2, pp. 82-89, 2002. 3, 12

[6] I. Baldine, A. Bragg, G. Evans, M. Pratt, M. Singhai, D. Stevenson, R. Uppalli, "JumpStart Deployments in Ultra-High-Performance Optical Networking Testbeds," *IEEE Communications Magazine*, vol. 43, no. 11, pp. S18-S25, November 2005. 12

[7] A. L. Barradas, M. C. R. Medeiros, "Preplanned Optical Burst Switched Routing Strategies Considering the Streamline Effect," *Photonic Network Communications*, vol. 19, no. 2, pp. 161-169, 2009. 76

[8] T. Battestilli, H. Perros, "An Introduction to Optical Burst Switching," *IEEE Communications Magazine*, vol. 41, no. 8, pp. S10-S15, August 2003. 2, 14

[9] L. Battestilli, H. Perros, "A Performance Study of an Optical Burst Switched Network with Dynamic Simultaneous Link Possession," *Elsevier Computer Networks*, vol. 50, no. 2, pp. 219-236, 2006. 21, 24, 72

[10] L. Battestilli, H. Perros, "Performance Evaluation of an OBS Network as a Tandem Network of $IPP/M/W/W$ Nodes," *Proceedings of APARM 2010*, 2-4 December 2010, Wellington, New Zealand. 21, 24

[11] L. Battestilli, H. Perros, S. Chukova, "Burst Lost Probabilities in a Network with Simultaneous Link Possession: A Single-Node Decomposition Algorithm," *IET Communications*, vol. 3, no. 3, pp. 441-453, March 2009. 21

[12] N. Bhatnagar, "Model of a Queue with Almost Self-Similar or Fractal-Like Traffic," *Proceedings of the IEEE Global Telecommunications Conference 1997, (IEEE GLOBECOM 1997)*, vol. 3, pp. 1424-1428, November 1997. 54

[13] A. Brandt, M. Brandt, "On the Moments of Overflow and Freed Carried Traffic for the $GI/M/C/0$ System," *Methodology and Computing in Applied Probability*, vol. 4, no. 1, pp. 69-82, March 2002. 36, 49

[14] G. Bretschneider, "Extension of the Equivalent Random Method to Smooth Traffic," *Proceedings of the International Teletraffic Congress 1973, (ITC 1973)*, vol. 7, pp. 411/1-411/9, 1973. 36

[15] H. Buchta , E. Patzak, “Analysis of the Physical Impairments on Maximum Size and Throughput of SOA-Based Optical Burst Switching Nodes,” *IEEE/OSA Journal of Lightwave Technology*, vol. 26, no. 16, pp. 2821-2830, 2008. 26, 27

[16] H. Buchta , E. Patzak, J. Saniter, S. F. Raub, “Impact of SOA Gain Saturation and Dynamics on the Throughput of Optical Burst Switching Nodes,” *Proceedings of the Optical Fiber Communication Conference 2004, (OFC 2004)*, vol. 2, pp. 1-3, Los Angeles, USA, 23-27 February 2004. 27

[17] H. Buchta , C. Gauger, E. Patzak, “Maximum Size and Throughput of SOA-Based Optical Burst Switching Nodes With Limited Tuning-Range Wavelength Converters and FDL Buffers,” *IEEE/OSA Journal of Lightwave Technology*, vol. 26, no. 16, pp. 2919-2927, 2008. 8, 26, 27, 28, 30

[18] F. Callegati, “Optical Buffers for Variable Length Packets,” *IEEE Communications Letters*, vol. 4, no. 9, September 2000. 19

[19] J. C. S. Castro, J. M. F. Pedro, P. P. Monteiro, “Routing and Buffer Placement Optimization in Optical Burst Switched Networks,” *Proceedings of the 33rd IEEE Conference on Local Computer Networks 2008*, pp. 353-360, 14-17 Oct. 2008. 21, 23, 24, 99

[20] H. M. Chaskar, S. Verma, R. Ravikanth, “A Framework to Support IP over WDM Using Optical Burst Switching,” *Proceedings of the Optical Networks Workshop*, January 2000. 8

[21] J. Y. Choi, J. S. Choi, M. Kang, “Dimensioning Burst Assembly Process in Optical Burst Switching Networks,” *IEICE Communications Transactions*, vol. E88-B, no. 10, October 2005. 10

[22] J. Y. Choi, J. S. Choi, M. Kang, “Node Dimensioning in Optical Burst Switching Networks,” *Photonic Network Communications*, vol. 13, no. 2, pp. 207-216, October 2006. 10

[23] K. Christodoulopoulos, E. Varvarigos, K. Vlachos, “A New Burst Assembly Scheme Based on the Average Packet Delay and its Performance for TCP Traffic,” *Elsevier Optical Switching and Networking*, vol. 4, no. 2, pp. 200-212, May 2007. 10

[24] M. E. Crovella, A. Bestavros, “Self-Similarity in World Wide Web Traffic: Evidence and Possible Causes,” *IEEE/ACM Transactions on Networking*, vol. 5, no. 6, pp. 835-846, December 1997. 10, 21

[25] K. Deb, “An Efficient Constraint Handling Method for Genetic Algorithms,” *Computer Methods in Applied Mechanics and Engineering*, vol. 186, no. 2-4, pp. 311-338, June 2000. 106, 109, 112

[26] K. Deb,“Multi-Objective Genetic Algorithms: Problem Difficulties and Construction of Test Problems,” *Evolutionary Computation*, vol. 7, pp. 205-230, 1999. 123

[27] L. E. N. Delbrouck, “A Unified Approximate Evaluation of Congestion Functions for Smooth and Peaky Traffics,” *IEEE Transactions on Communications*, vol. COM-29, no. 2, February 1981. 21, 36, 37

[28] L. E. N. Delbrouck, “The Uses of Kosten’s System in the Provisioning of Alternate Trunk Groups Carrying Heterogeneous Traffic,” *IEEE Transactions on Communications*, vol. COM-31, no. 2, pp. 741-749, 1983. 21, 36, 37, 38, 72, 81

[29] I. de Miguel, R. Vallejos, A. Beghelli, R. Duran, “Genetic Algorithm for Joint Routing and Dimensioning of Dynamic WDM Networks ,” *IEEE/OSA Journal of Optical Communications and Networking*, vol. 1, no. 7, pp. 608-621, December 2009. 22, 99

[30] P. J. Deschamps, “Analytic Approximation of Blocking Probabilities in Circuit Switched Communication Networks,” *IEEE Transactions on Communications*, vol. COM-27, no. 3, March 1979. 40

[31] K. Dolzer, C. Gauger, “On Burst Assembly in Optical Burst Switching Networks - A Performance Evaluation of Just-Enough-Time,” *Proceedings of the 17th International Teletraffic Congress, (ITC 2001)*, pp. 149-160, 2001. 12

[32] M. Duser, P. Bayvel, “Analysis of a Dynamically Wavelength-Routed Optical Burst Switched Network Architecture,” *IEEE/OSA Journal of Lightwave Technology*, vol. 20, no. 4, pp. 574-585, April 2002. 8

[33] V. Eramo, M. Listanti, and A. Germoni , “Cost Evaluation of Optical Packet Switches Equipped With Limited-Range and Full-Range Converters for Contention Resolution,” *IEEE/OSA Journal of Lightwave Technology*, vol. 26, no. 4, pp. 390-407, 2008. 116

[34] P. Fan, C. Feng, Y. Wang, N. Ge, “Investigation of the Time-Offset-Based QoS Support with Optical Burst Switching in WDM Networks,” *Proceedings of the IEEE International Conference on Communications, (IEEE ICC 2002)*, vol. 5, pp. 2682-2686, New York, USA, 28 April 2002 - 2 May 2002. 10, 20

[35] A. G. Fayoumi, A. P. Jayasumana, “Performance Model of an Optical Switch using Fiber Delay Lines for Resolving Contention,” *Proceedings of the IEEE International Conference on Local Computer Networks*, pp. 178-186, October 2003. 72

[36] H. Feng , E. Patzak, J. Saniter, “Size and Cascadability Limits of SOA Based Burst Switching Nodes,” *Proceedings of the 28th European Conference on Optical Communication 2002, (ECOC 2002)*, pp. 1-2, Copenhagen, Denmark, 8-12 September 2002. 27

[37] L. Galdino, J. Maranhao, M. T. Furtado, E. Moschim, L. H. F. Bonani, R. Durand, “Sparse Partial Optical Code and Wavelength Conversion Architecture in Hybrid WDM/OCDM OBS Networks,” *Proceedings of the 18th International Conference on Telecommunications 2011, (ICT 2011)*, pp. 211-215, 8-11 May 2011. 22

[38] C. M. Gauger, “Contention Resolution in Optical Burst Switching Networks,” *COST 266*, Workgroup 2, Technical Committee Telecommunications, pp. 62-82, July 2002. 15, 16, 23, 26, 27, 28, 31, 32

[39] C. M. Gauger, “Optimized Combination of Converter Pools and FDL Buffers for Contention Resolution in Optical Burst Switching,” *Photonic Network Communications*, vol. 8, no. 2, pp. 139-148, 2004. 16, 26

[40] C. M. Gauger, H. Buchta, E. Patzak, “Integrated Evaluation of Performance and Technology - Throughput of Optical Burst Switching Nodes Under Dynamic Traffic,” *IEEE/OSA Journal of Lightwave Technology*, vol. 26, no. 13, pp. 1969-1979, July 2008. 8, 11, 16, 26, 28, 29, 30, 31, 91, 100

[41] A. Ge, F. Callegati, L. S. Tamil, “On Optical Burst Switching and Self-Similar Traffic,” *IEEE Communications Letters*, vol. 4, no. 3, March 2000. 11

[42] A. Girard, *Routing and Dimensioning in Circuit-Switched Networks*, Addison-Wesley Longman Publishing Company, 1990. 10, 11, 20, 21, 33, 34, 35, 36, 38, 39, 40, 50, 53, 69, 70, 96

[43] M. Glabowski, A. Kaliszan, “Simulator of Full-Availability Group with Bandwidth Reservation and Multi-Rate Bernoulli-Poisson-Pascal Traffic Streams,” *Proceedings of EUROCON 2007*, pp. 2271-2277, 9-12 September 2007. 53

[44] D. E. Goldberg, *Genetic Algorithms in Search, Optimization and Machine Learning*, Addison-Wesley Longman Publishing Company, 1989. 106, 111, 112

[45] M. F. Hayat, F. Z. Khan, H. R. van As, “Performance Model for an OBS Node with a Shared Wavelength Converter Pool and an FDL Buffer per Link ,” *Proceedings of the 15th International Conference on Optical Network Design and Modeling 2011, (ONDM 2011)*, pp. 1-6, Bologna, Italy, 8-10 February 2011. 20, 24

[46] W. Helly, “Two Doctrines for the Handling of Two-Priority Traffic by a Group of N Servers,” *Operations Research*, vol. 10, pp. 268-269, March-April 1962. 42

[47] H. Ishibuchi, T. Murata, “A Multi-Objective Genetic Local Search Algorithm and its Application to Flowshop Scheduling,” *IEEE Transactions on Systems, Man, and Cybernetics, Part C: Applications and Reviews*, vol. 28, no. 3, pp. 392-403, August 1998. 110, 115

[48] C. F. Hsu, T. L. Liu, N. F. Huang, "Performance Analysis of Deflection Routing in Optical Burst-Switched Networks," *Proceedings of the 21st Annual Joint Conference of the IEEE Computer and Communications Societies 2002, (IEEE INFOCOM 2002)*, pp. 66-73, New York, USA, November 2002. 18

[49] Y. Hsueh et al.,"Traffic Grooming on WDM Rings Using Optical Burst Transport," *IEEE/OSA Journal of Lightwave Technology*, vol. 24, no. 1, pp. 44-53, February 2006. 7

[50] D. K. Hunter, M. C. Chia, I. Andonovic, "Buffering in optical packet switches," *IEEE/OSA Journal of Lightwave Technology*, vol. 16 no. 12, pp. 20812094, December 1998. 14, 15, 16

[51] Janardan, K. J., 'Moments of Certain Series Distributions and their Applications', *SIAM Journal on Applied Mathematics*, vol. 44, no. 4, pp. 854-868, August 1984. 49

[52] P. J. Jue, V. M. Vokkarane, *Optical Burst Switched Networks*, Springer, 2005. 7, 8, 11, 12, 15, 16, 17

[53] S. Katz, "Statistical Performance Analysis of a Switched Communication Network," *Proceedings of the International Teletraffic Congress*, vol. 5, 1967. 36

[54] F. P. Kelly, "Blocking Probabilities in Large Circuit Switched Networks," *Advances in Applied Probability*, vol. 18, pp. 473-505, 1986. 21, 69, 70, 77

[55] M. G. Khair, B. Kantarci, J. Zheng, H. T. Mouftah, "Optimization for Fault Localization in All-Optical Networks," *IEEE/OSA Journal of Lightwave Technology*, vol. 27, no. 21, pp. 4832-4840, November 2009. 69

[56] J. Kim, J. Cho, S. Das, D. Gutierrez, M. Jain, C. F. Su, R. Rabbat, T. Hamada, L. G. Kazovsky, "Optical Burst Transport: A Technology for the WDM Metro Ring Networks," *IEEE/OSA Journal of Lightwave Technology*, vol. 25, no. 1, pp. 93-101, January 2007. 7

[57] L. Kleinrock, *Queuing Systems Volume I: Theory*, John Wiley & Sons, 1975. 10, 33, 34, 71

[58] M. Klinkowski, M. Pioro, D. Careglio, M. Marciniak, J. Sole-Pareta, "Non-Linear Optimization for Multi-Path Source Routing in OBS Networks," *IEEE Communications Letters*, vol. 11, no. 12, pp. 1016-1018, 2007.

[59] B. Komatireddy, N. Charbonneau and V. M. Vokkarane, "Source-Ordering for Improved TCP Performance over Load-Balanced Optical Burst-Switched (OBS) Networks," *Photonic Network Communications*, vol. 19, no. 1, pp. 1-8, 2009. 18

[60] A. Konak, D. W. Coit, A. E. Smith, "Multi-Objective Optimization using Genetic Algorithms," *Elsevier Reliability Engineering and System Safety*, vol. 91, pp. 992-1007, January 2006. 108, 123, 139

[61] A. Kuczura, D. Bajaj, "A Method of Moments for the Analysis of a Switched Communication Network's Performance," *IEEE Transactions on Communications*, vol. COM-27, pp. 185-193, 1977. 36

[62] K. G. Kwak, E. G. Coffman, "Retransmission in OBS Networks with Fiber Delay Lines," *Proceedings of the fourth International Conference on Broadband Communications, Networks and Systems 2007 (BROADNETS 2007)*, pp. 243-249, 10-14 September 2007, Raleigh, NC, USA. 72

[63] T. Legrand, H. Nakajima, P. Gavignet, B. Cousin, "Labelled OBS Test Bed for Contention Resolution Study," *Proceedings of the 5th International Conference on Broadband Communications, Networks and Systems, 2008 (BROADNETS 2008)*, pp. 82-87 , 8-11 September 2008. 3, 58, 91

[64] Z. Liang, S. Xiao, "Performance Evaluation of Single-Wavelength Fiber Delay Line Buffer with Finite Waiting Places," *IEEE/OSA Journal of Lightwave Technology*, vol. 26, no. 5, pp. 520-527, March 2009. 20

[65] J. Liu, T. T. Lee, X. Jiang, S. Horiguchi "Blocking and Delay Analysis of Single Wavelength Optical Buffer with General Packet Size Distribution," *IEEE/OSA Journal of Lightwave Technology*, vol. 27, no. 8, pp. 955-966, April 2009. 20

[66] X. Lu, B. L. Mark, “Performance Modeling of Optical-Burst Switching with Fiber Delay Lines,” *IEEE Transactions on Communications*, vol. 52, no. 12, pp. 2175-2183, December 2004. 10, 17, 20, 21, 24, 26, 27, 55, 56, 57, 58, 72, 83, 99

[67] G. F. Lucio, M. Paredes-Farrera, E. Jammeh, M. Fleury, M. J. Reed, “OPNET Modeler and Ns-2: Comparing the Accuracy of Network Simulators for Packet-Level Analysis using a Network Testbed,” *Proceedings of the 3rd WEAS International Conference on Simulation, Modelling and Optimization 2003, (ICOSMO 2003)*, pp. 700-707, 2003. 52

[68] G. Maier, A. Pattavina, “Generalized Space-Equivalent Analysis of Optical Cross-Connect Architectures,” *Proceedings of the twentieth Annual Joint Conference of the IEEE Computer and Communications Societies (IEEE INFOCOM 2001)*, vol. 1, pp. 159-168, Anchorage, AK , USA, 22-26 April 2001. 17

[69] F. Masetti, et al., “Design and Implementation of a Multi-Terabit Optical Burst/Packet Router Prototype,” *Proceedings of the Optical Fiber Communication Conference 2002, (OFC 2002)*, pp. FD1-1 - FD1-3, Texas, USA, 17-22 March 2002. 3, 8

[70] Matworks, *Matlab*, URL:http://www.mathworks.co.uk/products/matlab/index.html, last visited December 2011. 64

[71] Matsuura, M., Kishi, N., Miki, T., ‘Ultrawideband Wavelength Conversion Using Cascaded SOA-Based Wavelength Converters’, *IEE/OSA Journal of Lightwave Technology*, vol. 25, no. 1, pp. 38-45, January 2007. 17

[72] C. McArdle, D. Tafani, T. Curran, A. Holohan, L. P. Barry, “Renewal Model of a Buffered Optical Burst Switch,” *IEEE Communications Letters*, vol. 5, no. 1, pp. 91-93, January 2011. 16, 52, 53

[73] C. McArdle, D. Tafani, L. P. Barry, “Equivalent Random Analysis of a Buffered Optical Switch with General Interarrival Times” Proc. *2009 International Symposium*

on Performance Evaluation of Computer and Telecommunication Systems, (SPECTS 2009), vol. 41, pp. 238-245, Istanbul, Turkey, July 2009. 49

[74] C. McArdle, D. Tafani, L. P. Barry, A. Holohan, T. Curran, "Simplified Overflow Analysis of an Optical Burst Switch with Fibre Delay Lines," *Proc. Sixth International Conference on Broadband Communications Networks and Systems, (Broadnets 2009)*, Madrid, Spain, September 2009. 138

[75] Y. Mingwu, W. Aijun, L. Zengji, "Blocking Probability of Asynchronous Optical Burst/Packet Switches with Limited Range Wavelength Conversion," *IEEE/OSA Photonics Technology Letters*, vol. 18, no. 2, pp. 1302-1304, June 2006. 21

[76] Y. Mingwu, L. Zengji, W. Aijun, "Accurate and Approximate Evaluations of Asynchronous Tunable-Wavelength-Converter Sharing Schemes in Optical Burst-Switched Networks," *IEEE/OSA Journal of Lightwave Technology*, vol. 23, no. 10, pp. 2807-2815, 2005. 20

[77] Z. Michalewicz, "A Survey of Constraint Handling Techniques in Evolutionary Computation Methods," *Proceedings of the 4th Annual Conference on Evolutionary Programming*, MIT Press, 1995. 108

[78] Z. Michalewicz, *Genetic Algorithms + Data Structures = Evolution Programs*, Springer-Verlag, 2nd Edition, 1994. 112, 114

[79] X. Mountrouidou, H. Perros, "On the departure process of burst aggregation algorithms in optical burst switching," *Computer Networks: The International Journal of Computer and Telecommunications Networking*, vol. 53, no. 3, pp. 247-264, February 2009. 11

[80] X. Mountrouidou, H. Perros, "A Discrete-Time Queueing Network Model of a Hub-Based OBS Architecture," *Springer Telecommunication Systems*, vol. 41, no. 3, pp. 173-184, July 2009. 21, 24

[81] D. Morat, J. Aracil, "On the Use of Balking for Estimation of the Blocking Probability for OBS Routers with FDL, " *Proceedings of ICOIN 2006*, pp. 399 408, 2006.

[82] B. Mukherjee, *Optical WDM Networks*, Optical Network Series, Springer, 2006. 1, 2, 15, 16, 18, 23, 26, 27

[83] G. L. Nemhauser, L. A. Wolsey, *Integer and combinatorial optimization*, John Wiley & Sons Inc., 1988. 102

[84] D. T. Nightingale, "Computation with Smooth Traffics and the Wormald Chart," *Proceedings of the International Teletraffic Congress 1977, (ITC 1977)*, vol. 8, pp. 145.1-145.7, 1977. 36

[85] Opnet Technologies, *Opnet Modeler*, URL:http://www.opnet.com/index.html, last visited December 2011. 25, 52, 68

[86] W. S. Park, M. Shin, H. W. Lee, S. Chong, "A Joint Design of Congestion Control and Burst Contention Resolution for Optical Burst Switching Networks," *IEEE/OSA Journal of Lightwave Technology*, vol. 27, no. 17, pp. 3820-3830, August 2009.

[87] S. Peng, Z. Li, Y. He, A. Xu, "TCP Window-Based Flow-Oriented Dynamic Assembly Algorithm for OBS Networks," *IEEE/OSA Journal of Lightwave Technology*, vol. 7, n. 6, pp. 670-678, 2009. 10

[88] M. H. Phung, K.C. Chua, G. Mohan, M. Motani, T.C. Wong, "The Streamline Effect in OBS Networks and its Application in Load Balancing," *Proceedings of the 2nd International Conference on Broadband Networks 2005, (Broadnets 2005)*, vol. 1, pp. 283-290, October 2005. 77

[89] R. M. Potter, "The Equivalent Non Random Method and Restrictions Imposed on Renewal Overflow Systems by the Specification of a Finite Number of Overflow Traffic Moments," *Proceedings of the International Teletraffic Congress 1979 (ITC 1979)*, vol. 9, pp. potter-1-potter-6, 1979. 36

[90] R. M. Potter, "Explicit Formulae for All Overflow Moments of the Kosten and Brockmeyer Systems with Renewal Input," *Australian Telecommunication Research*, vol. 13, pp. 39-49, 1980. 50

[91] V. Puttasubbappa, H. Perros, “Performance Analysis of Limited-Range Wavelength Conversion in an OBS Switch,” Telecommunications System Journal, vol. 31, no. (2-3), pp. 227-246, March 2006. 21

[92] X. Qin, Y. Yang, “Blocking Probability in WDM Multicast Switching Networks with Limited Wavelength Conversion,” *Second IEEE International Symposium on Network Computing and Applications*, pp. 322-329, 2003. 17

[93] C. Qiao, M. Yong, “Optical Burst Switching (OBS) - a New Paradigm for an Optical Internet,” *Journal of High Speed Networks*, vol. 8, no. 1, pp. 69-84, January 1999. 2, 7

[94] C. Raffaelli, M. Savi, “Cost Comparison of All-Optical Packet Switches with Shared Wavelength Converters,” *Proceedings of the 9th International Conference on Transparent Optical Networks, 2007 (ICTON 2007)*, vol. 3, pp. 209-212, July 2007. 116

[95] A. Rajabi, A. Khonsari, A. Dadlani, “On Modeling Optical Burst Switching Networks with Fiber Delay Lines: A Novel Approach,” *Elsevier Computer Communications*, vol. 33, no. 2, pp. 240-249, February 2010. 20, 24, 26, 72

[96] R. Ramaswami, K. N. Sivarajan, G. H. Sasaki, *Optical Networks: A Practical Perspective*, Morgan Kaufman Publishers, Elsevier, 2010. 1, 2

[97] Y. Rapp, “Planning of Junction Network in a Multi-exchange Area. II Extensions of the Principles and Applications,” *Ericsson Technics*, no. 2, pp. 187-240, 1965. 40

[98] P. Reviriego, A. M. Guidotti, C. Raffaelli, J. Aracil, “Blocking Models of Optical Burst Switches with Shared Wavelength Converters: Exact Formulations and Analytical Approximations,” *Photonic Network Communications*, vol. 16, no. 1, 2008. 17, 20, 24

[99] W. Rogiest, D. Fiems, K. Laevens, and H. Bruneel, “Tracing an Optical Buffer’s Performance: An Effective Approach,” *Lecture Notes in Computer Science*, NETCOOP 2007, Special Issue, 4465: pp. 185-194, 2007. 20

[100] W. Rogiest, D. Fiems, K. Laevens, H. Bruneel, "Exact Performance Analysis of FDL Buffers with Correlated Arrivals," *IFIP International Conference on Wireless and Optical Communications Networks*, 2007. 20

[101] W. Rogiest, D. Fiems, K. Laevens, H. Bruneel, "Modeling the Performance of FDL Buffers with Wavelength Conversion," *IEEE Transactions on Communications*, vol. 57, no. 12, pp. 3703-3711, December 2009. 16

[102] W. Rogiest, K. Laevens, D. Fiems, H. Bruneel, "Quantifying the Impact of Wavelength Conversion on the Performance of Fiber Delay Line Buffers," *Proceedings of the 3rd International Conference on Broadband Communications, Networks and Systems, (Broadnets 2006)*, pp. 1-10, San Jose, California, USA, October 2006. 16, 20, 26

[103] Z. Rosberg, , H. L. Vu, M. Zukerman, J. White, "Performance Analyses of Optical Burst-Switching Networks," *IEEE Journal on Selected Areas in Communications*, vol. 21, no. 7, September 2003. 10, 21, 70

[104] Z. Rosberg, H. L. Vu, M. Zukerman, J. White, "Blocking Probabilities of Optical Burst Switching Networks based on Reduced Load Fixed Point Approximations," *Proceedings of the 22nd Annual Joint Conference of the IEEE Computer and Communications Societies 2003, (IEEE INFOCOM 2003)*, vol. 3, pp. 2008-2018, San Francisco, USA, 30 March - 3 April 2003. 21

[105] Z. Rosberg, A. Zalesky, H. L. Vu, M. Zukerman, "Analysis of OBS Networks With Limited Wavelength Conversion," *IEEE/ACM Transactions on Networking*, vol. 14, no. 5, pp. 1118-1127, October 2006. 17, 21, 24, 69, 71, 77, 78

[106] A. Rostami, A. Wolisz, "Modeling and Synthesis of Traffic in Optical Burst-Switched Networks," *IEEE/OSA Journal of Lightwave Technology*, vol. 25, no. 10, pp. 2942-2952, October 2007. 11, 31

[107] A. Sahasrabudhe, D. Manjunath, “Performance of Optical Burst Switched Networks: a Two Moment Analysis,” *Elsevier Computer Networks*, vol. 50, no. 18, pp. 3550-3563, December 2006. 21, 22, 24, 72

[108] J. N. T. Sanghapi, H. Elbiaze, M. F. Zhani, “Adaptive Burst Assembly Mechanism for OBS Networks Using Control Channel Availability,” *Proceedings of the 9th International Conference on Transparent Optical Networks 2007, (ICTON 2007)*, pp. 96-100, August 2007. 10

[109] J. Segarra, V. Sales, J. Prat, “An All-Optical Access-Metro Interface for Hybrid WDM/TDM PON Based on OBS,” *IEEE/OSA Journal of Lightwave Technology*, vol. 25, no. 4, pp. 1002-1016 , April 2007. 7

[110] M. Schlosser, E. Patzak, P. Gelpke, ‘Impact of Deflection Routing on TCP Performance in Optical Burst Switching Networks,” *Proceedings of the 7th International Conference of Transparent Optical Networks 2005, (ICTON 2005)*, vol. 1, pp. 220-223, July 2005. 18

[111] B. Shihada, P. H. Ho, “Transport Control Protocol in Optical Burst Switched Networks: Issues, Solutions and Challenges,” *IEEE Communications Surveys and Tutorials*, vol. 10, no. 2, pp. 70-86, July 2008. 18, 19

[112] D. Tafani, C. McArdle, L. P. Barry, “Analytical Model of Optical Burst Switched Networks with Share-per-Node Buffers,” *Proceedings of the 16th IEEE Symposium on Computers and Communications 2011 (ISCC 2011)*, pp. 512-518, Corfu, 28 June - 01 July 2011.

[113] J. Teng, G. N. Rouskas, “Routing Path Optimization in Optical Burst Switched Networks,” *Proceedings of the Optical Network Design and Modeling Conference 2005 (ONDM 2005)*, pp. 1-10, 7-9 February, 2005. 22

[114] H. Tode, K. Hamada, K. Murakami, “ORGAN: Online Route and Wavelength Design Based on Genetic Algorithm for OPS Networks,” *Proceedings of the 14th Con-*

ference on Optical Network Design and Modeling 2010, (ONDM 2010), pp. 1-6, February 2010.

[115] J. Triay, C. Cervello-Pastor, "Delay Analysis of Slotted OBS Networks Under DAOBS MAC Protocol," *IEEE Communications Letters*, vol. 15, no. 8, pp. 878-880, August 2011. 69

[116] T. Tripathi, K. N. Sivarajan, "Computing Approximate Blocking Probabilities in Wavelength Routed All-Optical Networks with Limited-Range Wavelength Conversion," *Proceedings of the 18th Annual Joint Conference of the IEEE Computer and Communications Societies 1999, (IEEE INFOCOM 1999)*, vol. 1, pp. 329-336, New York, USA, 21-25 March 1999. 21

[117] J. S. Turner, "Terabit Burst Switching," *Journal of High Speed Networks*, vol. 8, no. 1, March 1999. 2

[118] R. Van Caenegem, D. Colle, M. Pickavet, P. Demeester, J. M. Martinez, F. Ramos, J. Marti, "From IP over WDM to All-Optical Packet Switching: Economical View," *IEEE/OSA Journal of Lightwave Technology*, vol. 24, no. 4, pp. 1638-1645, April 2006. 116

[119] T. Venkatesh, T. L. Sujatha, C. Siva Ram Murthy, "A Novel Burst Assembly Algorithm for Optical Burst Switched Networks Based on Learning Automata," *Springer Lecture Notes in Computer Science*, vol. 4534/2007, pp. 368-377, 2007. 10

[120] B. Wang, N. Lella, "Dynamic Contention Resolution in Optical Burst Switched Networks with Partial Wavelength Conversion and Fiber Delay Lines," *Proceedings of the IEEE Global Telecommunications Conference 2004, (IEEE GLOBECOM 2004)*, vol. 3, pp. 1862-1866, January 2005. 16

[121] J. Y. Wei, R. I. McFarland Jr., "Just-In-Time Signaling for WDM Optical Burst Switching Networks," *IEEE/OSA Journal of Lightwave Technology*, vol. 18, no. 12, pp. 2019-2037, 2000. 12

[122] J. White, *Modelling and Dimensioning of Optical Burst Switched Networks*, Ph.D. Dissertation, Department of Electrical and Electronic Engineering, University of Melbourne, May 2007. 21, 70

[123] J. White, M. Zukerman, H. L. Vu, "A Framework for Optical Burst Switching Network Design," *IEEE Communications Letters*, vol. 6, no. 6, June 2002. 10

[124] R. I. Wilkinson, "Theories for Toll Traffic Engineering in the USA," *Bell System Technical Journal*, vol. 35, pp. 421-514, 1954. 20, 35

[125] E. W. M. Wong, J. Baliga, M. Zukerman, A. Zalesky, G. Raskutti, "A New Method for Blocking Probability Evaluation in OBS/OPS Networks With Deflection Routing," *IEEE/OSA Journal of Lightwave Technology*, vol. 27, no. 23, pp. 5335-5347, 2009. 18, 24, 70, 72

[126] K. Xi, S. Arakawa, M. Murata, "How Many Wavelength Converters Do We Need?," *Proceedings of the 15th International Conference on Optical Network Design and Modeling 2005, (ONDM 2005)*, pp. 347-358, 7-9 February 2005. 17, 22

[127] C. Xiaowen, L. Bo,Z. Zhensheng, "A Dynamic RWA Algorithm in a Wavelength-Routed All-Optical Network with Wavelength Converters," *Proceedings of the 22nd Annual Joint Conference of the IEEE Computer and Communications Societies 2003, (IEEE INFOCOM 2003)*, vol. 3, pp. 1795-1804, San Francisco, USA, 30 March - 3 April 2003. 17

[128] Y. Xiong, M. Vandenhoute, H. C. Cankaya, "Control Architecture in Optical Burst-Switched WDM Networks," *IEEE Journal on Selected Areas in Communications*, vol. 18, no. 10, October 2000. 13, 14, 43

[129] J. Xu, C. Qiao, J. Li, G. Xu, "Efficient Channel Scheduling Algorithms in Optical Burst Switched Networks," *Proceedings of the 22nd Annual Joint Conference of the IEEE Computer and Communications Societies 2003, (IEEE INFOCOM 2003)*, vol. 3, pp. 1795-1804, San Francisco, USA, 30 March - 3 April 2003. 14

[130] L. Xu, H. G. Perros, G. N. Rouskas, "A Queueing Network Model of an Edge Optical Burst Switching Node," *Proceedings of the 22nd Annual Joint Conference of the IEEE Computer and Communications Societies 2003, (IEEE INFOCOM 2003)*, vol. 3, pp. 1795-1804, San Francisco, USA, 30 March - 3 April 2003. 20, 24

[131] S. Yao, B. Mukherjee, S. Dixit, "Advances in Photonic Packet Switching: an Overview," *IEEE Communications Magazine*, vol. 38, no. 2, February 2000. 2

[132] H. Yang, M. Maier, M. Reisslein, W.M. Carlyle, "A Genetic Algorithm-Based Methodology for Optimizing Multiservice Convergence in a Metro WDM Network," *IEEE/OSA Journal of Lightwave Technology*, vol. 21, no. 5, pp. 1114-1133, July 2003. 115

[133] M. Yoo, C. Qiao, "Just-Enough-Time (JET): a High Speed Protocol for Bursty Traffic in Optical Networks," *Proceedings of IEEE/LEOS Technologies for a Global Information Infrastructure 1997*, pp. 79-90, 1997. 12

[134] M. Yoo, C. Qiao, S. Dixit, "QoS Performance of Optical Burst Switching in IP-Over-WDM Networks," *IEEE Journal on Selected Areas in Communications*, vol. 18, no. 10, October 2000. 10, 14, 17, 20, 23

[135] X. Yu, Y. Chen, C. Qiao, "Performance Evaluation of Optical Burst Switching with Assembled Burst Traffic Input," *Proceedings of the IEEE Global Telecommunications Conference 2002, (IEEE GLOBECOM 2002)*, vol. 3, 2318-2322, Taipei, Taiwan, 17-21 November 2002. 11

[136] X. Yu, J. Li, X. Cao, Y. Chen, C. Qiao, "Traffic Statistics and Performance Evaluation in Optical Burst Switched Networks," *IEEE/OSA Journal of Lightwave Technology*, vol. 22, no. 12, pp. 2722-2738, December 2004. 11

[137] X. Yu, C. Qiao, Y. Liu, "TCP Implementations and False Time Out Detection in OBS Networks," *Proceedings of 23rd Annual Joint Conference of the IEEE Computer and Communications Societies 2004, (IEEE INFOCOM 2004)*, vol. 3, pp. 358-366, Hong Kong, 7-11 March 2004. 18

[138] A. Zalesky, H. L. Vu, "Designing an Optimal Scheduler Buffer in OBS Networks," *IEEE/OSA Journal of Lightwave Technology*, vol. 26, no. 14, July 2008. 10

[139] A. Zalesky, H. L. Vu, Z. Rosberg, E. W. M. Wong, M. Zukerman, "Stabilizing Deflection Routing in Optical Burst Switched Networks," *IEEE Journal on Selected Areas in Communications*, vol. 25, no. 6, pp. 3-19, August 2007. 18

[140] T. Zhang, K. Lu, J. Jue, "An Analytical Model for Shared Fiber-Delay Line Buffers in Asynchronous Optical Packet and Burst Switches," *Proceedings of the IEEE International Conference on Communications 2005, (IEEE ICC 2005)*, vol. 3, pp. 1636-1640, Seoul, South Korea, 16-20 May 2005. 20, 26

[141] T. Zhang, K. Lu, J. Jue, "Shared Fiber Delay Line Buffers in Asynchronous Optical Packet Switches," *IEEE/OSA Journal on Selected Areas in Communications*, vol. 24, no. 4, pp. 118-127, April 2006. 20, 24